

2006

MODELING AND SIMULATION TECHNIQUES FOR HIGH SPEED VLSI INTERCONNECTS AND HIGH FREQUENCY MICROWAVE DEVICES

Madhusudanan Keezhveedi Sampath
Western University

Follow this and additional works at: <https://ir.lib.uwo.ca/digitizedtheses>

Recommended Citation

Keezhveedi Sampath, Madhusudanan, "MODELING AND SIMULATION TECHNIQUES FOR HIGH SPEED VLSI INTERCONNECTS AND HIGH FREQUENCY MICROWAVE DEVICES" (2006). *Digitized Theses*. 4979. <https://ir.lib.uwo.ca/digitizedtheses/4979>

This Thesis is brought to you for free and open access by the Digitized Special Collections at Scholarship@Western. It has been accepted for inclusion in Digitized Theses by an authorized administrator of Scholarship@Western. For more information, please contact wlsadmin@uwo.ca.

**MODELING AND SIMULATION TECHNIQUES FOR
HIGH SPEED VLSI INTERCONNECTS AND HIGH
FREQUENCY MICROWAVE DEVICES**

(Spine title: High Speed Interconnects and Microwave Devices)

(Thesis format: Monograph)

by

Madhusudanan Keezhveedi Sampath

Graduate Program in Engineering Science
Department of Electrical and Computer Engineering

A thesis submitted in partial fulfillment
of the requirements for the degree of
Master of Engineering Science

Faculty of Graduate Studies
The University of Western Ontario
London, Ontario, Canada

© Madhusudanan Keezhveedi Sampath 2006

THE UNIVERSITY OF WESTERN ONTARIO
FACULTY OF GRADUATE STUDIES

CERTIFICATE OF EXAMINATION

Supervisor

Dr. Anestis Dounavis

Examiners

Dr. Kazimierz Adamiak

Dr. Gerry Moschopoulos

Dr. A.G. Straatman

The thesis by

Madhusudanan Keezhveedi Sampath

entitled:

**Modeling and Simulation Techniques for High Speed VLSI
Interconnects and High Frequency Microwave Devices**

is accepted in partial fulfillment of the
requirements for the degree of
Master of Engineering Science

Date _____

Chair of the Thesis Examination Board

Abstract

This thesis contributes to the development of novel methods and techniques to combat the simulation difficulties involved in the VLSI interconnect analysis and the finite element method (FEM) based Full Wave problems. Two significant contributions were made to achieve this.

1. A new closed-form passive time-domain macromodeling algorithm for distributed lossy multiconductor interconnects is developed. The method is based on a sixth order FEM approximation and offers an efficient means to discretize interconnects compared to conventional lumped discretization while preserving the passivity of the macromodel. It is shown that due to the high efficiency of sixth order approximation, the proposed macromodel requires only a few elements to achieve good accuracy. In addition, the FEM macromodel can include frequency-dependent per-unit-length (p.u.l.) parameters for the interconnect lines.

2. A parametric model reduction methodology is developed for Fullwave FEM analysis of high frequency microwave devices. This method produces parametric reduced order models that are valid over a user defined range of design parameter values. Such an approach is significantly more CPU efficient in optimization and design space exploration problems since a new reduced model is not required when a parameter is modified. The method presented in this work performs multidimensional Krylov subspace based reduction directly on the conventional FEM system obtained through discretization of vector wave equation. Unlike the previous techniques, the new approach does not result in doubling the size of the original system to perform Krylov-based reduction and consequently results in a significantly smaller and more efficient reduced model.

Acknowledgements

This thesis project could not have been completed with this degree of success if it were not for the invaluable support of my supervisor Prof. Anestis Dounavis. I would like to begin by thanking my professor for introducing me to the area of interconnect modeling and model reduction problem, as well as inculcating me the enthusiasm in research. I wish to extend my appreciation and gratitude to him for all his encouragement, expert guidance, keen supervision and friendly approach throughout my master's program.

I am also thankful to Prof. Roni Khazaka at the McGill University for his contribution in this research. His ideas, comments and feedback were always welcome and appreciated. In addition, I would like to thank all the professors, staff and students at the Electrical and Computer Engineering Department at the University of Western Ontario for their supportive and friendly manner. Finally, I wish to thank all my colleagues and friends for their support, encouragement and enjoyable experience.

Last but not the least I leave a special note to my parents, K.S Sampath and S. Leelavathi. I am also very much grateful to my sisters, Chitra and Subashree. Without these special people, I would not have had the opportunity to complete this study.

Contents

Preliminary Pages

Certificate of Examination.....	ii
Abstract.....	iii
Acknowledgements.....	iv

Introduction..... 1

1.1 – Background and Motivation	1
1.1.1 – <i>VLSI Interconnect Analysis</i>	2
1.1.2 – <i>Microwave Systems Analysis</i>	4
1.2 – Objectives	6
1.2.1 – <i>Addressing Interconnect Simulation Difficulties</i>	6
1.2.2 – <i>Addressing Microwave Simulation Difficulties</i>	7
1.3 – Contributions.....	8
1.4 – Organization of Thesis.....	9

Background and Literature Review..... 11

2.1 – Introduction.....	11
2.2 – High Speed Interconnect Simulation	13
2.2.1 – <i>High Frequency Effects in Interconnects</i>	13
2.2.2 – <i>Interconnect Simulation Difficulties</i>	15
2.2.3 – <i>Interconnect Simulation based on Transmission Line Macromodels</i>	19
2.2.3.1 – Conventional Lumped Segmentation	19
2.2.3.2 – Method of Characteristics	20
2.2.3.3 – Exponential Padé-based Matrix-Rational Approximation	22
2.2.3.4 – Compact Finite-Differences Based Approximation	23
2.2.3.5 – Chebyshev Polynomials	25
2.3 – Full Wave Simulation of Microwave Systems	26
2.3.1 – <i>FEM formulation of Microwave Systems</i>	27
2.4 – Simulation Techniques based on Model Order Reduction (MOR)	30
2.4.1 – <i>Explicit Moment Matching Based MOR</i>	31
2.4.2 – <i>Implicit Moment Matching Based MOR</i>	34
2.4.3 – <i>Challenges in Traditional MOR Application to Full Wave FEM</i>	37

Development of a Passive Macromodeling Algorithm for Lossy Multiconductor

Interconnects..... 39

3.1 – Introduction.....	39
3.2 – Development of the Proposed Macromodel	41

3.3 – Passivity Considerations	51
3.4 – Frequency Dependent Parameters.....	56
3.5 – Y-Parameters and the Time-Domain Macromodel.....	58
3.6 – Numerical Examples.....	64
3.6.1 – Example 3.1.....	65
3.6.2 – Example 3.2.....	67
3.6.3 – Example 3.3.....	71
Parameterized Model Order Reduction Techniques for FEM based Full Wave	
Analysis.....	74
4.1 – Introduction.....	74
4.2 – Krylov MOR Techniques based on Linear First Order Representations.....	77
4.3 – Multidimensional Model Reduction Methodology.....	79
4.3.1 – <i>PMR Technique based on the State Space Approach</i>	79
4.3.1.1 – Formulation of the Parametric System	80
4.3.1.2 – Computation of Multidimensional Subspace	80
4.3.1.3 – Model Reduction through Congruent Transformation	81
4.3.2 – <i>PMR technique based on the Parametric Frequency Approach</i>	82
4.3.2.1 – Formulation of the Multidimensional System	83
4.3.2.2 – Parametric System Formulation	84
4.3.2.3 – Computation of the Multidimensional Subspace	84
4.3.2.4 – MOR Through Congruent Transformation	85
4.3.3 – <i>Selecting the Order of the Reduced Model</i>	88
4.3.4 – <i>Sparsification of the Reduced Model</i>	88
4.4 – Numerical Examples.....	91
4.4.1 – Example 4.1.....	91
4.4.2 – Example 4.2.....	97
4.4.3 – Example 4.3.....	104
Conclusion and Future Research	108
5.1 – Conclusion	108
5.2 – Suggestions for Future Research	109
References.....	111
Curriculum Vita.....	119

List of Tables

TABLE 3.1 69

TABLE 4.1 96

TABLE 4.2 96

TABLE 4.3 103

TABLE 4.4 107

TABLE 4.5 107

List of Figures

Figure 2.1: Roadmap- Interconnect complexity grows as devices shrink	13
Figure 2.2: Delay versus Technology	14
Figure 2.3: Interconnect Hierarchy	15
Figure 2.4: High-Speed Interconnect Effects	15
Figure 2.5: Lumped transmission line model.....	20
Figure 2.6: Circuit Equivalent of Method of Characteristics based transmission-line model.....	22
Figure 2.7: Block Arnoldi Algorithm for expansion about a complex frequency point	36
Figure 3.1: M^{th} Order Finite Element Discretization of Interconnect.....	42
Figure 3.2: An interconnect circuit for illustrating the FEM macromodel.....	43
Figure 3.3: Frequency response comparison for circuit in Figure 3.2 for $d= 1\text{cm}$ using first order FEM approaches	45
Figure 3.4: Frequency response comparison for circuit in Figure 3.2 for $d= 3\text{ cm}$ using sixth order FEM approaches	49
Figure 3.5: Illustration of Significance of Passivity	52
Figure 3.6: RL canonical circuit configuration.....	57
Figure 3.7a: Circuit topology for $R(s)+sL(s)$ for a three conductor transmission line	57
Figure 3.7b: Circuit representation of Z_{ij} , RL canonical configuration.....	58
Figure 3.8: Realization of the Interconnect Model	59
Figure 3.9: Realization of Ψ_1	60
Figure 3.10: Realization of Ψ_2	60
Figure 3.11: Realization of Ψ_1 for a three conductor transmission line	60
Figure 3.12: Realization of Ψ_2 for a three conductor transmission line	61
Figure 3.13: Y_{jk}^i circuit.....	61

Figure 3.14: Realization of Ψ_1 of a two conductor transmission line with frequency dependent p.u.l. resistance and inductance	62
Figure 3.15: Realization of Ψ_2 of a two conductor transmission line with frequency dependent p.u.l. resistance and inductance	62
Figure 3.16: Z_i circuit (RL canonical configuration)	62
Figure 3.17: Realization of Ψ_1 for a three conductor transmission line with frequency dependent p.u.l. resistance and inductance	63
Figure 3.18: Realization of Ψ_2 for a three conductor transmission line with frequency dependent p.u.l. resistance and inductance	63
Figure 3.19: Z_{jk}^1 circuit (RL canonical configuration)	64
Figure 3.20: Nonlinear interconnect circuit (Example 1)	66
Figure 3.21: Frequency response of Y_{11} (Example 1)	66
Figure 3.22: Transient response (Example 1)	67
Figure 3.23: On-chip coupled interconnect network (Example 2)	67
Figure 3.24: Transient response at node V_1 (Example 2).....	69
Figure 3.25: Transient response at node V_3 (Example 2).....	70
Figure 3.26: Transient response at node V_2 (Example 2).....	70
Figure 3.27: Transient response at node V_4 (Example 2).....	71
Figure 3.29: On-chip 9-coupled interconnect network.....	72
Figure 3.30: Transient response of line 5 (Example3).....	73
Figure 3.31: Transient response of line 1 (Example3).....	73
Figure 4.1: Dielectric Post inside WR90 waveguide ;d= 6 mm, c = 12 mm.....	93
Figure 4.2: Frequency response comparison of the magnitude of reflection coefficient for Example1 when $\epsilon_r = 6$	94
Figure 4.3: Frequency response comparison of the magnitude of reflection coefficient for Example1 when $\epsilon_r = 8$	94
Figure 4.4: Frequency response comparison of the magnitude of reflection coefficient for Example1 when $\epsilon_r = 10$	95
Figure 4.5: 3D comparison of the magnitude of reflection coefficient (S_{11}) for Example1 with different dielectric permittivity values.....	95

Figure 4.6: H-plane waveguide T-junction loaded with a partial height post. (Example 2).....	99
Figure 4.7: Frequency response comparison of the magnitude of reflection coefficient for Example2 at parameter values $\sigma = 5.889e7$ and $\epsilon_r = 1$	100
Figure 4.8: Frequency response comparison of the magnitude of reflection coefficient for Example2 at parameter values $\sigma = 0$ and $\epsilon_r = 1 - j0.1$	100
Figure 4.9: Frequency response comparison of the magnitude of reflection coefficient for Example2 at parameter values $\sigma = 0$ and $\epsilon_r = 4 - j0.25$	101
Figure 4.10: Comparison of Frequency response of S-parameters for Example2 for the case when post is a metal ($\sigma = 5.889e7$ and $\epsilon_r = 1$).	101
Figure 4.11: 3D comparison of the magnitude of S_{11} for Example2 when $\sigma = 0$ and at different dielectric permittivity values.....	102
Figure 4.12: 3D comparison of the magnitude of S_{21} for Example2 when $\sigma = 0$ and at different dielectric permittivity values.....	102
Figure 4.13: 3D comparison of the magnitude of S_{31} for Example2 when $\sigma = 0$ and at different dielectric permittivity values.....	103
Figure 4.14: H-plane waveguide bend (Example 3).....	105
Figure 4.15: Frequency response of the magnitude of the reflection coefficient (S_{11}) for Example 3 at different cut lengths of the Hbend waveguide.	106
Figure 4.16: 3D comparison of the magnitude of reflection coefficient (S_{11}) for example3 at different cut length values.	106

Abbreviations

AWE: Asymptotic Waveform Evaluation.

CFH: Complex Frequency Hopping.

EM: Electromagnetic.

FEM: Finite Element Method.

ITRS: International Technology Roadmap for Semiconductors

MNA: Modified Nodal Analysis

MTL: Multiconductor Transmission Line

MOR: Model Order Reduction.

NUTL: Nonuniform Transmission Line

ODE: Ordinary Differential Equation

PDE: Partial Differential Equation.

PRIMA: Passive Reduced-order Interconnect Macromodeling Algorithm

p.u.l: per unit length

RF: Radio Frequency.

TEM: Transverse electromagnetic.

VLSI: Very Large Scale Integration.

Chapter 1

Introduction

1.1 – Background and Motivation

The phenomenal growth in the field of high frequency technology has influenced the construction of different types of microwave, millimetre-wave, optical, RF and VLSI devices commonly used in mobile communications, radio links, optical communications, and various other automotive electronics systems. Rapid advances in the VLSI technology have significantly reduced the feature sizes of high-speed electronic circuits and increased the density of chips. As VLSI technology shrinks to deep sub-micron geometries, the propagation delay due to interconnects (wiring) begins to dominate the total chip delay. Interconnects have become a dominating factor in determining the circuit performance of high-speed VLSI systems. Also modern wireless systems involve electrically large electromagnetic (EM) structures (waveguides, antennas, circuits, and

components) that are very complex in both geometry and material composition [1]. There is a clear need for advanced analysis and design tools for predicting the performance and optimizing the parameters of such structures prior to costly prototype development. Moreover, wireless designers also demand that the simulation techniques be fast and run on relatively small computing platforms, such as standard desktop PCs [1]. Hence at higher frequencies both VLSI interconnects and microwave devices require extremely fast and accurate modeling and simulation techniques for the optimization and design space exploration.

1.1.1 – VLSI Interconnect Analysis

As the operating frequencies of VLSI systems increase, interconnects behave like transmission lines and effects such as ringing, signal delay, distortion, attenuation and crosstalk severely degrade the signal integrity of the system. These high frequency issues have made electrical interconnects a critical part in the signal integrity analysis [2]-[5]. Furthermore, skin effect losses in the conductors and shunt losses in the dielectrics also become prominent at higher frequencies and distributed models with frequency-dependent parameters are needed. Consequently, designers must consider interconnect analysis at the early stages of the design cycle to ensure circuit performance and reliability.

There are two major difficulties in modeling distributed interconnects in a circuit simulation environment. The first difficulty is due to the mixed frequency/time problem, which is encountered while linking distributed interconnects with nonlinear circuit el-

ements. This is because, distributed interconnects are described by partial differential equations that are best solved in the frequency-domain, whereas nonlinear elements are described only in the time-domain as nonlinear ordinary differential equations [5]. Hence, it is essential to model interconnects such that they can be directly included in a nonlinear circuit simulation environment. The second difficulty is due to the excessive CPU time associated with the simulation of interconnects. A significant amount of research has been done to address the simulation of distributed interconnects in the presence of nonlinear elements [11]-[40]. Approaches based on conventional lumped segmentation of interconnects provide a brute force solution to the problem of mixed frequency/time simulation [12]. However, these methods lead to large circuit matrices, rendering the simulation inefficient. There are two simulation strategies for modeling high speed interconnect lines. One approach is based on efficient modeling of each interconnect networks by developing macromodels for each transmission line network and other is based on model order reduction (MOR) techniques that reduce a large linear interconnect network (containing many interconnects) into a smaller network.

In the first approach of developing macromodels for each interconnect, transmission-line networks described by Telegrapher's equation which are partial differential equations (PDEs) are translated into a set of ordinary differential equations, through some kind of discretization. This approach is extremely important for the analysis of electrical networks as it allows the circuit designers to evaluate their designs in a circuit simulation environment. One of the key issues in macromodeling of transmission lines is the preservation of passivity. Since transmission lines are passive elements, passivity is an essential property to satisfy because stable but not passive macromodels can produce

unstable networks when connected to other passive loads. This can result in spurious oscillations and numerical instabilities during transient analysis. In recent years, the development of passive macromodels has been a topic of intense research [21]-[27].

Model order reduction techniques such as asymptotic waveform evaluation (AWE) [13], were proposed to reduce the dimension of large linear interconnect networks. The goal of these techniques is to approximate the behaviour of a large linear interconnect network with a smaller network, while maintaining the accuracy of the response. This is achieved by extracting only the dominant poles of the network which can be accomplished by explicitly matching the moments of the original system. However, due to the numerical instabilities, these explicit moment matching methods cannot generate high order models. Due to these deficiencies, more efficient and robust MOR algorithms based on implicit moment matching such as the Krylov subspace methods were proposed [18]-[24]. These methods are robust and can preserve the passivity of the reduced network [20]-[21].

One of the goals of this thesis is to develop an efficient and passive macromodel for transmission lines where the transmission line parameters can be lossy, coupled, and frequency dependent.

1.1.2 – Microwave Systems Analysis

The design of microwave waveguide structures like filters, couplers, junctions and resonators need extremely fast numerical simulations [6]-[9]. Microwave systems are

also based on PDEs such as the vector wave equation or Maxwell's equations and hence full wave techniques are required to accurately characterize these systems. Numerical methods, such as the Finite Element Method (FEM), have become indispensable tools for the accurate full wave analysis of microwave waveguide devices [6]-[10]. The key advantages of the FEM are its accuracy, versatility and its ability to handle complex materials (including anisotropic, lossy, non-linear etc) and geometries [6]-[8]. However it relies on the discretization of three dimensional space and thus results in very large systems of equations which are prohibitively expensive to solve. This problem is further exacerbated when one considers the typical design process which includes optimization and design space exploration and thus requires repeated simulation of the same problem for different parameter values.

Recently researchers from electromagnetics modelling and simulation community have focussed their attention to apply MOR techniques (that were originally used for reduction of large interconnect networks in circuit simulation area) for finite element analysis of three-dimensional microwave structures [41]-[53]. MOR technique has been proposed in the literature as an effective tool to combat the computational complexity and CPU cost of FEM, and various advances in this field have led to the successful application of numerically stable techniques such as Krylov subspace methods [45],[46],[48],[49],[50],[53]. However, all these methods conserve the original system moments only with respect to frequency. While this provides a significant CPU cost advantage when performing a single frequency sweep, a new reduced order model is required each time a parameter is modified in the studied structure. This results in a significant overhead and reduced efficiency when performing common design steps such

as optimization and design space exploration. Parameterized reduction methods have been proposed in the interconnect simulation area to address such concerns [26],[30],[31],[32],[34] however no such method existed for microwave problems.

In this thesis, a multidimensional reduction method applicable for microwave problems based on Full-Wave analysis is presented. The proposed approach uses a multidimensional Krylov subspace and thus results in a reduced system that matches the moments of the original system with respect to frequency as well as other design parameters. The resulting reduced model is therefore valid over the parameter ranges of interest, which eliminates the need to redo the reduction for each optimization point and thus results in significant CPU cost savings.

1.2 – Objectives

It is extremely important to address the increased computational complexity of VLSI, and microwave systems in order to fulfill the industrial demand for faster design cycle and shorter time to market for electronic products. The objective of this thesis is to develop a fast, efficient and accurate macromodeling technique for high speed VLSI interconnects simulation and to address the computational complexity involved in the simulation of FEM based microwave systems.

1.2.1 – Addressing Interconnect Simulation Difficulties

The first objective of this thesis is to address the simulation difficulties of interconnects by developing a general-purpose passive macromodeling algorithm for a

lossy multiconductor transmission lines. This technique is based on the direct discretization of transmission line equations using a high order finite element method approximation. This technique enables the circuit simulation environment to view interconnects as regular circuit components, regardless of what the electrical parameters might be. The macromodel can be used to model interconnects with frequency dependent per unit length (p.u.l) parameters and can be incorporated with passive model order reduction techniques.

1.2.2 – Addressing Microwave Simulation Difficulties

As a second objective, this thesis also serves to address the computational complexity involved in the FEM based microwave problems. The commonly used FEM model for a microwave system is derived from the approximation of the vector wave equation for electric field [7]. FEM discretization of the vector wave equation results in a very large system of matrix equations that are prohibitively time consuming to solve. MOR techniques have been proposed in literature to significantly reduce the CPU time required to simulate these large scale FEM problems. In addition to reducing the CPU expense of regular simulations using MOR, it is also important to predict the response of a microwave circuit due to the variation in the design parameters. A variation in the design parameter changes the overall system of equations and performing MOR process each time a design parameter is modified is not a feasible task. Therefore incorporating a set of design parameters within the reduced model can aid in addressing these issues. In this thesis, a methodology is proposed to form parametric reduced order models for microwave systems based on the FEM discretization of the vector wave equation. The

resulting reduced order model matches the characteristics of the original system in frequency as well as other design parameters.

Furthermore, the general form of the resulting matrix equation is not directly compatible with robust and stable MOR techniques such as the Krylov subspace methods [18],[49]. A number of methods [49]-[50], [51]-[52] are available in order to reformulate the FEM equations as a linear first order system such that their moments form a Krylov subspace; however, these methods have the effect of making the original system twice as large. Moreover they cannot handle complex frequency dependence which is introduced in the model due to frequency dependent material properties and frequency dependent boundary conditions. A new approach is developed in this thesis based on multidimensional Krylov subspace methods to address the Krylov incompatibility of the discrete FEM systems. The method presented performs multidimensional Krylov subspace based reduction directly on the conventional FEM system obtained through discretization of vector wave equation. The new approach does not result in doubling the size of the original system in order to perform Krylov based MOR. Furthermore, this approach is applicable to problems which include losses and can also handle FEM systems with complex frequency dependence.

1.3 – Contributions

The main contributions of this thesis are:

1. An efficient and passive macromodeling algorithm is developed for high speed VLSI interconnects (multiconductor transmission lines) using high order finite

element methods [38]. The proposed scheme is applicable to interconnects with lossy, coupled, and frequency dependent p.u.l. parameters. The macromodel can easily be linked with existing circuit simulators and can also be incorporated with passive model order reduction techniques available in literature [18]-[24].

2. A Parametric Model Order Reduction (PMR) Methodology for Finite Element Based Full-Wave Analysis is presented to significantly reduce the computational cost involved in the simulation of modern microwave systems [53]. The developed PMR technique is based on multidimensional Krylov subspace methods and generates parametric reduced order models which are functions of frequency as well as a function of design parameter of interest. The significant advantage of the PMR technique is that there is no need to redo the MOR process each time a design parameter is modified in the studied problem. This leads to significant CPU savings for applications such as optimization and design space exploration.

1.4 – Organization of Thesis

The organization of thesis is as follows. Chapter 2 begins by reviewing the effects of interconnects in modern high-speed VLSI devices. The difficulties in high speed interconnect simulation and the contributions made in macromodeling techniques in order to address these simulation difficulties are reviewed. Following this, the FEM based full wave analysis of microwave systems and the computational complexities involved in their analysis are studied. Chapter 2 ends with a discussion on MOR techniques for

addressing the computational difficulties in the analysis of large scale linear systems and the challenges involved in applying these MOR techniques to full wave FEM analysis of microwave problems are also investigated. In Chapter 3, a new general class of passive macromodeling algorithm for lossy multiconductor transmission lines is described. The algorithm is based on the sixth-order finite element method approximation. The development of the algorithm and proof for the passivity of the macromodeling algorithm is described. Several numerical examples to demonstrate the validity and efficiency of the developed macromodel are illustrated. Chapter 4 presents a parameterized model order reduction methodology for full-wave FEM analysis of microwave systems. The FEM formulation of the microwave system is reviewed and the development of the parametric reduced model is described in detail. Finally, numerical examples are presented to demonstrate the efficiency of the parameterized reduced order models obtained using the proposed technique. Chapter 5 presents a summary and a list of future work.

Chapter 2

Background and Literature Review

2.1 – Introduction

The increasing demand for higher operating speeds and the rapid advancements in the design technology have made the analysis of high frequency circuits and systems such as the VLSI and microwave devices extremely important. The increasing trend of VLSI technology towards miniature designs has made interconnects a dominating factor in determining the circuit performance [2]-[5]. If the interconnects are sufficiently long or the signal rise/fall times are comparable to the time of flight across the line, the interconnect delay will dominate gate delay, and the transmission line effects will have a severe impact on circuit performance. At low frequencies, interconnects behave as short-circuits. However, as frequency increases, interconnects gradually display resistive, capacitive and inductive effects. These effects can severely degrade the signal integrity of circuits and systems. Depending on the operating frequency and physical structure of interconnects different transmission line models are required. Each model offers different challenges to circuit simulators.

At very high frequencies of operation, the quasi-static models are no longer valid and full wave models are required to accurately characterize the high frequency effects. Electromagnetic systems such as the microwave waveguide devices and other such structures require full wave methods which directly solve the Maxwell's equation to predict the electromagnetic behaviour of systems. Full wave analysis of microwave problems require the computation of frequency responses over broad band of frequencies rather than at one or few isolated frequencies [7]. Such calculations can be extremely time consuming when a traditional frequency domain numerical method (such as the FEM) is used because a large set of algebraic equations must be solved repeatedly at many frequencies. This problem is further compounded when one considers the optimization process of microwave problems which involve a process of repeated simulations alternating with the adjustment of design parameters to reach a design goal. Therefore, there is a need to reduce this computational burden involved in the full wave analysis of FEM based microwave problems.

The chapter is organized as follows. The high-speed interconnect simulation is discussed in section 2.2 which reviews the high frequency effects, interconnect simulation difficulties and the various simulation techniques based on macromodeling methods. Section 2.3 describes the finite element based full wave analysis of microwave problems. Simulation techniques based on Model Order Reduction (MOR) algorithms are briefly described in section 2.4. Section 2.4 also considers the challenges faced by researches in application of traditional MOR methods for finite element based full wave problems.

2.2 – High Speed Interconnect Simulation

2.2.1 – High Frequency Effects in Interconnects

The driving force behind the impressive advancement of the VLSI circuit technology has been the rapid scaling of the feature size, i.e., the minimum dimension of the transistor. It decreased from 2 μm in 1985 to 0.35 μm in 1996. According to the International Technology Roadmap for Semiconductors (ITRS) [54], it will further decrease at the rate of 0.7 x per generation (consistent with Moore's Law) to reach 0.07 μm by 2010. Such rapid scaling has two profound impacts. First, it enables much higher degree of on-chip integration. The number of transistors per chip will increase by more than 2x per generation to reach 800 millions in the 0.07 μm technology. Second, it implies that the circuit performance will be increasingly determined by the interconnect performance. The interconnect design will play the most critical role in achieving the projected clock frequencies in the ITRS [54].

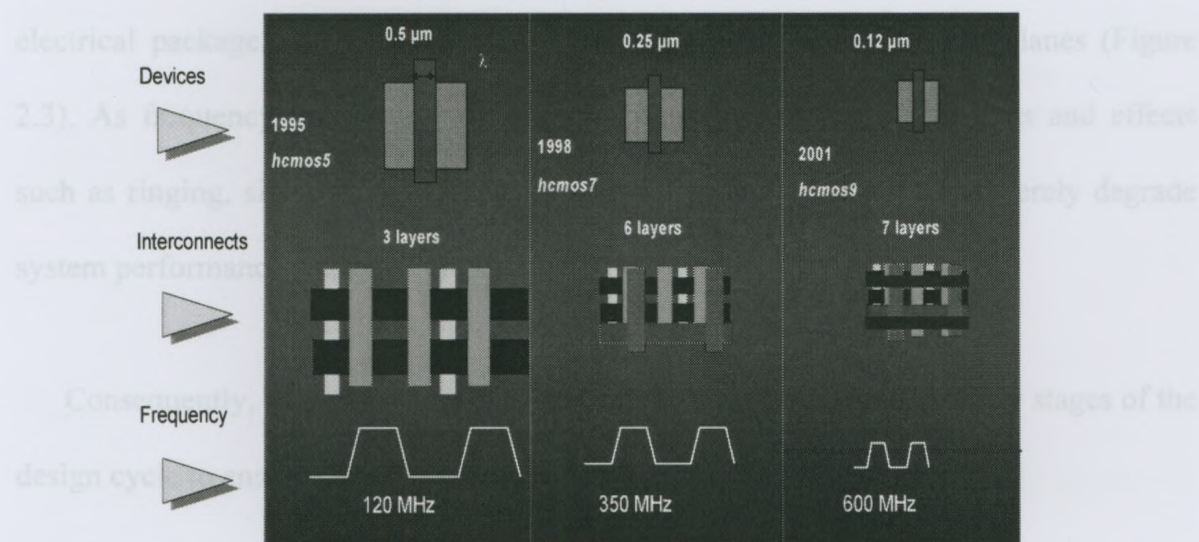
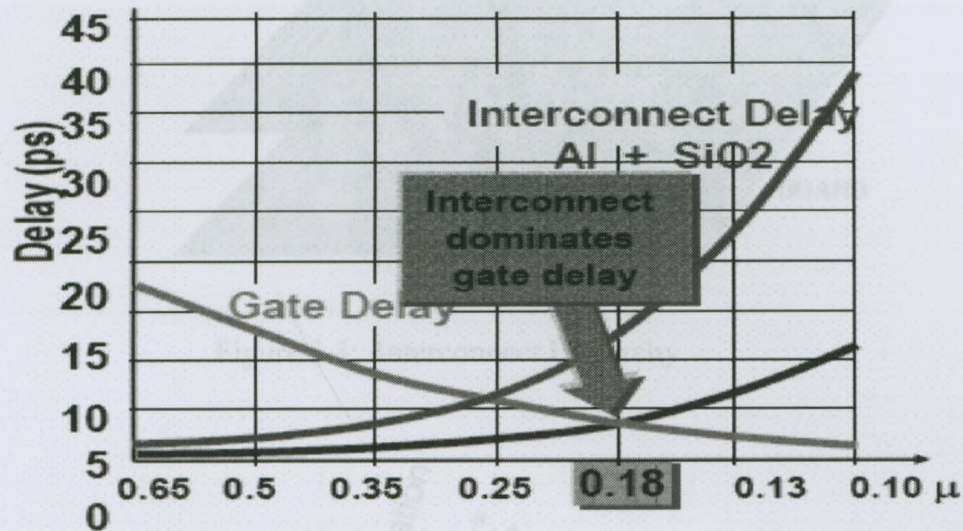


Figure 2.1: Roadmap- Interconnect complexity grows as devices shrink

Figure 2.1 shows the interconnect complexity grows as the device sizes shrink and Figure 2.2 shows that interconnect delay dominates gate delay as technology shrinks to deep-submicron geometries.



Source: ITRS Roadmap 1999

Figure 2.2: Delay versus Technology

Interconnects are present at different levels of technology such as digital chips, electrical packages, multi-chip modules, printed-circuit-boards and backplanes (Figure 2.3). As frequency increases, interconnects behave like transmission lines and effects such as ringing, signal delay, distortion, attenuation and crosstalk can severely degrade system performance (Figure 2.4) [5].

Consequently, designers must consider interconnect analysis at the early stages of the design cycle to ensure circuit performance and reliability.

The selection of the model depends on the physical interconnect structure as well as the operating frequency of the circuit. These two factors determine whether the modeling of interconnects is based on quasi-transverse electromagnetic (quasi-TEM) or full wave

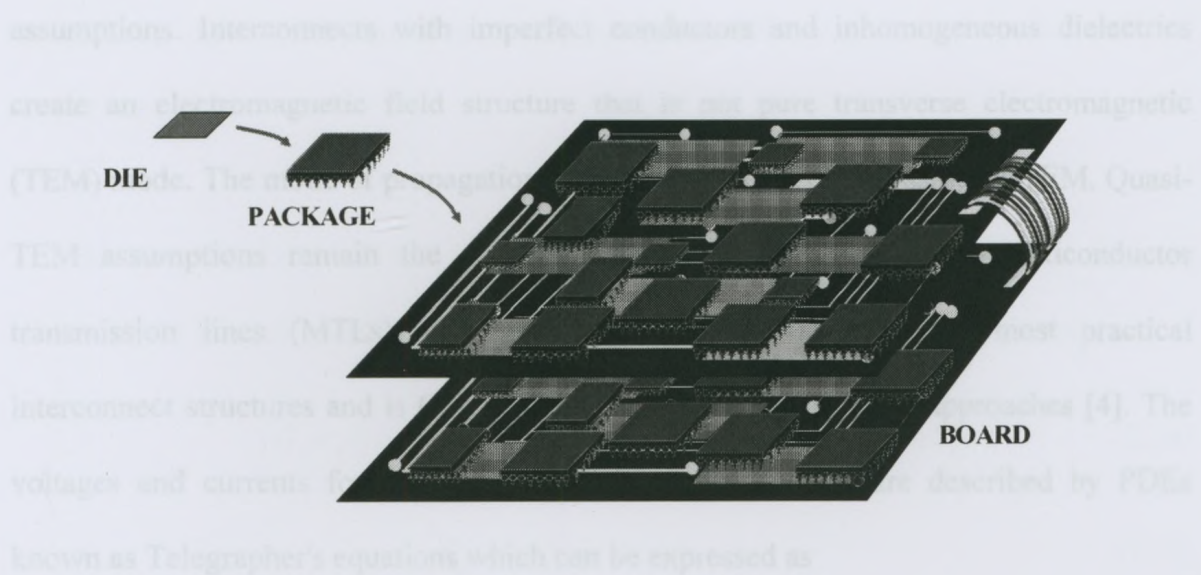


Figure 2.3: Interconnect Hierarchy

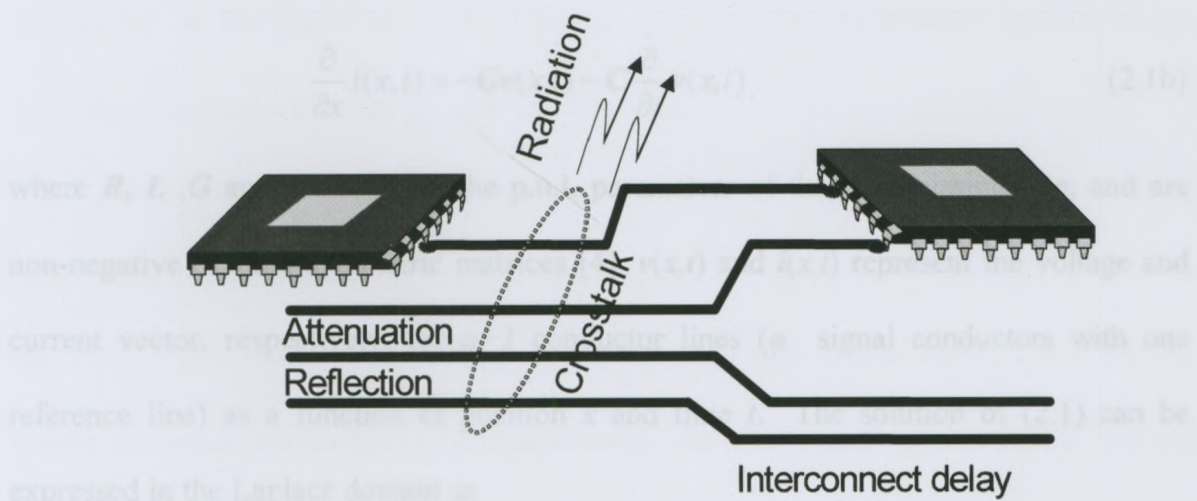


Figure 2.4: High-Speed Interconnect Effects

2.2.2 – Interconnect Simulation Difficulties

To simulate interconnects with circuit elements, electrical models are required. The selection of the model depends on the physical interconnect structure as well as the operating frequency of the circuit. These two factors determine whether the modeling of interconnects is based on quasi-transverse electromagnetic (quasi-TEM) or full wave

assumptions. Interconnects with imperfect conductors and inhomogeneous dielectrics create an electromagnetic field structure that is not pure transverse electromagnetic (TEM) mode. The mode of propagation of such lines is referred to as quasi-TEM. Quasi-TEM assumptions remain the dominant trend for analyzing lossy multiconductor transmission lines (MTLs), since the approximation is valid for most practical interconnect structures and is CPU efficient compared to full wave approaches [4]. The voltages and currents for the quasi-TEM distributed models are described by PDEs known as Telegrapher's equations which can be expressed as

$$\frac{\partial}{\partial x} \mathbf{v}(x,t) = -\mathbf{R}\mathbf{i}(x,t) - \mathbf{L} \frac{\partial}{\partial t} \mathbf{i}(x,t) \quad (2.1a)$$

$$\frac{\partial}{\partial x} \mathbf{i}(x,t) = -\mathbf{G}\mathbf{v}(x,t) - \mathbf{C} \frac{\partial}{\partial t} \mathbf{v}(x,t) \quad (2.1b)$$

where \mathbf{R} , \mathbf{L} , \mathbf{G} and $\mathbf{C} \in \mathbb{R}^{\varphi \times \varphi}$ are the p.u.l. parameters of the transmission line, and are non-negative definite symmetric matrices [4]. $\mathbf{v}(x,t)$ and $\mathbf{i}(x,t)$ represent the voltage and current vector, respectively, for $\varphi+1$ conductor lines (φ signal conductors with one reference line) as a function of position x and time t . The solution of (2.1) can be expressed in the Laplace domain as

$$\begin{bmatrix} \mathbf{V}(d,s) \\ \mathbf{I}(d,s) \end{bmatrix} = e^{\mathbf{Z}_t} \begin{bmatrix} \mathbf{V}(0,s) \\ \mathbf{I}(0,s) \end{bmatrix}, \quad \mathbf{Z}_t = (\mathbf{D} + s\mathbf{E})d \quad (2.2a)$$

$$\mathbf{D} = \begin{bmatrix} 0 & -\mathbf{R} \\ -\mathbf{G} & 0 \end{bmatrix}, \quad \mathbf{E} = \begin{bmatrix} 0 & -\mathbf{L} \\ -\mathbf{C} & 0 \end{bmatrix} \quad (2.2b)$$

where $\mathbf{V}(d,s)$, $\mathbf{I}(d,s)$ are the terminal voltage and current vectors of the transmission line; $\mathbf{V}(0,s)$, $\mathbf{I}(0,s)$ are the near end voltage and current vectors of the transmission line and d is the length of the transmission line. Equation (2.2) cannot be expressed in time domain

as ordinary differential equations, which makes it difficult to include with nonlinear circuit simulators.

The general form of the circuit equations for a multi-port nonlinear network consisting of lumped and distributed elements in Laplace domain can be expressed as

$$\left(\mathbf{G}_\phi \mathbf{x}_\phi(t) + \mathbf{C}_\phi \frac{d\mathbf{x}_\phi(t)}{dt} + \sum_{k=1}^{N_k} \mathbf{D}_k \mathbf{i}_k(t) + \mathbf{f}_\phi(\mathbf{x}_\phi(t)) \right) = \mathbf{b}_\phi(t) \quad (2.3a)$$

$$\mathbf{I}_k(s) = \mathbf{Y}_k(s) \mathbf{V}_k(s) \quad (2.3b)$$

where

$\mathbf{x}_\phi(t) \in \mathcal{R}^n$ is the vector of node voltages appended by independent voltage source currents, linear inductor currents, and port currents.

$\mathbf{G}_\phi, \mathbf{C}_\phi \in \mathcal{R}^{n \times n}$ are the constant matrices describing the lumped memoryless and memory elements of the network, respectively.

$\mathbf{D}_k = [d_{i,j} \in \{0,1\}]$ with a maximum of one nonzero in each row or column, is a selector matrix that maps the vector of currents entering the interconnect subnetwork k , into the node space \mathcal{R}^ϕ of the network where $i \in \{1, \dots, \phi\}$, $j \in \{1, \dots, 2m_k\}$, and m_k is the number of coupled conductors in the linear subnetwork k

$\mathbf{f}_\phi(\mathbf{x}_\phi(t))$ is a vector containing nonlinear functions of the nonlinear circuit elements of the network.

$\mathbf{b}_\phi(t) \in \mathcal{R}^\phi$ is a vector containing terms of independent voltages and current sources.

$\mathbf{Y}_k(s)$ is the admittance parameters for the interconnect subnetwork k , which can be obtained by converting $\mathbf{e}^{\mathbf{z}_i}$ in (2.2) into Y-parameters; $\mathbf{I}_k, \mathbf{V}_k$ are the Laplace terminal

current and voltage waveforms of the interconnect k and N_t is the number of interconnects.

There are two major difficulties involved in modeling distributed networks in a circuit simulation environment. The first difficulty is due to the mixed frequency/time problem, which is encountered while linking distributed transmission lines with nonlinear circuit elements. This is due to the fact that, distributed transmission lines are described by PDEs that are best solved in the frequency domain, whereas nonlinear elements are described only in time domain as nonlinear ordinary differential equations. In order to address this difficulty, numerical methods are required to convert the transmission line equations into ordinary differential equations, so that (2.3) can be expressed as

$$\mathbf{G}_\pi \mathbf{x}_\pi(t) + \mathbf{C}_\pi \frac{d\mathbf{x}_\pi(t)}{dt} + \mathbf{f}_\pi(\mathbf{x}_\pi(t)) = \mathbf{b}_\pi(t) \quad (2.4)$$

where the distributed elements are now explicitly combined in the MNA matrices of the overall network. The second difficulty is due to the excessive CPU time involved in the simulation of transmission lines. In time domain simulations it is required to solve nonlinear difference equations at every time point using Newton iterations. Since discretizing interconnects often leads to very large \mathbf{G}_π and \mathbf{C}_π matrices, this results in increased CPU cost for the simulation of transmission lines.

The objectives of interconnect simulation algorithms are to address the mixed frequency/time problem as well as to reduce the CPU time in simulations. The next section reviews some of the interconnect simulation techniques based on transmission line macromodels.

2.2.3 – Interconnect Simulation based on Transmission Line Macromodels

To simulate interconnects with nonlinear elements, macromodels are required to convert Telegrapher's equations into ordinary differential equations. The efficiency of macromodels is determined by its ability to address the mixed frequency/time problem as well as to handle large linear circuits without too much of CPU expense. Another way to classify transmission line macromodels is based on the passivity of the macromodel. Since transmission lines are passive elements, passivity is an important property to be satisfied since only passive macromodels can guarantee the stability of the overall network when terminated to other passive loads. This section reviews some of the interconnect simulation algorithms based on transmission line macromodels.

2.2.3.1 – Conventional Lumped Segmentation

The lumped segmentation approach approximates the Telegrapher's equation by applying the Euler's method which results in

$$\mathbf{v}_{d+1}(t) - \mathbf{v}_d(t) = -\Delta x \mathbf{R} \mathbf{i}_d(t) - \Delta x \mathbf{L} \frac{\partial}{\partial t} \mathbf{i}_d(t) \quad (2.5a)$$

$$\mathbf{i}_{d+1}(t) - \mathbf{i}_d(t) = -\Delta x \mathbf{G} \mathbf{v}_{d+1}(t) - \Delta x \mathbf{C} \frac{\partial}{\partial t} \mathbf{v}_{d+1}(t) \quad (2.5b)$$

where $d = [1, \dots, m]$, $\Delta x = d/m$ and m is the number of sections and d is the length of the interconnect. The circuit equivalent for this method consists of resistors, inductors and capacitors as shown in Figure 2.5.

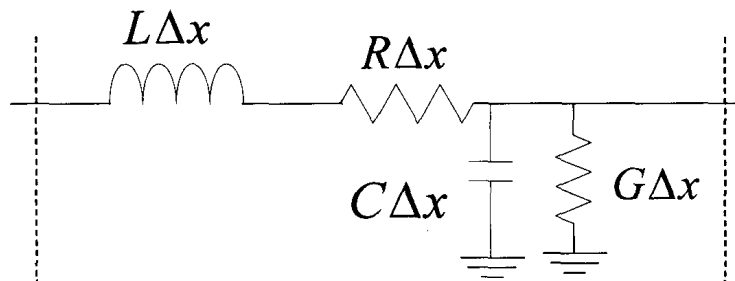


Figure 2.5: Lumped transmission line model

The conventional lumped method provides a direct method to discretized interconnects, however, the approximation is only valid if Δx is chosen to be a small fraction of the wavelength (i.e. $\lambda = v/f$, where λ is the wavelength, v is the velocity, and f is the frequency of interest). If the frequency of interest is high or if the interconnect is electrically long many lumped elements are required. This leads to large circuit sizes and the simulation becomes CPU inefficient. In order to overcome this difficulty, more sophisticated algorithms were proposed some of which are reviewed below.

2.2.3.2 – Method of Characteristics

The method of characteristics (MoC) [57] is able to represent lossless interconnects as ODEs containing time delays. The frequency domain solution of (2.1) for a two-conductor transmission line is

$$\begin{bmatrix} I_1 \\ I_2 \end{bmatrix} = \frac{1}{Z_0(1 - e^{-2\gamma l})} \begin{bmatrix} 1 + e^{-2\gamma l} & -2e^{-\gamma l} \\ -2e^{-\gamma l} & 1 + e^{-2\gamma l} \end{bmatrix} \begin{bmatrix} V_1 \\ V_2 \end{bmatrix} \quad (2.6a)$$

$$\gamma = \sqrt{(R + sL)(G + sC)} \quad (2.6b)$$

$$Z_0 = \sqrt{\frac{(R + sL)}{(G + sC)}} \quad (2.6c)$$

where γ is the propagation constant and Z_0 is the characteristic impedance. (2.6) can be further expressed as

$$V_1 = Z_0 I_1 + e^{-\gamma l} [2V_2 - e^{-\gamma l} (Z_0 I_1 + V_1)] \quad (2.7a)$$

$$V_2 = Z_0 I_2 + e^{-\gamma l} [2V_1 - e^{-\gamma l} (Z_0 I_2 + V_2)] \quad (2.7b)$$

Let us denote W_1 and W_2 as

$$W_1 = e^{-\gamma l} [2V_2 - e^{-\gamma l} (Z_0 I_1 + V_1)] \quad (2.8a)$$

$$W_2 = e^{-\gamma l} [2V_1 - e^{-\gamma l} (Z_0 I_2 + V_2)] \quad (2.8b)$$

After substituting (2.8) in (2.7),

$$V_1 = Z_0 I_1 + W_1 \quad (2.9a)$$

$$V_2 = Z_0 I_2 + W_2 \quad (2.9b)$$

Further substitution of (2.9) into (2.8) yields,

$$W_1 = e^{-\gamma l} [2V_2 - W_2] \quad (2.10a)$$

$$W_2 = e^{-\gamma l} [2V_1 - W_1] \quad (2.10b)$$

For a lossless transmission line, γ is purely imaginary and Z_0 is a real constant given by

$$\gamma = s\sqrt{LC} \quad Z_0 = \sqrt{\frac{L}{C}} \quad (2.11)$$

Equation (2.10) can be represented in time-domain by taking the Laplace inverse.

$$w_1(t + \tau) = 2v_2(t) - w_2(t) \quad (2.12a)$$

$$w_2(t + \tau) = 2v_1(t) - w_1(t) \quad (2.12b)$$

The circuit equivalent of (2.9) and (2.12) is shown in Figure 2.6.

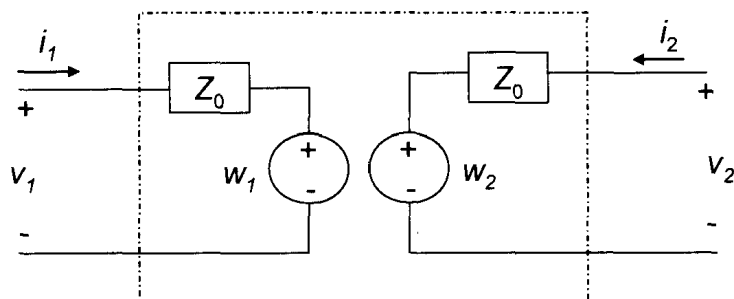


Figure 2.6: Circuit Equivalent of Method of Characteristics based transmission-line model

When the transmission line is lossy, γ is not purely imaginary and Z_0 is not a real constant and therefore a direct time domain representation is not possible. To overcome this situation, algorithms based on the generalized MoC use rational curve fitting to express Z_0 , W_1 , and W_2 in the time domain. For the case of multiconductor lines, the method of characteristics is applied through decoupling of transmission line equations [4]. The MoC macromodel can be shown to be passive for the case of lossless transmission lines; however, there is no guarantee of passivity for lossy transmission lines due to numerical curve fitting required to realize the macromodel [57]-[58].

2.2.3.3 – Exponential Padé-based Matrix-Rational Approximation

This algorithm converts the partial differential equations into time domain macromodels based on rational approximations of exponential matrices [25],[27]. The coefficients describing the discrete time-domain macromodel are computed using closed-form matrix rational approximation of exponential matrices and can be computed a priori.

This enables the development of transmission line macromodel analytically, in terms of predetermined (stored) constants and the given p.u.l. parameters. A brief description of the development of this macromodel is reviewed.

The exponential matrix e^Z in (2.2) can be expressed with a matrix rational approximation as

$$\mathbf{P}_M(\mathbf{Z})e^Z \approx \mathbf{Q}_N(\mathbf{Z}) \quad (2.13)$$

where $\mathbf{P}_M(\mathbf{Z}), \mathbf{Q}_N(\mathbf{Z})$ are polynomial matrices:

$$\mathbf{Q}_N(\mathbf{Z}) = \sum_{i=0}^N q_i \mathbf{Z}^i \quad \mathbf{P}_M(\mathbf{Z}) = \sum_{i=0}^N p_i \mathbf{Z}^i \quad (2.14)$$

After some mathematical manipulations, (2.13) can be translated into a macromodel represented by a set of ordinary differential equations, in a closed form in terms of the q_i and p_i coefficients and the p.u.l. parameters.

It can be proved that the matrix-rational approximation preserves the passivity of the reduced model [27] and can achieve better accuracy when compared to the conventional lumped segmentation model.

2.2.3.4 – Compact Finite-Differences Based Approximation

Compact Finite Differences can be used to convert Telegrapher's equation into ordinary differential equations [24]. Consider a two-conductor transmission line. The variations in space for the voltage $v(x,t)$ and current $i(x,t)$ expressed as

$$V(x, s) = \sum_{m=1}^P V_m(s) A_m(x) \quad (2.15a)$$

$$I(x, s) = \sum_{n=1}^Q I_n(s) B_n(x) \quad (2.15b)$$

where $A_m(x)$ and $B_n(x)$ are the known expansion functions and $I_n(s)$ and $V_m(s)$ are the unknown variables. It is to be assumed that the line is divided into M equal segments of length Δx . The unknown voltage $V(x, s)$ can be expressed in terms of node values at $x = k\Delta x$; where $k=0, 1, \dots, M$. The spatial derivatives of Telegrapher's equation are approximated using the following central difference operator as

$$\alpha_1 \frac{\partial f(x)}{\partial x} \Big|_{k+1} + \alpha_2 \frac{\partial f(x)}{\partial x} \Big|_k + \alpha_1 \frac{\partial f(x)}{\partial x} \Big|_{k-1} = \frac{f_{k+1/2} - f_{k-1/2}}{\Delta x} \quad (2.16)$$

Where $f(x)$ represents either $V(x)$ or $I(x)$, and k is the index node. The coefficients α_1 and α_2 are selected to obtain the desired truncation error criteria. The fourth order approximation is achieved as $\alpha_1 = 1/24$ and $\alpha_2 = 11/12$. Using (2.16) to discretize (2.1), results in

$$-\alpha_1 Z_{k+3/2} I_{k+3/2} - \alpha_2 Z_{k+1/2} I_{k+1/2} - \alpha_1 Z_{k-1/2} I_{k-1/2} = \frac{V_{k+1} - V_k}{\Delta x} \quad (2.17a)$$

$$k = 0, 1, \dots, M-2$$

$$-\alpha_1 Y_{k+1} V_{k+1} - \alpha_2 Y_k V_k - \alpha_1 Y_{k-1} V_{k-1} = \frac{I_{k+1/2} - I_{k-1/2}}{\Delta x} \quad (2.17b)$$

$$k = 0, 1, \dots, M-1$$

where $Z_k = Rk\Delta x + sLk\Delta x$ and $Y_k = Gk\Delta x + sCk\Delta x$. Using compact difference operators (2.17) can be expressed as ordinary differential equations.

Compact difference based on fourth order approximations achieve better accuracy with fewer variables when compared to the direct lumped segmentation approaches. Also the algorithm guarantees passivity of the macromodel by construction.

2.2.3.5 – Chebyshev Polynomials

A brief description of the macromodels obtained using Chebyshev polynomials is given here, a more detailed explanation is given in [11],[19]. For example, consider a two conductor transmission line. The variations in space for the voltage $v(x,t)$ and $i(x,t)$ current can be expressed in terms of Chebyshev polynomials as

$$v(x,t) = \sum_{n=0}^N a_n(t)T_n(x) \quad i(x,t) = \sum_{n=0}^N b_n(t)T_n(x) \quad (2.18)$$

where $T_n(x)$ is the n^{th} degree chebyshev polynomial. $a_n(t)$ and $b_n(t)$ are the unknown variables. The derivatives of the voltage and current with respect to x is given by

$$\frac{\partial}{\partial x} v(x,t) = \sum_{n=0}^N \hat{a}_n(t)T_n(x) \quad \frac{\partial}{\partial x} i(x,t) = \sum_{n=0}^N \hat{b}_n(t)T_n(x) \quad (2.19)$$

The relationship between $a_n(t)$ and $\hat{a}_n(t)$; $b_n(t)$ and $\hat{b}_n(t)$ are [11]

$$a_n(t) = \frac{1}{2n}(\hat{a}_{n-1}(t) - \hat{a}_{n+1}(t)) \quad b_n(t) = \frac{1}{2n}(\hat{b}_{n-1}(t) - \hat{b}_{n+1}(t)) \quad (2.20)$$

Using (2.18)-(2.20), and the orthogonal properties of the Chebyshev polynomials the Telegrapher's equations can be converted to ODEs.

The important feature of this algorithm is that the macromodel can be easily generated and extended for nonuniform transmission lines. This can be accomplished by expanding the line parameters in terms of chebyshev functions with respect to position x .

Chebyshev approximations are based on the order N in (2.18) and hence for higher orders it can achieve better accuracy when compared to the conventional lumped segmentation model and the compact difference macromodel which is based on the fourth order difference approximation. However, the algorithm does not guarantee the passivity of the resulting macromodel.

2.3 – Full Wave Simulation of Microwave Systems

High frequency microwave devices such as antennas, waveguides, filters, couplers and junctions are extremely complicated in geometrical structure and material properties. These devices are governed by PDEs such as the Maxwell's equations. The mathematical difficulties inherent in Maxwell's equation, the various cross-section geometries of conventional microwave devices, and the use of anisotropic, nonlinear, and lossy materials, considerably complicate the analysis of these devices. As operating frequencies increase, full wave methods which are based on the Maxwell's equation are essential in order to accurately predict high frequency electromagnetic behaviour of microwave devices. The FEM technique has now been a very popular approach for full wave electromagnetic modeling of high frequency microwave devices due to its accuracy, versatility and flexibility. However, the resulting system of equations after the FEM discretization is typically very large and cumbersome to solve. The computations of frequency responses of electromagnetic systems over a broad band require solving the large set of FEM systems repeatedly at many frequency points. Moreover, optimization process requires repeated simulation of the same problem for different design parameter

values. This can be computationally expensive. A brief review of the FEM formulation for the microwave systems is presented in the following section.

2.3.1 – FEM formulation of Microwave Systems

The FEM formulation begins with the discretization of the electric field vector wave equation

$$\nabla \times ([\mu_r]^{-1} \cdot \nabla \times \mathbf{E}) - k_0^2 [\varepsilon_r] \cdot \mathbf{E} = 0 \quad (2.21)$$

where $k_0^2 = \omega^2 \varepsilon_0 \mu_0$; ε_0 and μ_0 are the permittivity and permeability for the free space; ω is the angular frequency; $[\mu_r]$ and $[\varepsilon_r]$ are the relative permeability and permittivity tensors, respectively and \mathbf{E} is the electric field vector. For waveguide problems, on the conducting surfaces, the electric field satisfies the Dirichlet boundary condition as

$$\hat{n} \times \mathbf{E} = 0 \quad (2.22)$$

The boundary condition for the port i is given by [7]

$$\hat{n} \times \nabla \times \mathbf{E} + j\beta \hat{n} \times (\mathbf{E} \times \hat{n}) = -2j\beta \mathbf{E}^{inc} \text{ at } \Gamma_i \quad (2.23)$$

where β is the propagation constant of the dominant mode, Γ_i denotes the cross section of port i and \mathbf{E}^{inc} is the incident field. The propagation constant is given by $\beta = (\omega^2 \varepsilon_0 \mu_0 - k_i^2)^{1/2}$. For rectangular waveguides, $k_i^2 = ((m\pi/a)^2 - (n\pi/b)^2)$; where a , b are the width and height of the waveguide; m , n represents the mode numbers of the transverse electric or magnetic waves propagating through a waveguide. For waveguides of non-rectangular cross section k_i^2 can be obtained numerically.

The functional for the boundary value problem defined above in accordance with the general variational principle [7] is given by

$$F(\mathbf{E}) = \frac{1}{2} \iiint_V [(\nabla \times \mathbf{E}) \cdot [\boldsymbol{\mu}_r]^{-1} \cdot (\nabla \times \mathbf{E}) - k_0^2 \mathbf{E} \cdot [\boldsymbol{\varepsilon}_r] \cdot \mathbf{E}] dV + \sum_{i=1}^p \left\{ \iint_{\Gamma_i} \left[\frac{j\beta}{2} (\hat{\mathbf{n}} \times \mathbf{E}) \cdot (\hat{\mathbf{n}} \times \mathbf{E}) - 2j\beta \mathbf{E} \cdot \mathbf{E}^{inc} \right] dS \right\} \quad (2.24)$$

where p is the total number of ports. The FEM discretization of (2.24) when there is a finite conductivity using vector basis functions yields a matrix equation which can be expressed as

$$(\mathbf{A}_0 + \mathbf{A}_1 s + \mathbf{A}_2 s^2 + \mathbf{A}_3 j\beta(s)) \mathbf{e}_s = j\beta(s) \mathbf{b} \quad (2.25)$$

where $s=j\omega$ is the Laplace frequency variable; the propagation constant is expressed as $\beta(s)$ to emphasize that it is a function of frequency; the elements of the matrices \mathbf{A}_0 , \mathbf{A}_1 , \mathbf{A}_2 , \mathbf{A}_3 , and \mathbf{b} are given by

$$A_{0,ij} = \iiint_V \frac{1}{\boldsymbol{\mu}} \nabla \times \mathbf{N}_i \cdot \nabla \times \mathbf{N}_j dV \quad (2.26)$$

$$A_{1,ij} = \iiint_V \sigma \mathbf{N}_i \cdot \mathbf{N}_j dV \quad (2.27)$$

$$A_{2,ij} = \iiint_V \boldsymbol{\varepsilon} \mathbf{N}_i \cdot \mathbf{N}_j dV \quad (2.28)$$

$$A_{3,ij} = \iint_S \mathbf{S}_i \cdot \mathbf{S}_j dS \quad (2.29)$$

$$b_i = -2 \iint_S \mathbf{S}_i \cdot (\mathbf{E}^{inc} \times \hat{\mathbf{n}}) dS \quad (2.30)$$

where \mathbf{S}_i denote the vector basis functions. Also $\mathbf{S}_i = \hat{\mathbf{n}} \times \mathbf{N}_i$, where \mathbf{N}_i are the vector basis functions that have a unit tangential component at edge i ; $\mathbf{A}_0 \in \mathfrak{R}^{N \times N}$, $\mathbf{A}_1 \in \mathfrak{R}^{N \times N}$, $\mathbf{A}_2 \in \mathfrak{R}^{N \times N}$ and $\mathbf{A}_3 \in \mathfrak{R}^{N \times N}$ are the sparse matrices obtained through the finite element

formulation; $\mathbf{e}_s \in \mathfrak{R}^N$ is the vector of unknown variables in the approximation of \mathbf{E} ; $\mathbf{b} \in \mathfrak{R}^N$ is the known vector determined from the incident field and N is the total number of variables in the FEM formulation.

When there is no finite conductivity, equation (2.25) can be further simplified as

$$\left(\tilde{\mathbf{A}}_0 + \tilde{\mathbf{A}}_1 k + \tilde{\mathbf{A}}_2 k^2\right) \mathbf{e}_k = \mathbf{kb} \quad (2.31)$$

where $\mathbf{e}_k \in \mathfrak{R}^N$ is the vector of unknown variables in the approximation of \mathbf{E} and $k = j\beta(s)$.

The matrices $\tilde{\mathbf{A}}_0$, $\tilde{\mathbf{A}}_1$, and $\tilde{\mathbf{A}}_2$ are derived using the system matrices in (2.25) as

$$\tilde{\mathbf{A}}_0 = \mathbf{A}_0 - (k_i^2 / \varepsilon_0 \mu_0) \mathbf{A}_2 \quad (2.32)$$

$$\tilde{\mathbf{A}}_1 = \mathbf{A}_3 \quad (2.33)$$

$$\tilde{\mathbf{A}}_2 = (1 / \varepsilon_0 \mu_0) \mathbf{A}_2 \quad (2.34)$$

The calculation of S -parameters over a broad spectrum requires the solution of (2.25) or (2.31) at many frequency points. Such calculations can be very time consuming since the solution of (2.25) or (2.31) at a given frequency point requires inverting a matrix that is typically formed by tens or even hundred of thousands of finite element equations. Krylov subspace based MOR techniques provide a mechanism to generate reduced order models from the detailed FEM description. However, a new reduced order model is required each time a parameter is modified in the studied structure resulting in significant overhead when performing common design steps such optimization and design space exploration. Furthermore, the general form of the discretization of vector wave equation is incompatible with Krylov subspace based MOR methods. Equation (2.25) and (2.31) exhibit both linear and quadratic dependence with respect to s and k respectively;

whereas Krylov subspace methods require linear dependency of s and k respectively in the discrete model. In addition, the presence of the frequency dependent propagation constant $\beta(s)$ in (2.25) further hinders the application of the Krylov MOR techniques to these problems.

The following section discusses the MOR techniques as originally proposed for reduction of large interconnect networks in the circuit area and the difficulties involved in applying the traditional MOR methods to full wave FEM problems are also described.

2.4 – Simulation Techniques based on Model Order Reduction (MOR)

A large linear system usually has a many number of poles, however only a small percentage of these poles are dominant. By capturing only the dominant poles, MOR techniques are able to convert a large system into a much smaller system while still maintaining the accuracy of the original solution. This significantly reduces the CPU expense of the simulations without compromising accuracy.

The general form of the circuit equations comprising of distributed transmission lines as in (2.4) consists of matrices \mathbf{G}_π and \mathbf{C}_π which are very large. Also, the matrix form resulting from the full wave FEM formulation as in (2.25) and (2.31) consists of matrices \mathbf{A}_0 , \mathbf{A}_1 , \mathbf{A}_2 and \mathbf{A}_3 which are very large too. In general, both distributed transmission lines and full wave FEM problems leads to very large systems of equations that are required to be solved repeatedly many times at different parameter values.

In order to address these computational complexities, MOR methods were originally proposed to reduce large interconnect networks in circuit simulation [13],[15],[16][18], [20]-[24], [30]-[32]. The encouraging results of these methods in the circuit simulation area have prompted interest in their application to FEM based full wave problems [41]-[53].

MOR techniques are broadly classified as

1. Approaches based on explicit moment matching based on direct Padé approximants [13],[15],[16]and
2. Implicit moment matching based on projecting large matrices on its dominant eigenspace [18],[20]-[24],[32].

The following two subsections reviews the mathematical implementation of these two types of MOR approaches.

2.4.1 – Explicit Moment Matching Based MOR

Explicit moment matching techniques [5] use direct Padé approximants to capture the frequency impulse response of networks. Consider a single-input single-output linear system and let $H(s)$ be the transfer function. $H(s)$ can be expressed using Taylor series expansion as

$$H(s) \approx m_0 + m_1s + m_2s^2 + \dots \quad (2.35)$$

where m_i is referred to as the i^{th} moment of $H(s)$. In order to form a reduced order model, the series expansion of (2.35) is converted to a rational function using a Padé approximation as

$$H(s) \approx m_0 + m_1 s + m_2 s^2 + \dots + m_{N+L-1} s^{N+L-1} \approx \frac{a_0 + a_1 s + \dots + a_L s^L}{1 + b_1 s + \dots + b_N s^N} \quad (2.36)$$

The coefficients a_i and b_i are obtained by cross-multiplying the denominator of (2.36) and matching equal powers of s , as

$$\begin{bmatrix} m_{L-M+1} & m_{L-M+2} & m_{L-M+3} & \cdots & m_L \\ m_{L-M+2} & m_{L-M+3} & m_{L-M+4} & \cdots & m_{L+1} \\ m_{L-M+3} & m_{L-M+4} & m_{L-M+5} & \cdots & m_{L+2} \\ \vdots & \vdots & \vdots & \ddots & \vdots \\ m_L & m_{L+1} & m_{L+2} & \cdots & m_{N+L-1} \end{bmatrix} \begin{bmatrix} b_N \\ b_{N-1} \\ b_{N-2} \\ \vdots \\ b_1 \end{bmatrix} = \begin{bmatrix} m_{L+1} \\ m_{L+2} \\ m_{L+3} \\ \vdots \\ m_{L+N} \end{bmatrix} \quad (2.37)$$

$$\begin{aligned} a_0 &= m_0 \\ a_1 &= m_1 + b_1 m_0 \\ &\dots \\ a_L &= m_L + \sum_{i=1}^{\min(L,N)} b_i m_{L-i} \end{aligned} \quad (2.38)$$

To generate a reduced order model, the moments of the network need to be computed. Consider the system in (2.4) for the case of a linear network expressed in Laplace domain as

$$(\mathbf{G}_\pi + s\mathbf{C}_\pi)\mathbf{X}_\pi(s) = \mathbf{b}_\pi \quad (2.39)$$

After multiplying by \mathbf{G}_π^{-1} ,

$$(\mathbf{I}_\pi - s\mathbf{A}_\pi)\mathbf{X}_\pi(s) = \mathbf{R}_\pi \quad (2.40)$$

where \mathbf{I}_π is the identity matrix and

$$\mathbf{A}_\pi = -\mathbf{G}_\pi^{-1}\mathbf{C}_\pi \quad \mathbf{R}_\pi = \mathbf{G}_\pi^{-1}\mathbf{B}_\pi \quad (2.41)$$

Replacing the $X_\pi(s)$ with a Taylor series expansion, yields

$$(\mathbf{I}_\pi - s\mathbf{A}_\pi)(\mathbf{M}_0 + \mathbf{M}_1s + \mathbf{M}_2s^2 + \dots) = \mathbf{R}_\pi \quad (2.42)$$

Now, equating the coefficients of similar powers of s on both sides of (2.42), gives

$$\mathbf{M}_0 = \mathbf{R}_\pi \quad (2.43a)$$

$$\mathbf{M}_i = -\mathbf{A}_\pi \mathbf{M}_{i-1} \quad ; i > 0 \quad (2.43b)$$

Equation (2.43) gives a closed form relationship for the computation of moments \mathbf{M}_i .

Finally, for a specific output node of interest, the moments are converted to a rational function as described by (2.36)-(2.38). As shown from (2.41)-(2.43), only one matrix inversion is required to compute the moment. This significantly reduces the simulation time of linear circuits which require many matrix inversions at each frequency or time point.

Explicit moment matching techniques such as these based on single Padé expansion is referred to as asymptotic waveform evaluation (AWE) [13],[42],[43]. However, in general if the rational approximation contains more than eight poles, a single Padé expansion can produce an inaccurate result since (2.37) becomes ill-conditioned as the order of the Padé approximation increases. In addition, Padé approximants may produce unstable poles and provide no estimates for error bounds. Another difficulty with explicit moment matching techniques is that there is no guarantee that the reduced order model is passive.

2.4.2 – Implicit Moment Matching Based MOR

Implicit moment matching techniques use Krylov subspace approaches to project large matrices on its dominant eigenspace [18]. Krylov subspace methods require linear frequency dependence in the system and its application has found great success for reducing large linear networks in circuit simulation research area [20]-[24]. In order to explain the concept of implicit moment matching techniques, consider a linear system in (2.40). Krylov subspace techniques aim to approximate A_π with a reduced matrix that preserves the leading eigenvalues (those with the largest magnitude). This is performed by calculating the moments of the system to create the following matrix \mathbf{K} .

$$\mathbf{K} = [\mathbf{M}_0 \quad \mathbf{M}_1 \quad \mathbf{M}_2 \quad \dots \quad \mathbf{M}_{q-1}] \quad (2.44)$$

Using (2.43),

$$\mathbf{K} = [\mathbf{R}_\pi \quad \mathbf{R}_\pi \mathbf{A}_\pi \quad \mathbf{R}_\pi \mathbf{A}_\pi^2 \quad \mathbf{R}_\pi \mathbf{A}_\pi^3 \quad \dots \quad \mathbf{R}_\pi \mathbf{A}_\pi^{q-1}]; \quad \mathbf{K} \in \mathfrak{R}^{\pi \times k} \quad (2.45)$$

where π is the size of the original network, k is the number of columns in \mathbf{K} defined as $k = qN_p$, and N_p denotes the number of ports. The matrix \mathbf{K} formed by the moments is an ill-conditioned matrix and therefore the first step in Krylov MOR is to construct a well conditioned orthonormal matrix \mathbf{Q} such that

$$\text{colspan}(\mathbf{Q}) = \text{colspan}(\mathbf{K}) \quad (2.46a)$$

$$\mathbf{Q}^T \mathbf{Q} = \mathbf{I}_k \quad (2.46b)$$

The orthonormal matrix \mathbf{Q} is generated by making use of a numerically well conditioned algorithm say the Arnoldi technique [76] which exploits the nice relationship between

successive moments in (2.45). The orthonormal bases \mathbf{Q} of the generated Krylov subspace contains the eigen vectors corresponding to the leading eigenvalues of the \mathbf{A}_π matrix. The next step is to use the matrix \mathbf{Q} to perform congruence transformation and generate the reduced system. This is done by pre-multiplying \mathbf{Q}^T on both sides of (2.39) and performing a change of variables in (2.39) as

$$\mathbf{X}_\pi = \mathbf{Q}\mathbf{Z}_k \quad (2.47)$$

where \mathbf{Z}_k is the reduced order system variable. This results in the following reduced system given by

$$(\hat{\mathbf{G}}_k + s\hat{\mathbf{C}}_k)\mathbf{Z}_k(s) = \hat{\mathbf{b}}_k \quad (2.48)$$

where the reduced matrices are given by

$$\hat{\mathbf{G}}_k = \mathbf{Q}^T \mathbf{G}_\pi \mathbf{Q} \quad \hat{\mathbf{C}}_k = \mathbf{Q}^T \mathbf{C}_\pi \mathbf{Q} \quad \hat{\mathbf{b}}_k = \mathbf{Q}^T \mathbf{b}_\pi \quad (2.49)$$

Here $\mathbf{Q} \in \mathbb{R}^{\pi \times k}$, $\mathbf{X}_\pi \in \mathbb{R}^{\pi \times 1}$, $\mathbf{Z}_k \in \mathbb{R}^{k \times 1}$, $\mathbf{G}_\pi \in \mathbb{R}^{\pi \times \pi}$, $\mathbf{C}_\pi \in \mathbb{R}^{\pi \times \pi}$, $\mathbf{b}_\pi \in \mathbb{R}^{\pi \times 1}$ and the dimensions of the reduced matrix are $\hat{\mathbf{G}}_k \in \mathbb{R}^{k \times k}$, $\hat{\mathbf{C}}_k \in \mathbb{R}^{k \times k}$, $\hat{\mathbf{b}}_k \in \mathbb{R}^{k \times 1}$ where π is the original number of unknowns and k is the reduced number of unknowns. It is to be noted that $k \ll \pi$. The response of the reduced system is obtained by (2.48) and is transformed to the original system using (2.47).

The traditional way of constructing the orthonormal matrix is using the Modified Gram Schmidt algorithm. This technique explicitly calculates the moment vectors and can lead to numerically inaccurate results due to the fact that higher order moments tend to be parallel. To obtain numerically accurate results, the Arnoldi process [76] is used which takes advantage of the recursive relationship between the moments and enables the

computation of the moments in an implicit fashion. The basic steps involved in the Arnoldi process for multi-port systems which requires a complex frequency expansion point is shown in Figure 2.7.

(Block Arnoldi Algorithm)

```

arnoldi ( input  $\mathbf{G}, \mathbf{C}, \mathbf{B}, s_0$ ; output  $\mathbf{Q}$  )
{
   $\mathbf{M} = (\mathbf{G} + s_0 \mathbf{C})^{-1}$ 
   $\mathbf{R} = \mathbf{M}\mathbf{B}$ 
   $z_0 = \mathbf{R}$ 
   $[\mathbf{Q}_0, \mathfrak{R}] = qr(\text{Real}(z_0) \text{ Imag}(z_0))$ 
  For  $j \leftarrow 1$  to  $k$ 
     $z_j = -\mathbf{M}\mathbf{C}q_{j-1}$ 
    For  $i \leftarrow 0$  to  $j-1$ 
       $\mathbf{h} \leftarrow q_i^T z_j$ 
       $z_j \leftarrow z_j - q_i \mathbf{h}$ 
    End
     $[\mathbf{Q}_j, \mathfrak{R}] = qr(\text{Real}(z_j) \text{ Imag}(z_j))$ 
  End
   $\mathbf{Q} = [\mathbf{Q}_0 \ \mathbf{Q}_1 \ \mathbf{Q}_2 \ \mathbf{Q}_3 \ \dots \ \mathbf{Q}_k]$ 
  Return ( $\mathbf{Q}$ )
}

```

Figure 2.7: Block Arnoldi Algorithm for expansion about a complex frequency point $s = s_0$

Here qr refers to the modified Gram-Schmidt orthonormalization procedure. This is used to orthonormalize the real and imaginary parts of the complex vector z_j . In each iteration, $j \in [1, k]$, the algorithm generates p columns of the matrix \mathbf{z} , where p is the number of ports. The point of expansion is a complex frequency and therefore each p^{th} column in itself is a block with real and imaginary parts of the complex vector. The inner for loop in the algorithm is a block orthogonalization procedure that orthogonalizes the new matrix

block generated at every i^{th} iteration with respect to all the previous block matrices $z_0, z_1, z_2, \dots, z_j$. The net result of the algorithm is that it generates the orthonormal matrix Q which can be used to obtain the reduced system by means of congruence transformation.

The application of the Krylov subspace methods has been very successful for the reduction of large interconnect networks. However there are certain challenges when one considers applying these methods to FEM based full wave problems.

2.4.3 – Challenges in Traditional MOR Application to Full Wave FEM

While implicit moment matching techniques such as the Krylov subspace methods produce an efficient and accurate reduced model, these techniques suffer from a major drawback when applied to optimization and design space problems of full wave FEM analysis. This is due to the fact that the reduced order models obtained using the current techniques would no longer be valid when a design parameter is modified. Hence using traditional MOR techniques, a new reduced order model is required each time a parameter is modified in the studied structure which means that MOR process has to be repeated each time a parameter is varied. This is a computationally intensive task when performing optimization problems.

Another major challenge with applying Krylov subspace based reduction to FEM based microwave applications, is that the matrix equations resulting from the

conventional FEM discretization of the vector wave equation exhibits linear, quadratic and complex frequency dependence (due to frequency dependent material properties and frequency dependent boundary conditions); however, Krylov-based MOR requires only a linear frequency dependence in the matrix form of the discrete electromagnetic problem [49]. This limits the direct application of Krylov subspace MOR methods to these problems. One way to make the full wave FEM problems Krylov compatible is to use techniques [51]-[53] that convert the conventional FEM equations into a linear first order system by including extra unknown variables in the system. However, these methods have the effect of doubling the size of the original system. Furthermore, they do not have the flexibility to handle complex frequency dependence which is introduced due to frequency dependent material properties and frequency dependent boundary conditions.

Another alternative FEM formulation for electromagnetic problems is based on the discretization of Maxwell's equations. Its matrix form exhibits a linear dependence in frequency and hence this approach is directly compatible with Krylov subspace methods [46],[48],[49]. However, approaches based on the discretization of Maxwell's equations include both the electric and magnetic field components in the electromagnetic system. This also has the impact of almost doubling the size of the system which is to be reduced.

Chapter 3

Development of a Passive Macromodeling Algorithm for Lossy Multiconductor Interconnects

3.1 – Introduction

In this chapter a new general-purpose passive macromodel based on the direct discretization of transmission line equations is described using a high order FEM approximation. A significant amount of research has been done in literature to address the simulation of transmission lines in the presence of nonlinear element by developing transmission line macromodels [21]-[27]. Among these methods, macromodels based on the direct discretization of transmission line equations such as the pseudospectral methods (chebyshev polynomials) [19], and compact finite differences [24] have been proposed. The key advantage of these methods is the simplicity of the construction of

their SPICE models. This simplicity can also deal with the passivity of the macromodel in a straightforward manner by ensuring the equivalent circuit representations of the p.u.l. impedance matrix $\mathbf{R}(s)+s\mathbf{L}(s)$ and admittance matrix $\mathbf{G}(s)+s\mathbf{C}(s)$ are passive. Methods based on the Chebyshev polynomials provide higher order accuracy but do not guarantee the passivity of the macromodel. Methods based on the compact difference approximation provide fourth-order accuracy, however, extending these methods to higher orders while preserving the passivity of macromodel is a challenging task. The formulation of the proposed macromodel is based on a sixth order FEM approximation and ensures the passivity of the macromodel. In addition, the method can be generalized to higher orders finite element approximations. The proposed model is suitable for inclusion in general-purpose circuit simulators and overcomes the mixed frequency/time simulation difficulties encountered during the transient analysis. The key features of the algorithm are: the macromodel can be formulated analytically in terms of predetermined coefficients and the p.u.l. parameters; the passivity of the macromodel can be guaranteed by construction; the macromodel can be used to model interconnects with frequency dependent p.u.l. parameters and can be incorporated with passive model order reduction techniques.

The organisation of the chapter is as follows. A review of the transmission line equations and the development of the proposed macromodel are described in section 3.2. Section 3.3 specifies the necessary conditions to ensure passivity for the proposed macromodel. Section 3.4 describes the behaviour of the frequency dependent p.u.l. parameters and provides a scheme to model frequency dependent parameters in the proposed macromodel. The time domain macromodel implementation using circuit

realizations is described in section 3.5. Numerical examples showing the validity of the proposed sixth order FEM based macromodel are provided in section 3.6.

3.2 – Development of the Proposed Macromodel

Transmission lines are governed by Telegrapher's equations which can be expressed in the Laplace domain as

$$\partial V(x, s) / \partial x = -(\mathbf{R} + s\mathbf{L})\mathbf{I}(x, s) \quad \partial \mathbf{I}(x, s) / \partial x = -(\mathbf{G} + s\mathbf{C})\mathbf{V}(x, s) \quad (3.1)$$

where s is the Laplace transform variable; x is the position variable; \mathbf{R} , \mathbf{L} , \mathbf{G} and $\mathbf{C} \in \mathfrak{R}^{\phi \times \phi}$ are the p.u.l. parameters of the transmission line, and are nonnegative definite symmetric matrices [4]. $\mathbf{V}(x, s)$ and $\mathbf{I}(x, s) \in \mathfrak{R}^{\phi}$ represent the voltage and current vector, respectively, for $\phi+1$ conductor lines (ϕ signal conductors with one reference line).

Among classical numerical techniques, FEM is widely used to numerically solve transmission lines which are based on partial differential equations [4]. However in [4], transmission lines models are based on low order finite element approximations. This section describes how a high order FEM can be used to derive an efficient and passive macromodel for transmission lines. FEM divides the line into a finite number of elements and the transmission line voltages and currents along each element are approximated by means of known basis functions. For ease of presentation and without loss of generality consider a 2-conductor transmission line. The e^{th} element shown in Figure. 3.1 can be described as

$$V^e(x, s) = \sum_{i=0}^M N_i^e(x) V_i^e(x, s) \quad I^e(x, s) = \sum_{i=0}^M N_i^e(x) I_i^e(x, s) \quad (3.2)$$

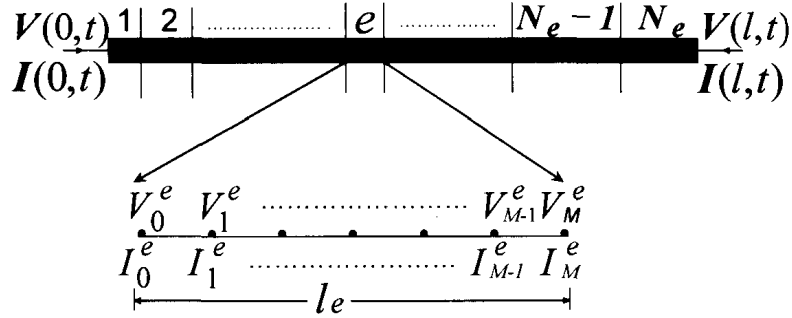


Figure 3.1: M^h Order Finite Element Discretization of Interconnect

where M is the order of the finite element approximation, $V_i^e(x,s)$ and $I_i^e(x,s)$ are the voltage and current node variables illustrated in Figure. 3.1. The nodes of each element, say $[x_i, i = 0, \dots, M]$ are uniformly spaced and the finite element basis function $N_i^e(x)$ has a value of one at the node $x = x_i$ and a zero value at all the other nodes. These basis functions are derived based on an M^{th} order generating polynomial for an M^{th} order finite element approximation as [6]

$$N_i(x) = \frac{\prod_{j=0, j \neq i}^M (x - x_j)}{\prod_{j=0, j \neq i}^M (x_i - x_j)} \quad (3.3)$$

Substituting (3.2) into Telegrapher's equation in (3.1), we can formulate the weak form using weighted residual methods such as the Galerkin formulation as

$$\int_0^{l_e} \left(\sum_{j=0}^M N_j^e(x) \frac{\partial N_i^e(x)}{\partial x} V_i^e(x,s) \right) dx = -(R + sL) \int_0^{l_e} \left(\sum_{j=0}^M N_j^e(x) N_i^e(x) I_j^e(x,s) \right) dx \quad (3.4)$$

$$\int_0^{l_e} \left(\sum_{j=0}^M N_j^e(x) \frac{\partial N_i^e(x)}{\partial x} I_i^e(x,s) \right) dx = -(G + sC) \int_0^{l_e} \left(\sum_{j=0}^M N_j^e(x) N_i^e(x) V_j^e(x,s) \right) dx \quad (3.5)$$

where $j = [0, \dots, M]$; $N_i^e(x)$ and $N_j^e(x)$ are the basis functions of the finite element for node i and j ; l_e is the length of the finite element.

In order to better understand the development of FEM macromodel, let us consider a simple example in Figure 3.2 to illustrate the basic concept using a first order FEM element. Then the method is generalized to high order finite element approximations.

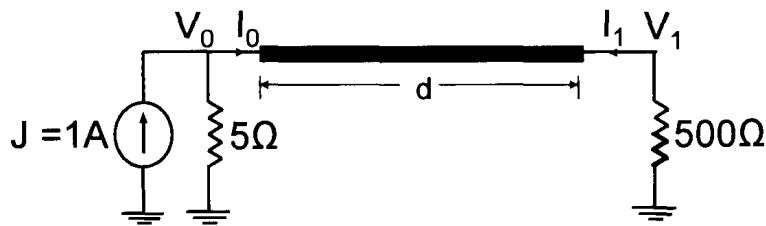


Figure 3.2: An interconnect circuit for illustrating the FEM macromodel

The first order element consists of two nodes (say x_0 and x_1), the voltages and currents at the two end nodes are denoted by (V_0, I_0) and (V_1, I_1) respectively. For the case when $M=1$, the first order basis functions $N_0^e(x)$ and $N_1^e(x)$ for nodes x_0 and x_1 of the e^{th} element can be obtained from (3.3) as

$$N_0(x) = \frac{(x-x_1)}{(x_0-x_1)}; \quad N_1(x) = \frac{(x-x_0)}{(x_1-x_0)} \quad (3.6)$$

The set of equations given by (3.4) and (3.5) for $M=1$ is solved using (3.6) to obtain the FEM matrix system for one first order element as

$$\begin{bmatrix} -1/2 & 1/2 \\ -1/2 & 1/2 \end{bmatrix} \begin{bmatrix} V_0 \\ V_1 \end{bmatrix} + \begin{bmatrix} Zd/3 & Zd/6 \\ Zd/6 & Zd/3 \end{bmatrix} \begin{bmatrix} I_0 \\ I_1 \end{bmatrix} = \begin{bmatrix} 0 \\ 0 \end{bmatrix} \quad (3.7a)$$

$$\begin{bmatrix} -1/2 & 1/2 \\ -1/2 & 1/2 \end{bmatrix} \begin{bmatrix} I_0 \\ I_1 \end{bmatrix} + \begin{bmatrix} Yd/3 & Yd/6 \\ Yd/6 & Yd/3 \end{bmatrix} \begin{bmatrix} V_0 \\ V_1 \end{bmatrix} = \begin{bmatrix} 0 \\ 0 \end{bmatrix} \quad (3.7c)$$

$$(3.7d)$$

where $Z = R + sL$, $Y = G + sC$ and d is the length of the element.

The Boundary Conditions (B.C) for the network in Figure 3.2 are given as

$$J = V_0 (1/5) + I_0 \quad (3.8a)$$

$$V_1 (1/500) + I_1 = 0 \quad (3.8b)$$

The traditional approach to solve the problem of Figure 3.2 governed by (3.7)-(3.8) is to eliminate two FEM equations out of the four equations in (3.7) by imposing the B.C in (3.8). One way of performing this is to use (3.7a) and (3.7c) along with the B.C to yield a system as

$$\begin{bmatrix} -1/2 & 1/2 \\ Zd/3 & Zd/6 \\ 1 & 0 \\ 0 & 1 \end{bmatrix} \begin{bmatrix} I_0 \\ I_1 \end{bmatrix} + \begin{bmatrix} Yd/3 & Yd/6 \\ -1/2 & 1/2 \\ 1/5 & 0 \\ 0 & 1/500 \end{bmatrix} \begin{bmatrix} V_0 \\ V_1 \end{bmatrix} = \begin{bmatrix} 0 \\ 0 \\ J \\ 0 \end{bmatrix} \quad (3.9)$$

Another way of performing this is to use (3.7b) and (3.7d) along with the B.C to result in a system as

$$\begin{bmatrix} -1/2 & 1/2 \\ Zd/6 & Zd/3 \\ 1 & 0 \\ 0 & 1 \end{bmatrix} \begin{bmatrix} I_0 \\ I_1 \end{bmatrix} + \begin{bmatrix} Yd/6 & Yd/3 \\ -1/2 & 1/2 \\ 1/5 & 0 \\ 0 & 1/500 \end{bmatrix} \begin{bmatrix} V_0 \\ V_1 \end{bmatrix} = \begin{bmatrix} 0 \\ 0 \\ J \\ 0 \end{bmatrix} \quad (3.10)$$

As an alternative approach to solve the network of Figure 3.2 which gives more accurate results, one can combine the equations in (3.7a)-(3.7b) and (3.7c)-(3.7d) and use those two equations along with the B.C. This can be accomplished by performing a transformation on (3.7a)-(3.7b) using a transformation matrix W_t as

$$W_t \begin{bmatrix} -1/2 & 1/2 \\ -1/2 & 1/2 \end{bmatrix} \begin{bmatrix} I_0 \\ I_1 \end{bmatrix} + W_t \begin{bmatrix} Yd/3 & Yd/6 \\ Yd/6 & Yd/3 \end{bmatrix} \begin{bmatrix} V_0 \\ V_1 \end{bmatrix} = \begin{bmatrix} 0 \\ 0 \end{bmatrix} \quad (3.11)$$

where $W_t = [1 \ 1]$ and (3.11) can be expressed as

$$[-1 \ 1] \begin{bmatrix} I_0 \\ I_1 \end{bmatrix} + [Yd/2 \ Yd/2] \begin{bmatrix} V_0 \\ V_1 \end{bmatrix} = \begin{bmatrix} 0 \\ 0 \end{bmatrix} \quad (3.12)$$

Similarly, performing a transformation on (3.7c)-(3.7d) using $W_t = [1 \ 1]$ as

$$W_t \begin{bmatrix} -1/2 & 1/2 \\ -1/2 & 1/2 \end{bmatrix} \begin{bmatrix} V_0 \\ V_1 \end{bmatrix} + W_t \begin{bmatrix} Zd/3 & Zd/6 \\ Zd/6 & Zd/3 \end{bmatrix} \begin{bmatrix} I_0 \\ I_1 \end{bmatrix} = \begin{bmatrix} 0 \\ 0 \end{bmatrix} \quad (3.13)$$

$$[-1 \ 1] \begin{bmatrix} V_0 \\ V_1 \end{bmatrix} + [Zd/2 \ Zd/2] \begin{bmatrix} I_0 \\ I_1 \end{bmatrix} = \begin{bmatrix} 0 \\ 0 \end{bmatrix} \quad (3.14)$$

Using (3.12) and (3.14) along with the B.C one can solve the problem as

$$\begin{bmatrix} -1 & 1 \\ Zd/2 & Zd/2 \\ 1 & 0 \\ 0 & 1 \end{bmatrix} \begin{bmatrix} I_0 \\ I_1 \end{bmatrix} + \begin{bmatrix} Yd/2 & Yd/2 \\ -1 & 1 \\ 1/5 & 0 \\ 0 & 1/500 \end{bmatrix} \begin{bmatrix} V_0 \\ V_1 \end{bmatrix} = \begin{bmatrix} 0 \\ 0 \\ J \\ 0 \end{bmatrix} \quad (3.15)$$

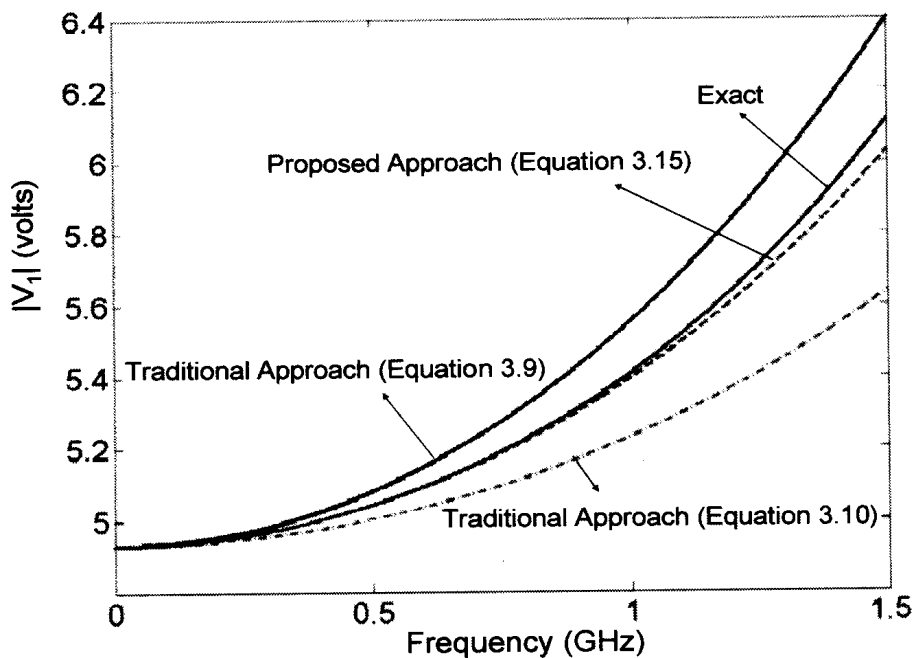


Figure 3.3: Frequency response comparison for circuit in Figure 3.2 for $d= 1\text{cm}$ using first order FEM approaches

It was observed that the approach of (3.15) achieved better accuracy when compared to the traditional approach of (3.9) and (3.10). Hence the proposed method took advantage of this technique in order to improve the accuracy of the FEM macromodel. Figure 3.3 shows the frequency response comparison between the traditional and proposed approaches of imposing B.C of the output voltage (V_1) for the circuit in Figure 3.2 which has a line length of $d=1$ cm and the interconnect per unit length parameters as $R= 1.93 \Omega/\text{cm}$, $G= 79e^{-9} \text{ S/cm}$; $L=2.97 \text{ nH/cm}$ and $C= 1.61 \text{ pF/cm}$. As seen from Figure 3.3, the errors in the traditional approach of (3.9) and (3.10) are large with respect to the exact solution obtained using transmission line stamp and are also almost equal in magnitude and opposite in direction. Hence in the proposed approach of combining the equations, the errors get cancelled and one achieves an accurate solution. As a result, the proposed method of handling B.C is more accurate when compared to traditional techniques.

A similar approach can be performed to obtain a high order (say sixth order) FEM system starting from the set of equations given by (3.4) and (3.5) and using sixth order generating polynomials as basis functions to derive the following system

$$\begin{bmatrix} \mathbf{A}_x & z\mathbf{B}_x \\ y\mathbf{B}_x & \mathbf{A}_x \end{bmatrix} \begin{bmatrix} \mathbf{V}_x^e \\ \mathbf{I}_x^e \end{bmatrix} = \begin{bmatrix} \mathbf{0} \\ \mathbf{0} \end{bmatrix} \quad (3.16)$$

$$\mathbf{V}_x^e = [V_0^e \quad V_1^e \quad V_2^e \quad V_3^e \quad V_4^e \quad V_5^e \quad V_6^e]^T \quad (3.17a)$$

$$\mathbf{I}_x^e = [I_0^e \quad I_1^e \quad I_2^e \quad I_3^e \quad I_4^e \quad I_5^e \quad I_6^e]^T \quad (3.17b)$$

$$A_x = \begin{bmatrix} -1 & 1776 & -5151 & 3967 & -732 & 267 & -587 \\ 2 & 1925 & 6160 & 5775 & 1925 & 1925 & 18480 \\ -1776 & 0 & 3078 & -2136 & 243 & -648 & 267 \\ \hline 1925 & 0 & 1925 & 1925 & 385 & 1925 & 1925 \\ 5151 & -3078 & 87 & -3807 & 243 & -732 & \\ \hline 6160 & 1925 & 0 & 77 & 6160 & 385 & 1925 \\ -3967 & 2136 & -87 & 0 & 87 & -2136 & 3967 \\ \hline 5775 & 1925 & 77 & 0 & 77 & 1925 & 5775 \\ 732 & -243 & 3807 & -87 & 0 & 3078 & -5151 \\ \hline 1925 & 385 & 6160 & 77 & 0 & 1925 & 6160 \\ -267 & 648 & -243 & 2136 & -3078 & 0 & 1776 \\ \hline 1925 & 1925 & 385 & 1925 & 1925 & 0 & 1925 \\ 587 & -267 & 732 & -3967 & 5151 & -1776 & 1 \\ \hline 18480 & 1925 & 1925 & 5775 & 6160 & 1925 & 2 \end{bmatrix} \quad (3.18)$$

$$B_x = \begin{bmatrix} 90269 & 42087 & 84855 & 10237 & 17175 & 3867 & 10237 \\ 3003 & 1001 & 2002 & 3003 & 1001 & 1001 & 6006 \\ 42087 & 258768 & 122175 & 113760 & 73035 & 34128 & 3867 \\ \hline 1001 & 1001 & 1001 & 1001 & 1001 & 1001 & 1001 \\ 84855 & 122175 & 327375 & 161550 & 242325 & 73035 & 17175 \\ \hline 2002 & 1001 & 1001 & 1001 & 2002 & 1001 & 1001 \\ 102370 & 113760 & 161550 & 1054400 & 161550 & 113760 & 102370 \\ \hline 3003 & 1001 & 1001 & 3003 & 1001 & 1001 & 3003 \\ 17175 & 73035 & 242325 & 161550 & 327375 & 122175 & 84855 \\ \hline 1001 & 1001 & 2002 & 1001 & 1001 & 1001 & 2002 \\ 3867 & 34128 & 73035 & 113760 & 122175 & 258768 & 42087 \\ \hline 1001 & 1001 & 1001 & 1001 & 1001 & 1001 & 1001 \\ 10237 & 3867 & 17175 & 102370 & 84855 & 42087 & 90269 \\ \hline 6006 & 1001 & 1001 & 3003 & 2002 & 1001 & 3003 \end{bmatrix} * \frac{1}{1000} \quad (3.19)$$

The superscript T denotes the transpose of the matrix and $z=(R+sL)l_e$ and $y=(G+sC)l_e$. A similar transformation can be performed on the sixth order FEM system using the transformation matrix W_t in order to obtain a more accurate FEM macromodel. The transformation matrix W_t and the proposed sixth order FEM system obtained using W_t are given as

$$W_t = \begin{bmatrix} 0 & 1 & 1 & 1 & 1 & 1 & 1 \\ 1 & 0 & 1 & 1 & 1 & 1 & 1 \\ 1 & 1 & 1 & 0 & 1 & 1 & 1 \\ 1 & 1 & 1 & 1 & 0 & 1 & 1 \\ 1 & 1 & 1 & 1 & 1 & 0 & 1 \\ 1 & 1 & 1 & 1 & 1 & 1 & 0 \end{bmatrix} \quad (3.20)$$

$$\begin{bmatrix} \mathbf{A}'_x & z\mathbf{B}'_x \\ y\mathbf{B}'_x & \mathbf{A}'_x \end{bmatrix} \begin{bmatrix} \mathbf{V}_x^e \\ \mathbf{I}_x^e \end{bmatrix} = \begin{bmatrix} \mathbf{0} \\ \mathbf{0} \end{bmatrix} \quad (3.21)$$

where

$$\mathbf{A}'_x = \mathbf{W}_t \mathbf{A}_x = \begin{bmatrix} -7551 & 10656 & -52641 & 5798 & -3177 & 954 & -799 \\ 1925 & 1925 & 15400 & 1925 & 1925 & 1925 & 15400 \\ -9057 & -6156 & 3078 & -1266 & 5913 & -162 & -129 \\ 3080 & 1925 & 385 & 385 & 3080 & 385 & 1925 \\ 9887 & -5904 & -261 & 348 & 1413 & -1548 & 1039 \\ 7700 & 1925 & 77 & 77 & 1540 & 1925 & 1925 \\ -1039 & 1548 & -1413 & -348 & 261 & 5904 & -9887 \\ 1925 & 1925 & 1540 & 77 & 77 & 1925 & 7700 \\ 129 & 162 & -5913 & 1266 & -3078 & 6156 & 9057 \\ 1925 & 385 & 3080 & 385 & 385 & 1925 & 3080 \\ 799 & -954 & 3177 & -5798 & 52641 & -10656 & 7551 \\ 15400 & 1925 & 1925 & 1925 & 15400 & 1925 & 1925 \end{bmatrix} \quad (3.22)$$

$$\mathbf{B}'_x = \mathbf{W}_t \mathbf{B}_x = \begin{bmatrix} 137 & 3933 & -207 & 7 & -387 & 63 & -7 \\ 616 & 7700 & 550 & 22 & 2200 & 1100 & 1100 \\ 69 & 8073 & 27 & 27 & -27 & 27 & -3 \\ 550 & 7700 & 616 & 110 & 220 & 1100 & 200 \\ -37 & -81 & 1269 & 157 & 0 & 27 & 37 \\ 550 & 550 & 1540 & 385 & 0 & 550 & 1100 \\ 37 & 27 & 0 & 157 & 1269 & -81 & -37 \\ 1100 & 550 & 0 & 385 & 1540 & 550 & 550 \\ -3 & 27 & -27 & 27 & 27 & 8073 & 69 \\ 200 & 1100 & 220 & 110 & 616 & 7700 & 550 \\ -7 & 63 & -387 & 7 & -207 & 3933 & 137 \\ 1100 & 1100 & 2200 & 22 & 550 & 7700 & 616 \end{bmatrix} \quad (3.23)$$

The same circuit in Figure 3.2 was solved for one sixth order FEM element using the proposed method and traditional method of imposing B.C. Figure 3.4 compares the frequency response at the output node (V_1) for $d=3$ cm using sixth order FEM element for both the approaches of imposing B.C. As shown, the proposed method matched more accurately at higher frequencies when compared to the traditional approach.

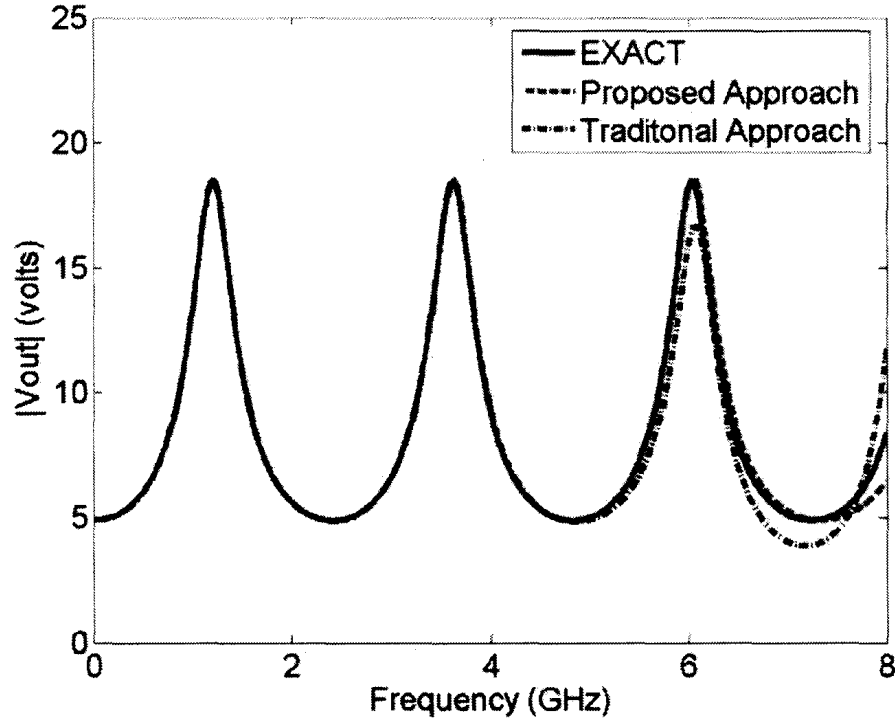


Figure 3.4: Frequency response comparison for circuit in Figure 3.2 for $d= 3$ cm using sixth order FEM approaches

For MTLs containing $\phi+1$ conductors the system of equations are similar to (3.21) and are expressed as

$$\begin{bmatrix} \tilde{\mathbf{A}}_x & \tilde{\mathbf{B}}_x \\ \tilde{\mathbf{C}}_x & \tilde{\mathbf{A}}_x \end{bmatrix} \begin{bmatrix} \mathbf{V}_x^e \\ \mathbf{I}_x^e \end{bmatrix} = \begin{bmatrix} \mathbf{0} \\ \mathbf{0} \end{bmatrix} \quad (3.24)$$

where $\tilde{\mathbf{A}}_x$ is obtained by multiplying each element of \mathbf{A}'_x by the identity matrix \mathbf{I} of size $\phi \times \phi$; $\tilde{\mathbf{B}}_x$ is obtained by multiplying each element of \mathbf{B}'_x with $\mathbf{Z} = (\mathbf{R} + s\mathbf{L})l_e$ and $\tilde{\mathbf{C}}_x$ is obtained by multiplying each element of \mathbf{B}'_x with $\mathbf{Y} = (\mathbf{G} + s\mathbf{C})l_e$ as

$$\tilde{A}_x = \begin{bmatrix} \frac{-7551}{1925} I & \frac{10656}{1925} I & \frac{-52641}{15400} I & \frac{5798}{1925} I & \frac{-3177}{1925} I & \frac{954}{1925} I & \frac{-799}{15400} I \\ \frac{9057}{1925} I & \frac{-6156}{1925} I & \frac{3078}{1925} I & \frac{-1266}{1925} I & \frac{5913}{1925} I & \frac{-162}{1925} I & \frac{-129}{1925} I \\ \frac{3080}{9887} I & \frac{1925}{-5904} I & \frac{385}{-261} I & \frac{385}{-348} I & \frac{3080}{1413} I & \frac{385}{-1548} I & \frac{1925}{1039} I \\ \frac{7700}{-1039} I & \frac{1925}{1548} I & \frac{77}{-1413} I & \frac{77}{-348} I & \frac{1540}{261} I & \frac{1925}{5904} I & \frac{1925}{-9887} I \\ \frac{1925}{129} I & \frac{1925}{162} I & \frac{1540}{-5913} I & \frac{77}{1266} I & \frac{77}{-3078} I & \frac{1925}{6156} I & \frac{7700}{9057} I \\ \frac{1925}{799} I & \frac{385}{-954} I & \frac{3080}{3177} I & \frac{385}{-5798} I & \frac{385}{52641} I & \frac{1925}{-10656} I & \frac{3080}{7551} I \\ 15400 & 1925 & 1925 & 1925 & 15400 & 1925 & 1925 \end{bmatrix} \quad (3.25)$$

$$\tilde{B}_x = \begin{bmatrix} \frac{137}{616} Z & \frac{3933}{7700} Z & \frac{-207}{550} Z & \frac{7}{22} Z & \frac{-387}{2200} Z & \frac{63}{1100} Z & \frac{-7}{1100} Z \\ \frac{69}{550} Z & \frac{8073}{7700} Z & \frac{27}{616} Z & \frac{27}{110} Z & \frac{-27}{220} Z & \frac{27}{1100} Z & \frac{-3}{200} Z \\ \frac{-37}{550} Z & \frac{-81}{550} Z & \frac{1269}{1540} Z & \frac{157}{385} Z & \frac{0}{550} Z & \frac{27}{550} Z & \frac{37}{1100} Z \\ \frac{37}{1100} Z & \frac{27}{550} Z & \frac{0}{385} Z & \frac{157}{1540} Z & \frac{1269}{550} Z & \frac{-81}{550} Z & \frac{-37}{1540} Z \\ \frac{-3}{200} Z & \frac{27}{1100} Z & \frac{-27}{220} Z & \frac{27}{110} Z & \frac{27}{616} Z & \frac{8073}{7700} Z & \frac{69}{550} Z \\ \frac{200}{-7} Z & \frac{1100}{63} Z & \frac{220}{-387} Z & \frac{110}{7} Z & \frac{616}{-207} Z & \frac{7700}{3933} Z & \frac{550}{137} Z \\ \frac{1100}{1100} Z & \frac{1100}{1100} Z & \frac{2200}{2200} Z & \frac{22}{22} Z & \frac{550}{550} Z & \frac{7700}{7700} Z & \frac{616}{616} Z \end{bmatrix} \quad (3.26)$$

$$\tilde{C}_x = \begin{bmatrix} \frac{137}{616} Y & \frac{3933}{7700} Y & \frac{-207}{550} Y & \frac{7}{22} Y & \frac{-387}{2200} Y & \frac{63}{1100} Y & \frac{-7}{1100} Y \\ \frac{69}{550} Y & \frac{8073}{7700} Y & \frac{27}{616} Y & \frac{27}{110} Y & \frac{-27}{220} Y & \frac{27}{1100} Y & \frac{-3}{200} Y \\ \frac{-37}{550} Y & \frac{-81}{550} Y & \frac{1269}{1540} Y & \frac{157}{385} Y & \frac{0}{550} Y & \frac{27}{550} Y & \frac{37}{1100} Y \\ \frac{37}{1100} Y & \frac{27}{550} Y & \frac{0}{385} Y & \frac{157}{1540} Y & \frac{1269}{550} Y & \frac{-81}{550} Y & \frac{-37}{1540} Y \\ \frac{-3}{200} Y & \frac{27}{1100} Y & \frac{-27}{220} Y & \frac{27}{110} Y & \frac{27}{616} Y & \frac{8073}{7700} Y & \frac{69}{550} Y \\ \frac{200}{-7} Y & \frac{1100}{63} Y & \frac{220}{-387} Y & \frac{110}{7} Y & \frac{616}{-207} Y & \frac{7700}{3933} Y & \frac{550}{137} Y \\ \frac{1100}{1100} Y & \frac{1100}{1100} Y & \frac{2200}{2200} Y & \frac{22}{22} Y & \frac{550}{550} Y & \frac{7700}{7700} Y & \frac{616}{616} Y \end{bmatrix} \quad (3.27)$$

It should be noted that the FEM macromodel is formulated in terms of predetermined coefficients (derived from the FEM approximation) and by the p.u.l. parameters. The

system of equations obtained from the assembly of system in (3.21) and (3.24) including the boundary conditions can be expressed as

$$(s\mathbf{C}_\pi + \mathbf{G}_\pi)\mathbf{X}_\pi = \mathbf{B}_\pi \quad (3.28)$$

\mathbf{C}_π is due to the assembly of element matrices of p.u.l. inductance and capacitance parameters; \mathbf{G}_π is due to the assembly of element matrices of the p.u.l. resistance and conductance parameters as well as the \mathbf{A}'_x , $\tilde{\mathbf{A}}_x$ matrices; \mathbf{X}_π is a vector containing the voltage and current coefficients; \mathbf{B}_π is a vector formed by forcing voltage and/or current sources applied at the boundaries of the interconnect. Equation (3.28) can be expressed in time domain as

$$\frac{d\mathbf{X}_\pi}{dt} \mathbf{C}_\pi + \mathbf{G}_\pi \mathbf{X}_\pi = \mathbf{B}_\pi \quad (3.29)$$

Once the macromodel is expressed in terms of (3.29), it can be linked into nonlinear circuit simulators such as the SPICE.

3.3 – Passivity Considerations

Passivity is an important property to satisfy because stable but not passive macromodels can produce unstable networks when connected to other passives loads. In order to better explain this, consider a macromodel proposed in [86] and shown in Figure 3.5. It is to be noted that when the stable but non-passive macromodel is connected to a passive inductor and capacitor, the overall network becomes unstable (i.e., poles are on the right hand side of the imaginary axis). As a result, spurious oscillations may be produced in the transient analysis due to network instability resulting in accurate time domain responses.

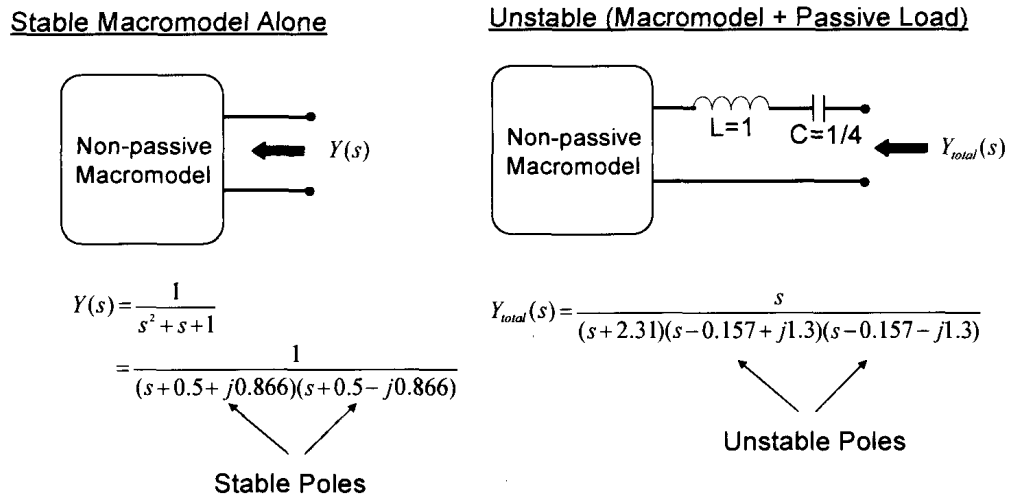


Figure 3.5: Illustration of Significance of Passivity

A linear network with admittance matrix $\mathbf{Y}(s)$ is said to be passive if and only if

1. $\mathbf{Y}(s^*) = \mathbf{Y}^*(s)$, where “*” is the complex conjugate operator.
2. $\mathbf{Y}(s)$ a positive real matrix, that is the product $\mathbf{z}^{*T}(\mathbf{Y}^T(s^*) + \mathbf{Y}(s))\mathbf{z} \geq 0$ for all complex values of s satisfying $\text{Re}(s) > 0$ and any arbitrary vector \mathbf{z} .

The first condition implies that the coefficients of the rational function matrix generated by the proposed macromodel must be real. The second condition states that $\mathbf{Y}(s)$ must be a positive real matrix for all $\text{Re}(s) > 0$, since the real part of $\mathbf{Y}(s)$ is $1/2[\mathbf{Y}^T(s^*) + \mathbf{Y}(s)]$.

To prove that the sixth order FEM macromodel is passive, the system of equations described by (3.21) and (3.24) are converted to the Y-parameters. For a 2-conductor line the Y-parameters of (3.21) for the e^{th} element (Figure. 3.1) is defined as

$$Y(s) = \begin{bmatrix} Y_{11} & Y_{12} \\ Y_{21} & Y_{22} \end{bmatrix} = \Psi_1 + \Psi_2; \quad (3.28a)$$

$$Y_{11} = \left. \frac{I_0^e}{V_0^e} \right|_{V_6^e=0} \quad Y_{12} = \left. \frac{I_0^e}{V_6^e} \right|_{V_6^e=0} \quad Y_{22} = \left. \frac{I_6^e}{V_6^e} \right|_{V_6^e=0} \quad Y_{21} = \left. \frac{I_6^e}{V_0^e} \right|_{V_6^e=0} \quad (3.28b)$$

The matrices Ψ_1 and Ψ_2 are expressed in terms of congruent transforms as

$$\Psi_1 = W_1^T \begin{bmatrix} H_1 & 0 \\ 0 & 0 \end{bmatrix} W_1 \quad \Psi_2 = W_2^T \begin{bmatrix} H_2 & 0 \\ 0 & 0 \end{bmatrix} W_2; \quad (3.29a)$$

$$W_1 = \begin{bmatrix} 1 & -1 \\ 0 & 1 \end{bmatrix} \quad W_2 = \begin{bmatrix} 1 & 1 \\ 0 & 1 \end{bmatrix} \quad (3.29b)$$

$$H_1 = \frac{1}{84} \frac{(z^3 y^3 + 840z^2 y^2 + 75600zy + 665280)}{(z^2 y^2 + 240zy + 7920)z} \quad (3.30a)$$

$$H_2 = 21 \frac{(y^2 z^2 + 240yz + 7920)y}{y^3 z^3 + 840y^2 z^2 + 75600yz + 665280} \quad (3.30b)$$

Since the coefficients describing H_1 and H_2 are real, Y-parameters of (3.28) satisfy the first passivity condition $Y(s^*) = Y^*(s)$. If H_1 and H_2 are positive real, then Ψ_1 and Ψ_2 are also positive real since they are expressed in terms of congruence transformation of a positive real function. The following facts are used to prove that H_1 and H_2 are positive real.

Lemma 1: The sum of two positive real functions or matrices of similar dimensions is positive real [60].

Lemma 2: The inverse of a positive real function or matrix (if the inverse exists) is positive real [60].

To prove that H_1 is positive real the rational function is expressed as continued fractions as

$$H_1 = \kappa_6 y + (\kappa_5 z + (\kappa_4 y + (\kappa_3 z + (\kappa_2 y + (\kappa_1 z)^{-1})^{-1})^{-1})^{-1})^{-1} \quad (3.31a)$$

The coefficients κ_i , for $i=1,2,\dots,6$ are derived from (3.30a) and are all positive values $\kappa_i > 0$. Since $z = (R + sL)l_e$ and $y = (G + sC)l_e$ are positive-real functions (due to the fact the line parameters are nonnegative matrices [4], H_1 is positive real (from Lemma 1 and 2). Similarly H_2 can also be expressed as a continued fraction as

$$H_2 = (\kappa_6 z + (\kappa_5 y + (\kappa_4 z + (\kappa_3 y + (\kappa_2 z + (\kappa_1 y)^{-1})^{-1})^{-1})^{-1})^{-1})^{-1} \quad (3.31b)$$

where the κ_i coefficients of (3.31b) are the same as (3.31a). As a result, H_2 is positive real. Thus the Y-parameters of (3.28) are positive real since Ψ_1 and Ψ_2 are expressed in terms of congruence transformation of positive real functions.

Using similar approach, we can prove that the sixth order FEM macromodel is passive for a multiconductor line. For a multiconductor line, the system of equations described by (3.24) are converted to the Y-parameters which is defined as

$$Y(s) = \begin{bmatrix} Y_{11} & Y_{12} \\ Y_{21} & Y_{22} \end{bmatrix} = \Psi_1 + \Psi_2; \quad (3.32)$$

As before, the matrices Ψ_1 and Ψ_2 are expressed in terms of congruent transforms as

$$\Psi_1 = W_1^T \begin{bmatrix} H_1 & 0 \\ 0 & 0 \end{bmatrix} W_1 \quad \Psi_2 = W_2^T \begin{bmatrix} H_2 & 0 \\ 0 & 0 \end{bmatrix} W_2; \quad (3.33a)$$

$$W_1 = \begin{bmatrix} I & -I \\ 0 & I \end{bmatrix} \quad W_2 = \begin{bmatrix} I & I \\ 0 & I \end{bmatrix} \quad (3.33b)$$

where I is the identity matrix.

$$\mathbf{H}_1 = \frac{I}{84} \left[(z^2 y^2 + 240zy + 7920)z \right]^{-1} \left[z^3 y^3 + 840z^2 y^2 + 75600zy + 665280 \right] \quad (3.34a)$$

$$\mathbf{H}_2 = 2I \left[y^3 z^3 + 840y^2 z^2 + 75600yz + 665280 \right]^{-1} \left[(y^2 z^2 + 240yz + 7920)y \right] \quad (3.34b)$$

Since the coefficients describing \mathbf{H}_1 and \mathbf{H}_2 are real, Y-parameters of (3.32) satisfy the first passivity condition $\mathbf{Y}(s^*) = \mathbf{Y}^*(s)$. Again, if \mathbf{H}_1 and \mathbf{H}_2 are positive real, then Ψ_1 and Ψ_2 are also positive real since they are expressed in terms of congruence transformation of a positive real function. Similar to the two conductor line proof, to prove that \mathbf{H}_1 is positive real the rational function is expressed as continued fractions as

$$\mathbf{H}_1 = \kappa_6 y + (\kappa_5 z + (\kappa_4 y + (\kappa_3 z + (\kappa_2 y + (\kappa_1 z)^{-1})^{-1})^{-1})^{-1})^{-1} \quad (3.35a)$$

The coefficients κ_i , for $i=1,2,\dots,6$ are derived from (3.34a) and are all positive values $\kappa_i > 0$. Since $z = (\mathbf{R} + s\mathbf{L})l_e$ and $y = (\mathbf{G} + s\mathbf{C})l_e$ are positive-real functions (due to the fact the line parameters are nonnegative matrices [4]) \mathbf{H}_1 is positive real (from Lemma 1 and 2). Similarly \mathbf{H}_2 can also be expressed as a continued fraction as

$$\mathbf{H}_2 = (\kappa_6 z + (\kappa_5 y + (\kappa_4 z + (\kappa_3 y + (\kappa_2 z + (\kappa_1 y)^{-1})^{-1})^{-1})^{-1})^{-1})^{-1} \quad (3.35b)$$

A similar technique can be used to show that \mathbf{H}_2 is positive real. Thus the Y-parameters of (3.32) are positive real as Ψ_1 and Ψ_2 are expressed in terms of congruence transformation of positive real functions. In addition, the proposed method can be used to obtain passive macromodels using higher order FEM approximation.

3.4 – Frequency Dependent Parameters

As frequency increases the proximity, edge and skin effects causes the p.u.l. resistance and inductance to become a function of frequency. Typically, the p.u.l. parameters are often characterized by tabulated data obtained from measurements or through an electromagnetic field solver [4]. One way to model the frequency dependent p.u.l. parameters is to use a rational approximation as

$$\mathbf{Z}(s) = \mathbf{R}(s) + s\mathbf{L}(s) = \frac{\mathbf{N}_z}{D_z} = \frac{\mathbf{F}_k s^k + \dots + \mathbf{F}_0}{w_{k-1} s^{k-1} + \dots + 1} \quad (3.36)$$

where \mathbf{N}_z is a polynomial matrix and D_z is a scalar polynomial.

However as discussed by the passivity considerations in section 3.3, in order to preserve the passivity of the transmission line macromodel with frequency dependent parameters it is required for the functions $\mathbf{Z}(s) = \mathbf{R}(s) + s\mathbf{L}(s)$ to be positive real. One way to ensure the passivity of a macromodel with frequency dependent parameters, is to use the passivity verification and correction methodologies proposed in [86],[95]. An alternative approach is to fit the p.u.l. parameters to positive real functions which are represented using passive circuit elements. Since the circuit element approach can be easily linked to nonlinear circuit simulators, this technique was used by the proposed method and is discussed next.

For the sake of simplicity of presentation, the discussion will focus on a two-conductor line and then extend to multiconductor lines. The circuit configuration shown in Figure 3.6 has been proposed to model skin effect of interconnects [94]. The proposed

method matches the input impedance of the circuit with tabulated data values of $R(s)+sL(s)$. by ensuring each element of Figure 3.6 is nonnegative, the resulting network remains passive and the rational function formed by the input impedance is positive real.

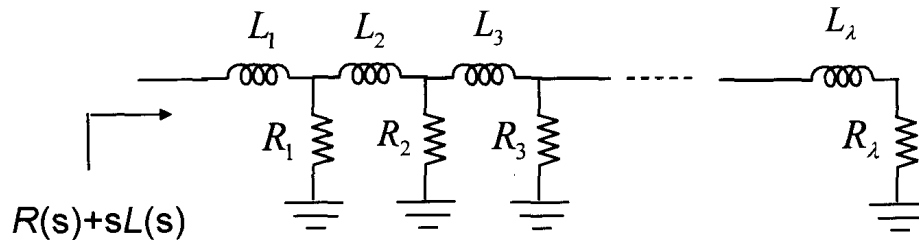


Figure 3.6: RL canonical circuit configuration

For the case of multiconductor transmission lines, the circuit topology is composed of resistors, inductors and ideal transformers. As an example, Figure 3.7 shows the circuit topology for a four conductor case that represents $R(s)+sL(s)$, where each Z_{ij} box represents an RL circuit configuration shown in Figure 3.7b.

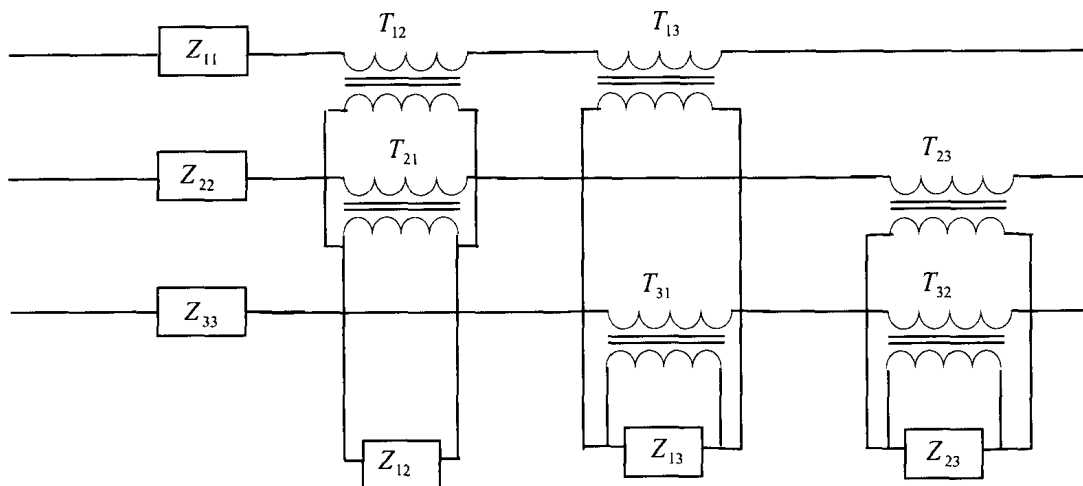


Figure 3.7a: Circuit topology for $R(s)+sL(s)$ for a three conductor transmission line

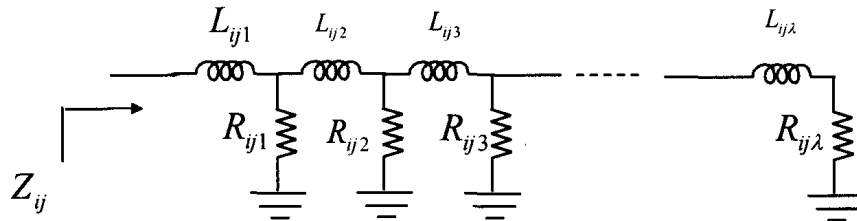


Figure 3.7b: Circuit representation of Z_{ij} , RL canonical configuration

3.5 – Y-Parameters and the Time-Domain Macromodel

In order to make the proposed interconnect model useful to nonlinear circuit simulators, the model must be expressed as ordinary differential equations. There are many ways to convert rational functions to ordinary differential equations. One way is to directly represent the Y-parameter rational functions of the macromodel in terms of Laplace transfer functions and then use the Laplace function of the HSPICE simulator [60] to link the macromodel with nonlinear elements in a circuit simulator environment. The other approaches are to represent rational functions in terms of state space equations either in the controllable, observable, or Jordan canonical form [87]-[88]. One could also directly link the system in (3.21) and (3.24) as ordinary differential equations into a circuit simulator. However the matrices of (3.21) and (3.24) are dense. Often it is desirable to represent the system in terms of sparse matrices to improve CPU efficiency of simulations. Hence an alternative approach to link to nonlinear circuit simulators is to use circuit elements. The advantage of using circuit elements is that the macromodel can

be realized without having knowledge or access to the internals of the circuit simulator. Moreover, the circuit realization models can be much faster in terms of simulation time due to the fact that they result in diagonally dominant, band limited and highly sparse matrices when compared to directly linking (3.21) and (3.24).

The realization of the Y-parameters of the macromodel for a single conductor line given by

$$\begin{bmatrix} I(0,s) \\ -I(l_e,s) \end{bmatrix} = \begin{bmatrix} Y_{11} & Y_{12} \\ Y_{21} & Y_{22} \end{bmatrix} \begin{bmatrix} V(0,s) \\ V(l_e,s) \end{bmatrix}; \quad Y(s) = \begin{bmatrix} Y_{11} & Y_{12} \\ Y_{21} & Y_{22} \end{bmatrix} = \Psi_1 + \Psi_2 \quad (3.37)$$

is shown in Figure 3.8. In order to implement Ψ_1 and Ψ_2 , the rational functions H_1 and H_2 given by

$$H_1 = \kappa_6 y + (\kappa_5 z + (\kappa_4 y + (\kappa_3 z + (\kappa_2 y + (\kappa_1 z)^{-1})^{-1})^{-1})^{-1})^{-1} \quad (3.38a)$$

$$H_2 = (\kappa_6 z + (\kappa_5 y + (\kappa_4 z + (\kappa_3 y + (\kappa_2 z + (\kappa_1 y)^{-1})^{-1})^{-1})^{-1})^{-1} \quad (3.38b)$$

in terms of partial fraction expansion can be realized by means of a ladder circuit as shown in Figure 3.9 and Figure 3.10. Similarly the circuit models can be extended for multiconductor transmission lines. An example of a three conductor line is shown in Figure 3.11 to Figure 3.13.

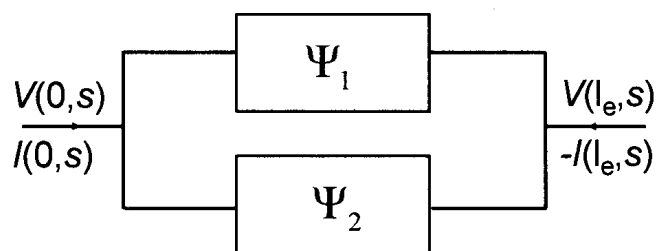


Figure 3.8: Realization of the Interconnect Model

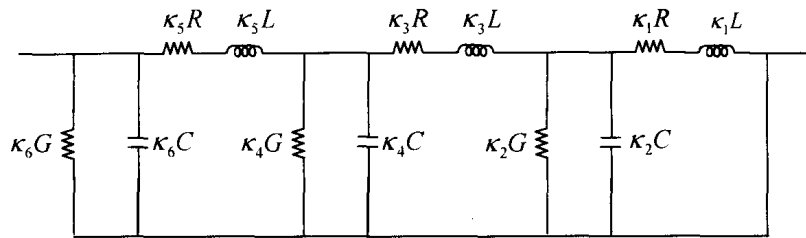


Figure 3.9: Realization of Ψ_1

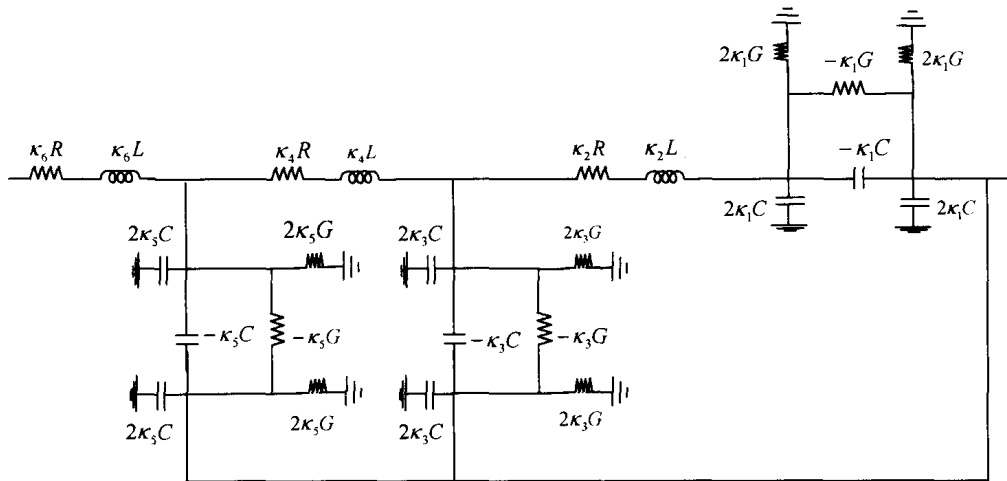


Figure 3.10: Realization of Ψ_2

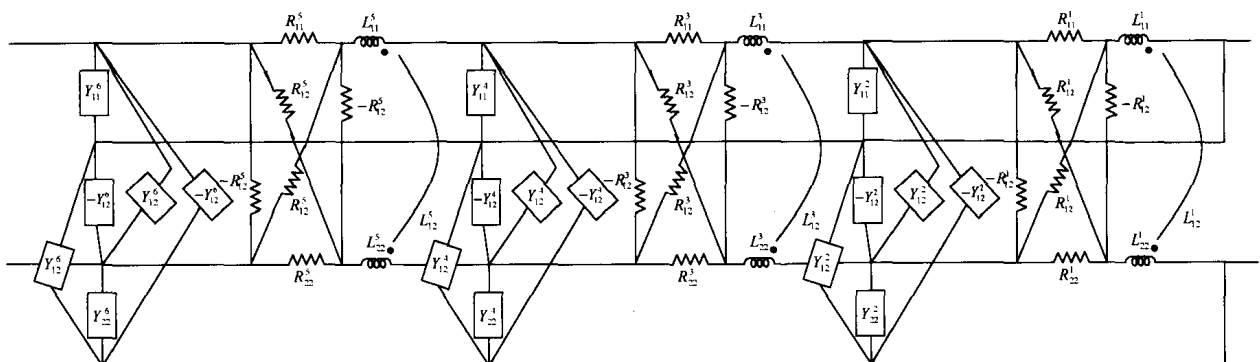


Figure 3.11: Realization of Ψ_1 for a three conductor transmission line

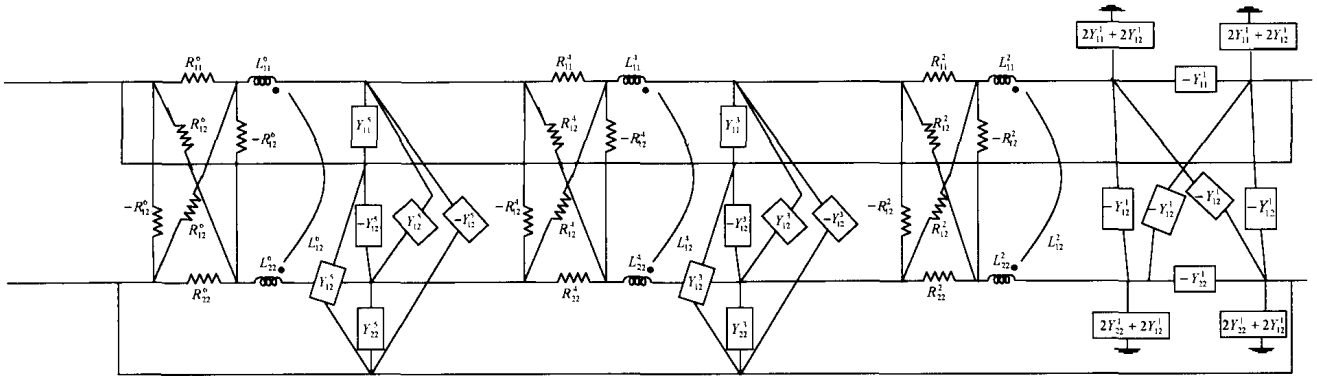


Figure 3.12: Realization of Ψ_2 for a three conductor transmission line

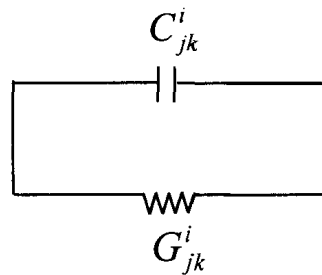


Figure 3.13: Y_{jk}^i circuit

For the case of frequency dependent parameters, the circuit realization of a two conductor transmission line with frequency dependent p.u.l. resistance and inductance is shown in Figure 3.14 to Figure 3.16. The coefficient λ in the Figure 3.16 corresponds to the number of sections required to model the frequency dependent parameters.

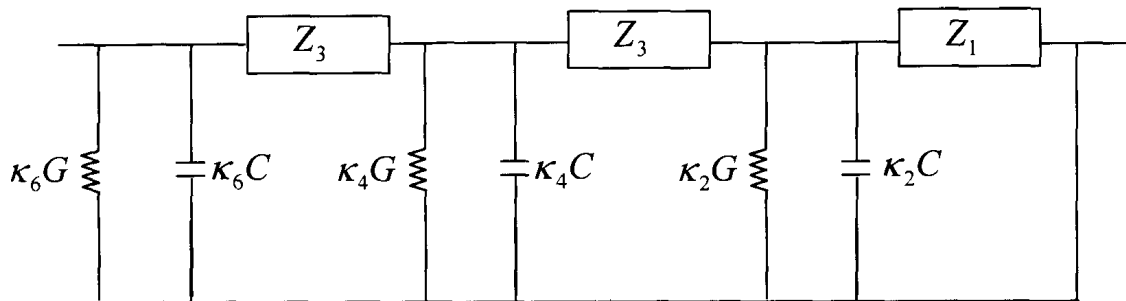


Figure 3.14: Realization of Ψ_1 of a two conductor transmission line with frequency dependent p.u.l. resistance and inductance

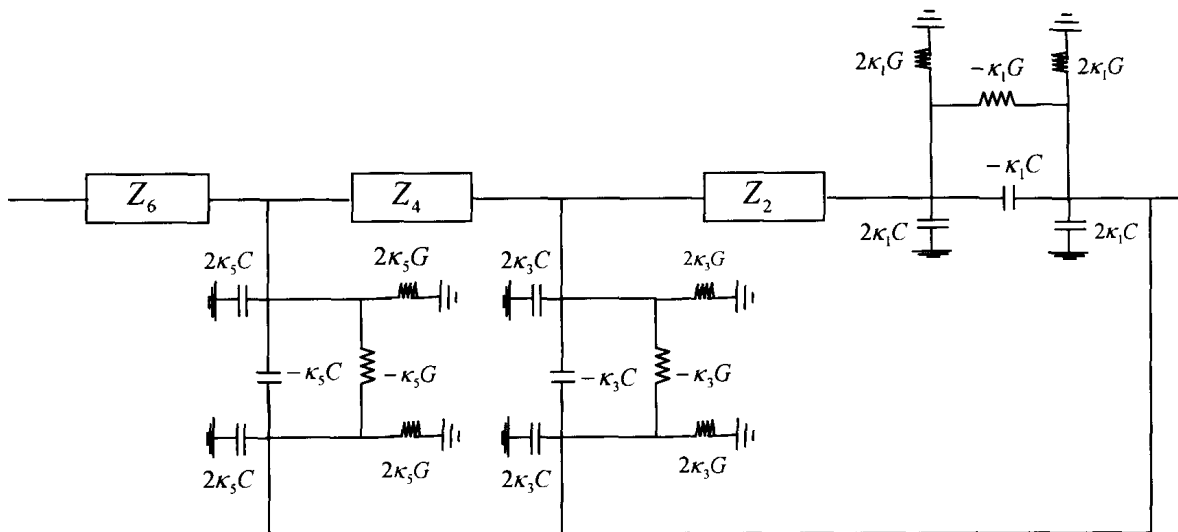


Figure 3.15: Realization of Ψ_2 of a two conductor transmission line with frequency dependent p.u.l. resistance and inductance

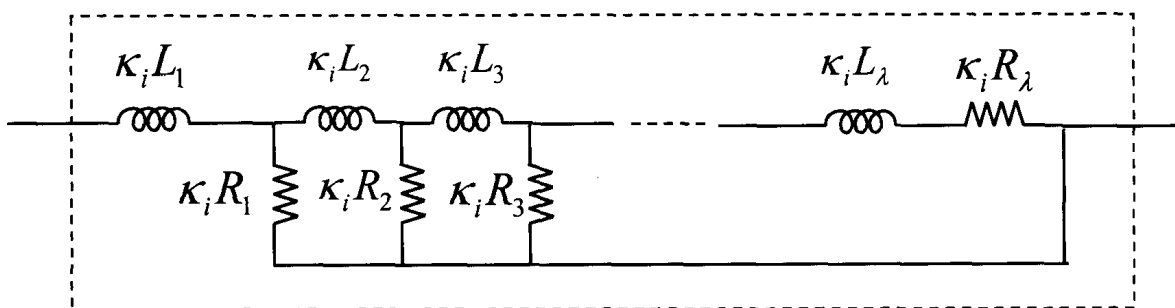


Figure 3.16: Z_i circuit (RL canonical configuration)

In similar lines, the circuit realization can also be extended to multiconductor transmission lines with frequency dependent parameters. An example of a three conductor transmission line is shown in Figure 3.17 to Figure 3.19.

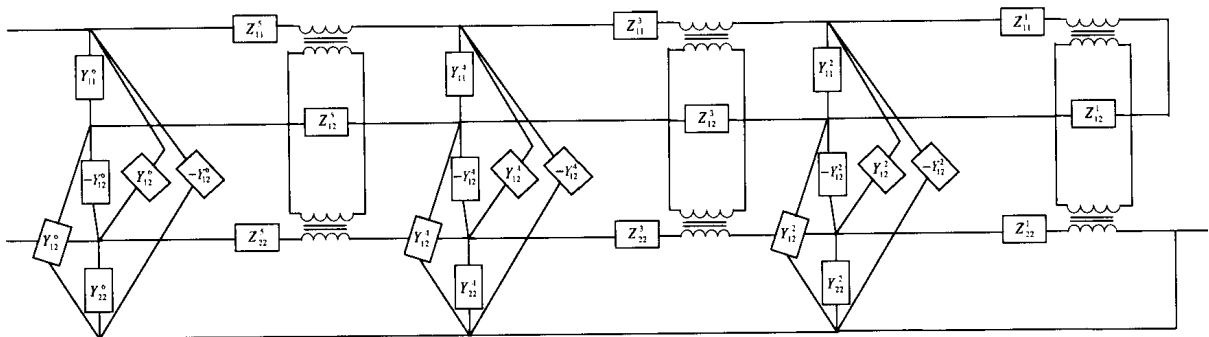


Figure 3.17: Realization of Ψ_1 for a three conductor transmission line with frequency dependent p.u.l. resistance and inductance

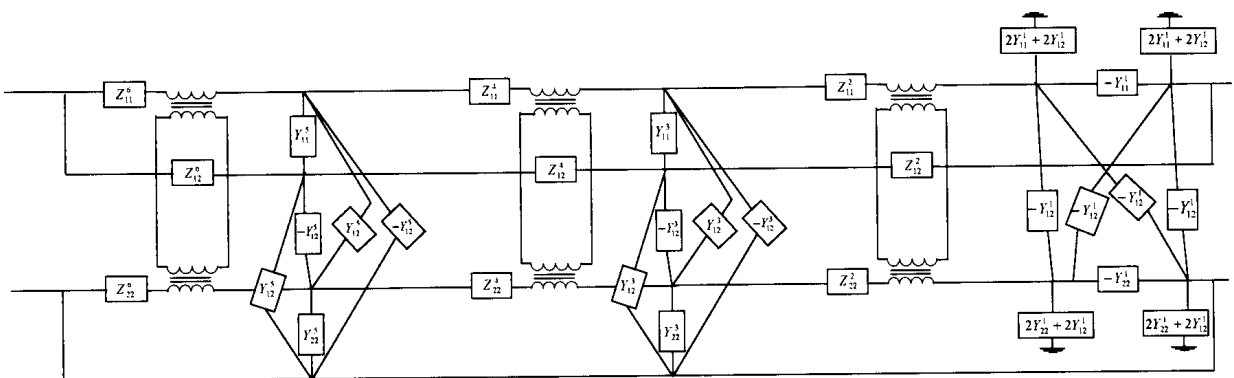


Figure 3.18: Realization of Ψ_2 for a three conductor transmission line with frequency dependent p.u.l. resistance and inductance

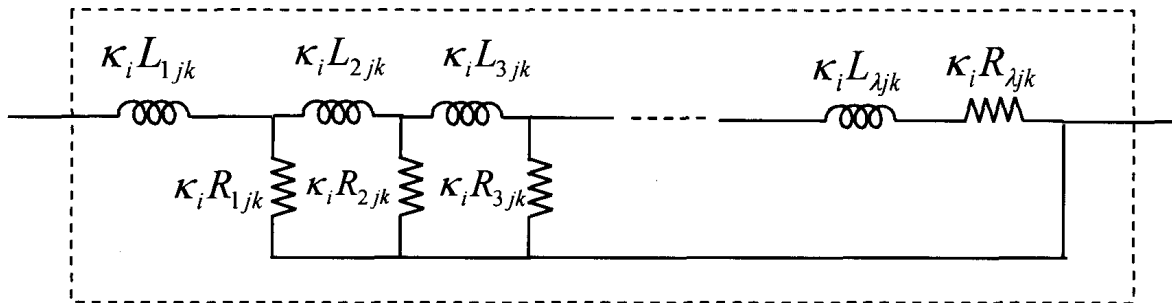


Figure 3.19: Z_{jk}^i circuit (RL canonical configuration)

3.6 – Numerical Examples

Three examples are presented in this section to demonstrate the validity and efficiency of the proposed macromodel. Since the developed macromodeling algorithm is proposed to simulate VLSI interconnects, all the three examples considered here are to test on-chip interconnects used in modern VLSI and packaging systems. The first example deals with a packaging interconnection system, the second considers an on-chip two coupled interconnect network with frequency dependent per unit length parameters, and the third example represents an on-chip 9-coupled interconnect network. The results given by the proposed method are compared with the conventional lumped segmentation model [12], and/or the “exact” analysis of the transmission line equation. Within the context of this section, “exact” analysis refers to direct solution of Telegrapher’s equations through eigenvalue/eigenvector analysis. All simulations were performed in HSPICE [60] using a Sun blade 1500 workstation.

3.6.1 – Example 3.1

Packaging interconnection system with nonlinear termination:

The nonlinear circuit shown in Figure 3.20 was proposed in [19]. The two systems of coupled interconnects are identical, with length 5cm and p.u.l. parameters given by:

$R_{11} = R_{22} = R_{33} = 3.448 \Omega / \text{cm}$; $L_{11} = L_{22} = L_{33} = 4.976 \text{nH/cm}$, $L_{12} = L_{21} = L_{23} = L_{32} = 0.765 \text{nH/cm}$,
 $L_{13} = L_{31} = 0.152 \text{nH/cm}$; $C_{11} = C_{22} = C_{33} = 1.082 \text{pF/cm}$, $C_{12} = C_{21} = C_{23} = C_{32} = -0.197$
 pF/cm , $C_{13} = C_{31} = -0.006 \text{pF/cm}$. Figure 3.21 shows a comparison of the magnitude of Y_{11}

for the linear subnetwork of Figure 3.20 obtained using the proposed method (2 sixth order FEM elements), conventional lumped model (60 sections) and the “exact” response. Within the context of this section, “exact” analysis refers to direct solution of Telegrapher’s equations through eigenvalue/eigenvector analysis. For their respective orders, the frequency response of the proposed matches the conventional lumped model and the ‘exact’ frequency response up to 7 GHz. The transient response at node 2 and 3 corresponding to a 5V input pulse with fall/rise time 0.1ns and a pulse width of 1ns is shown in Figure 3.22. Both the proposed and the conventional lumped model give similar results. In this example, the lumped-segmentation model introduces 540 new equations to the MNA matrix whereas the proposed introduces 108 equations (80% savings). On a Sun blade 1500 workstation, it takes HSPICE 13.27 sec to simulate the results with the conventional lumped segmentation model while the proposed method only requires 4.77 sec.

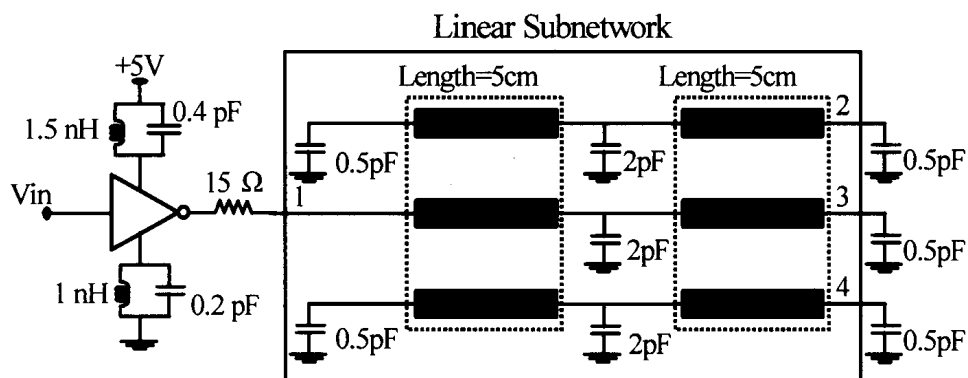


Figure 3.20: Nonlinear interconnect circuit (Example 1)

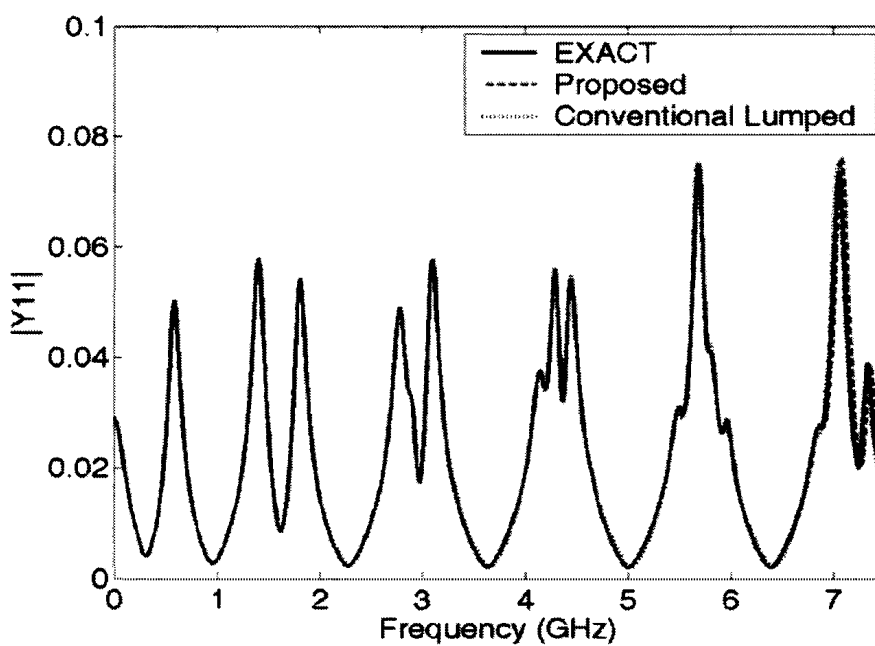


Figure 3.21: Frequency response of Y_{11} (Example 1)

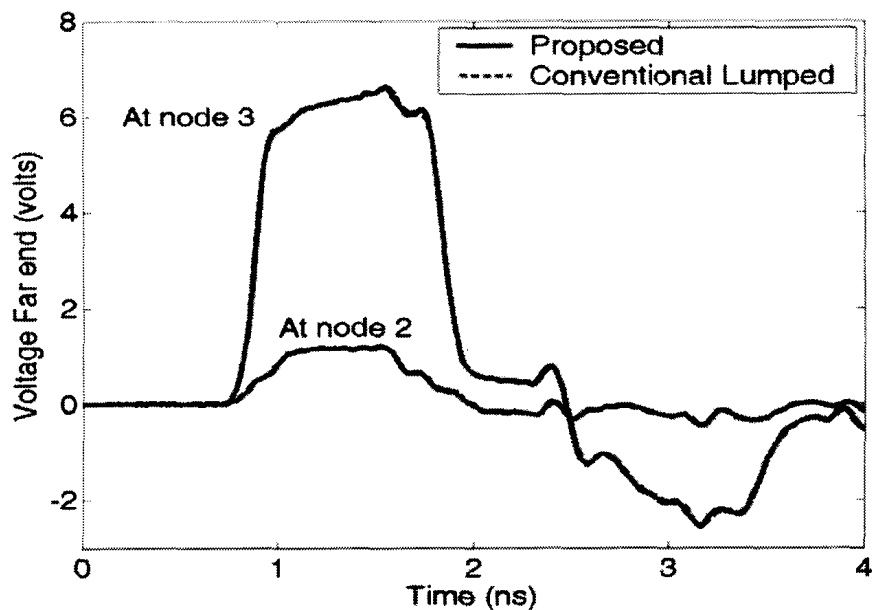


Figure 3.22: Transient response (Example 1)

3.6.2 – Example 3.2

On-chip 2-coupled interconnect network with frequency dependent p.u.l. parameters

An on-chip coupled interconnect network with frequency dependent parameters proposed in [89] is shown in Figure 3.23. The length of the interconnect network is 0.5 cm and the per unit length parameters are given in Table 3.1.

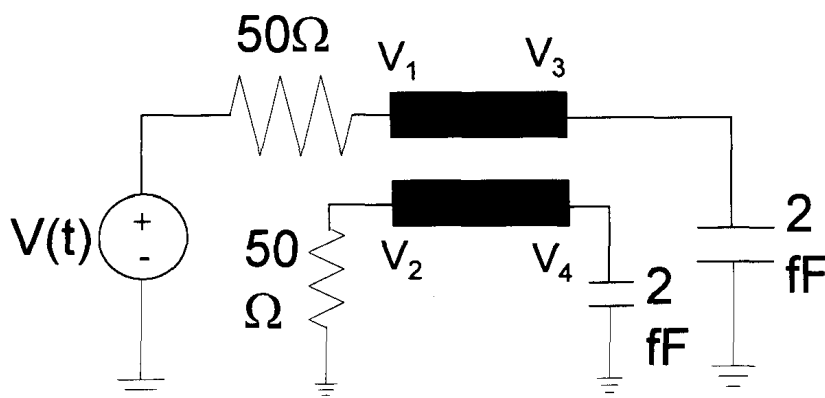


Figure 3.23: On-chip coupled interconnect network (Example 2)

The frequency dependent data are modeled using 2 RL section for $R_{11}(s) + sL_{11}(s)$ and 2 RL section for $R_{12}(s) + sL_{12}(s)$ using the scheme described in section 3.4. The time-domain responses corresponding to an input step of 1V and a rise time of 0.07 ns for the nodes V1 and V3 of the active line is shown in Figure 3.24 and Figure 3.25. The results of the proposed macromodel (one sixth order element) are in good agreement with the results of the conventional lumped segmentation (32 sections). Figure 3.26 and Figure 3.27 shows the transient response at the nodes V2 and V4 of the victim line. For their respective orders, the proposed macromodel and the conventional lumped segmentation give similar responses as shown in Figure 3.26 and Figure 3.27. The responses produced by the proposed and the conventional lumped segmentation also matches results published in [89]. In this example, the proposed method required 80% fewer variables when compared to the lumped-segmentation model. The CPU times taken to simulate the results with conventional lumped model was 0.82 sec, while the proposed method took 0.17 sec.

TABLE 3.1
Frequency dependent p.u.l. data, Frequency in GHz, Resistor in $K\Omega$,
and Inductor in μH (EXAMPLE 3.2)

Freq.	R11	R12	R22	L11	L12	L22
0.0000	54.980e-3	0.0	333.700e-3	14.024e-3	11.186 e-3	14.1697 e-3
0.0010	56.440e-3	1.4094e-3	335.550e-3	14.024 e-3	11.186 e-3	14.1679 e-3
0.0033	56.442e-3	1.4130e03	335.555 e-3	14.023 e-3	11.186 e-3	14.1679 e-3
0.0066	56.447e-3	1.4220e-3	335.556 e-3	14.020 e-3	11.178 e-3	14.1607 e-3
0.0100	56.460e-3	1.4320e-3	335.570 e-3	14.000 e-3	11.167 e-3	14.1530 e-3
0.030	56.677e-3	1.4408e-3	335.785 e-3	13.840 e-3	11.012 e-3	14.0030 e-3
0.660	56.326e-3	2.0620e-3	336.430 e-3	13.365 e-3	10.557 e-3	13.5740 e-3
0.1000	58.260e-3	2.9540e-3	337.360 e-3	12.710 e-3	9.9300 e-3	12.9820 e-3
0.3000	63.800e-3	8.2570e-3	342.875 e-3	9.3000 e-3	6.6760 e-3	9.90400 e-3
0.6600	68.337e-3	12.560e-3	347.375 e-3	7.1279 e-3	4.6030 e-3	7.94560 e-3
1.0000	70.375e-3	14.454e-3	349.380 e-3	6.5050 e-3	4.0090 e-3	7.38400 e-3
3.5000	77.443e-3	20.320e-3	356.416 e-3	5.6750 e-3	3.2260 e-3	6.64500 e-3
6.6000	84.188e-3	24.549e-3	363.250 e-3	5.5130 e-3	3.0874 e-3	6.49600 e-3
10.000	92.682e-2	29.190e-3	371.725 e-3	5.4160 e-3	3.0180 e-3	6.40900 e-3

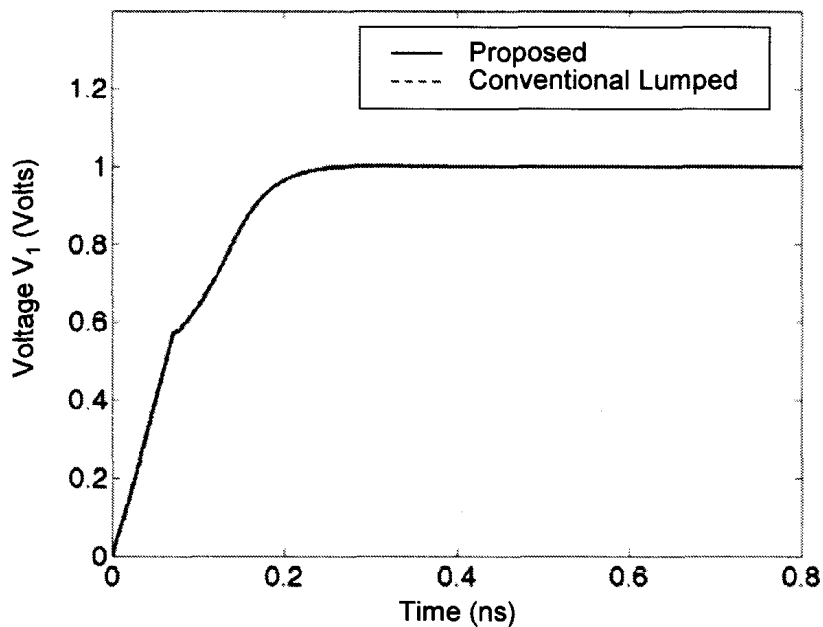
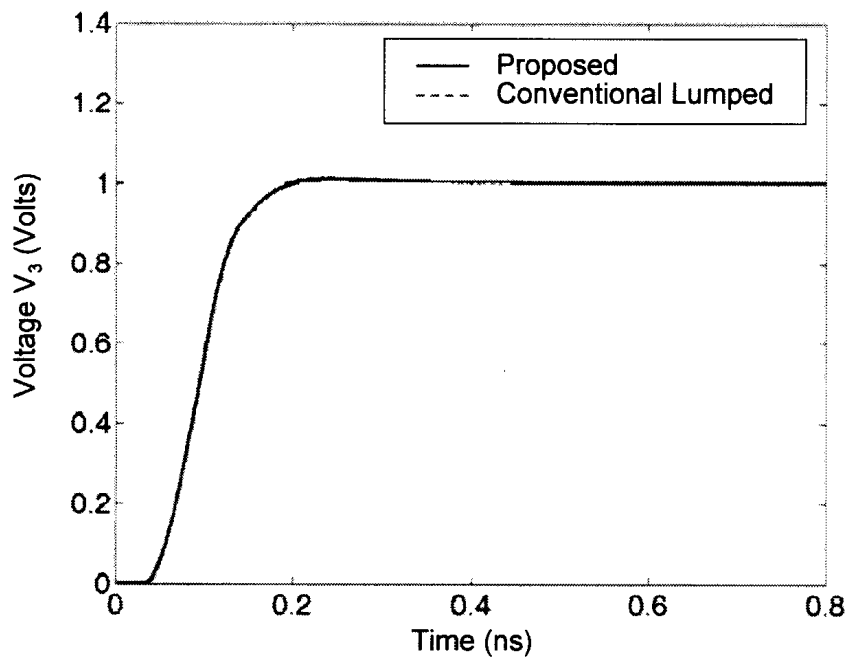
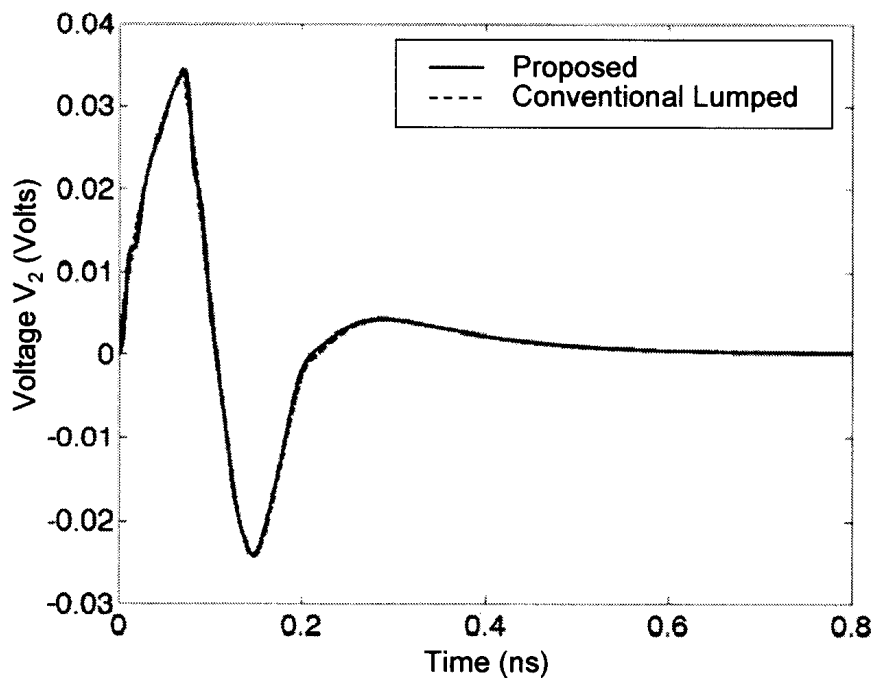


Figure 3.24: Transient response at node V_1 (Example 2)

Figure 3.25: Transient response at node V_3 (Example 2)Figure 3.26: Transient response at node V_2 (Example 2)

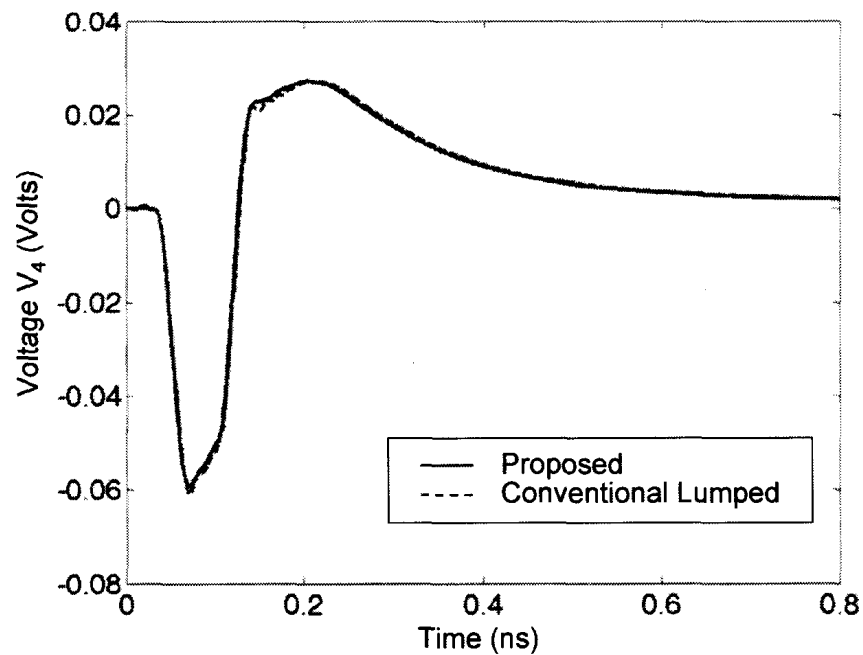


Figure 3.27: Transient response at node V_4 (Example 2)

3.6.3 – Example 3.3

On-chip 9-coupled frequency dependent interconnect network with nonlinear termination

Figure 3.28 shows the cross-section of a 9-coupled transmission line network terminated with a nonlinear inverter as shown in Figure 3.29. The frequency dependent p.u.l. resistance and inductance parameters $R(s), L(s)$ and the p.u.l. conductance and capacitance G, C for the structure of Figure 3.28 are determined by using the HSPICE field solver [61]. Dielectric losses are assumed to be negligible. The length of the line is 1 cm. The frequency dependent p.u.l. parameter in this example was modeled using 2 RL sections using the scheme described in section 3.4. As shown in Figure 3.29, at the near end all the source resistances are assumed to be 50Ω and at the far end all the load capacitances are assumed to be 0.1 pF. A unit step voltage with a rise time of 0.1 ns is

applied to the 50Ω resistor connected to the center line (line 5). Figure 3.30 and Figure 3.31 shows the transient response of the proposed (1 sixth order FEM element) and the conventional lumped model (30 sections) for the far and near end of line 5 and line 1. For their respective orders, the proposed and the conventional lumped model give similar results. In this example, the proposed method required 80% fewer variables when compared to the lumped-segmentation model. The CPU times required to simulate the results using the conventional lumped model was 10.89 sec, and using the proposed was 1.57 sec.

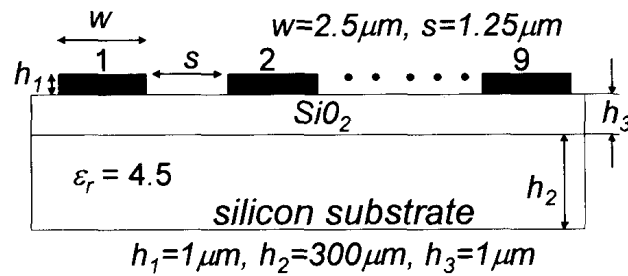


Figure 3.28: Cross-section of 9-coupled interconnect

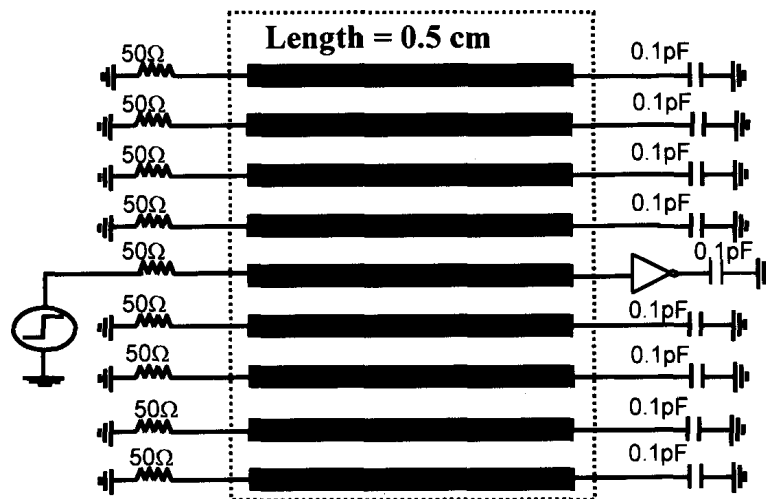


Figure 3.29: On-chip 9-coupled interconnect network

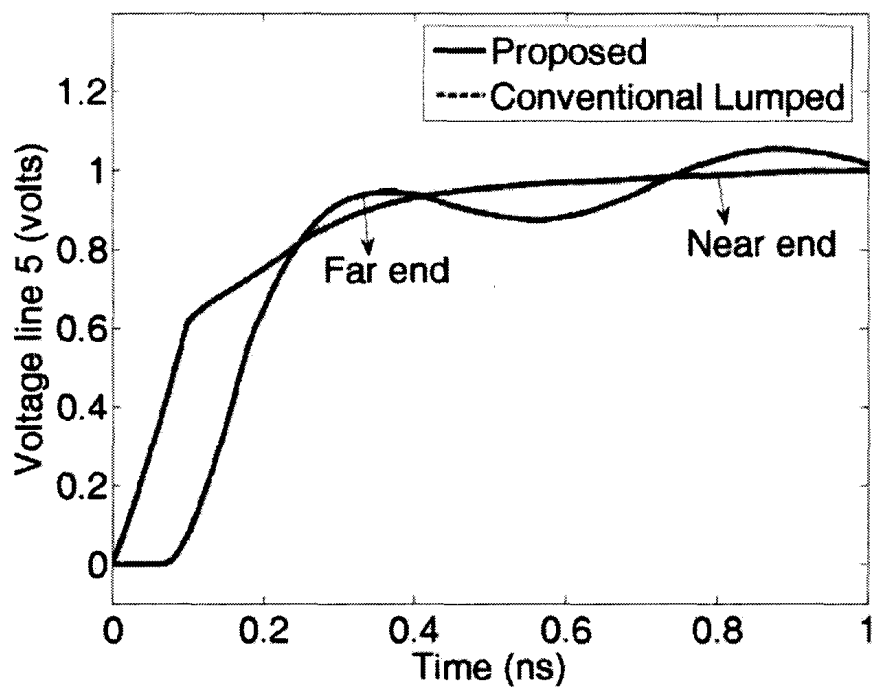


Figure 3.30: Transient response of line 5 (Example3)

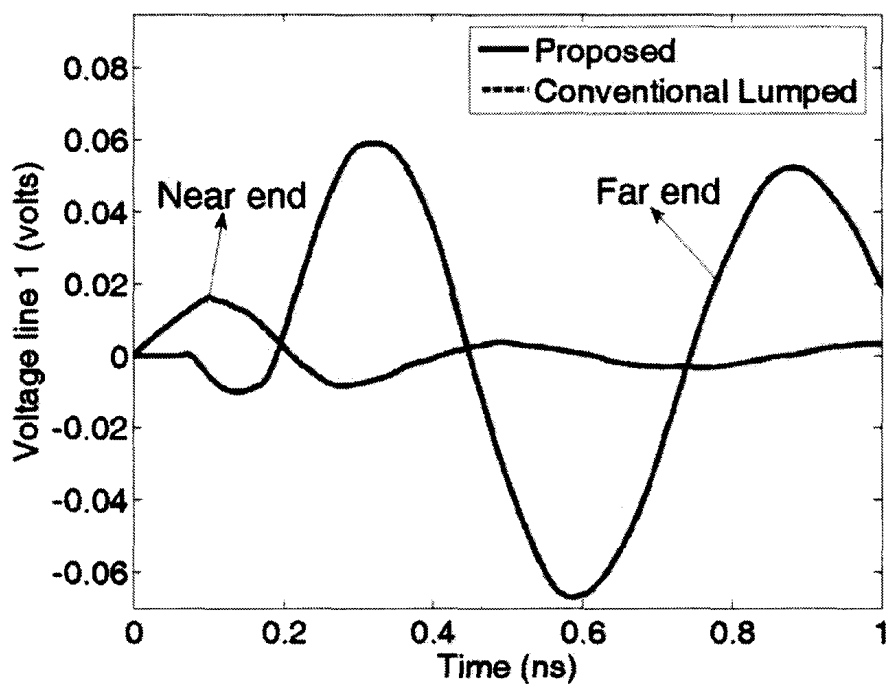


Figure 3.31: Transient response of line 1 (Example3)

Chapter 4

Parameterized Model Order Reduction Techniques for FEM based Full Wave Analysis

4.1 – Introduction

As operating frequencies increase full wave methods such as the Finite Element Method (FEM) become necessary for the analysis of high frequency circuit structures. Such techniques result in very large systems of equations, and model order reduction (MOR) was proven to be very effective in combating such increased complexity. Using traditional MOR, one has to generate a new reduced model each time a design parameter is modified, thus significantly reducing the CPU efficiency. In the recent years, researchers have focused on implicit moment matching techniques based on congruence transformation to derive reduced order models of FEM based microwave systems [45]-[50]. The methods are Krylov subspace methods, and take advantage of the Arnoldi

process in order to achieve more accurate reduced models when compared to explicit moment matching methods [41]-[43]. While they produce efficient and accurate reduced order models, these techniques suffer from a major disadvantage when applied to problems which require optimization and design space exploration. This is due to the fact that reduced order models obtained using current techniques would no longer be valid if a design parameter (such as material property for example) is modified. While Parametric Model Reduction (PMR) techniques have been developed for circuit applications [26], [30],[32] no such method exists which is applicable to FEM problems. Another major difficulty with applying Krylov subspace based reduction to FEM based microwave applications, is that the matrices arising from the FEM equations are not linearly dependent on frequency and thus the system moments do not naturally form a Krylov subspace. This makes it difficult to take advantage of the Arnoldi process. A number of methods [48]-[52] are available in order to reformulate the FEM equations as a linear first order system such that their moments form a Krylov subspace; however, these methods have the effect of making the original system twice as large and also they cannot handle complex frequency dependence introduced in the system due to the frequency dependent parameters.

In this chapter, a PMR method applicable for FEM analysis is proposed which produces parametric reduced order models that are valid over a user defined range of design parameter values. Such an approach is significantly more CPU efficient in optimization and design space exploration problems since a new reduced model is not required when a parameter is modified. The proposed method is based on a

multidimensional Krylov subspace which was used in [26],[30],[32] and has proven to be very effective for circuit problems. It can be shown [30] that the resulting reduced model matches the moments of the original system with respect to frequency as well as the other design parameters and is thus valid over the parameter range of interest. In this thesis, multidimensional Krylov subspace methods are further extended to address both the Krylov incompatibility of the discrete FEM systems and to include design parameters in the reduced order model. The method presented in this chapter performs multidimensional Krylov subspace based reduction directly on the conventional FEM system obtained through discretization of vector wave equation. The new approach does not result in doubling the size of the original system and thus results in a significantly smaller and more efficient reduced model. Furthermore, this technique is applicable to problems which include losses and can also handle FEM systems with complex frequency dependence that may arise due to frequency dependent material properties. Numerical examples demonstrate that this proposed methodology requires fewer unknown variables in the parametric reduced model when compared to reduction techniques that convert the FEM equations to a linear first order system.

The chapter is organized as follows. In Section 4.2 the MOR technique based on Krylov subspace methods that convert the FEM equations into a linear first order system are briefly reviewed. Section 4.3 describes the multidimensional model reduction methodology based on the multidimensional Krylov subspace methods in order to obtain parameterized reduced order models. Section 4.3.1 discusses the PMR technique based on the state space approach and section 4.3.2 presents a new PMR method referred to as the parametric frequency approach to address the Krylov incompatibility of microwave

FEM systems and to include design parameters in the reduced order model. Section 4.3.3 gives a brief note on selecting the order of the reduced model and section 4.3.4 describes the sparsification technique used to sparsify the reduced order models obtained using the PMR technique. Numerical examples are provided in section 4.4 followed by some concluding remarks in section 4.5.

4.2 – Krylov MOR Techniques based on Linear First Order Representations

The FEM formulation of the vector wave equation discussed in Chapter 2 results in a very large matrix system for the case when there is finite conductivity as

$$\left(A_0 + A_1 s + A_2 s^2 + A_3 j\beta(s)\right) \mathbf{e}_s = j\beta(s) \mathbf{b} \quad (4.1)$$

where $s=j\omega$ is the Laplace frequency variable; the propagation constant is expressed as $\beta(s)$ to emphasize that it is a function of frequency; the matrices A_0 , A_1 , A_2 , A_3 , and \mathbf{b} are as given in (2.26)-(2.30).

When there is no finite conductivity, the system in (4.1) is expressed as

$$\left(\tilde{A}_0 + \tilde{A}_1 k + \tilde{A}_2 k^2\right) \mathbf{e}_k = k \mathbf{b} \quad (4.2)$$

where $\mathbf{e}_k \in \mathbb{R}^N$ is the vector of unknown variables in the approximation of \mathbf{E} , $k=j\beta(s)$ and the matrices \tilde{A}_0 , \tilde{A}_1 , and \tilde{A}_2 , are as in (2.32)-(2.34).

Directly reducing (4.1) or (4.2) requires matching the moments of the system explicitly and thus the reduced model is limited to low order approximations [5]. On the other hand, Krylov subspace methods based on congruent transformations calculate the

moments of the system implicitly by taking advantage of the Arnoldi process [76] to achieve high order approximations. To apply Krylov subspace methods to FEM based microwave systems, techniques are available [48]-[52] to reformulate the FEM equations as a linear first order system. These techniques introduce extra unknown variables to convert the second order system of (4.2) to a linear first order representation as

$$(\mathbf{G}' + k\mathbf{C}')\mathbf{X}' = \mathbf{B}' \quad (4.3)$$

where

$$\mathbf{G}' = \begin{bmatrix} \tilde{\mathbf{A}}_1 & \mathbf{I}_N \\ -\tilde{\mathbf{A}}_0 & \mathbf{0} \end{bmatrix}; \mathbf{C}' = \begin{bmatrix} \tilde{\mathbf{A}}_2 & \mathbf{0} \\ \mathbf{0} & \mathbf{I}_N \end{bmatrix}; \mathbf{X}' = \begin{bmatrix} \mathbf{e}_k \\ \mathbf{e}'_x \end{bmatrix}; \mathbf{B}' = \begin{bmatrix} \mathbf{b} \\ \mathbf{0} \end{bmatrix} \quad (4.4)$$

$\mathbf{I}_N \in \mathfrak{R}^{N \times N}$ is the identity matrix and $\mathbf{e}'_x \in \mathfrak{R}^N$ is the vector of extra unknown variables.

The linear first order system of (4.3) is compatible with Krylov subspace methods but has twice the number of unknown variables than that of the conventional FEM system in (4.2). This increase in the number of unknown variables is undesirable since reducing an augmented system may not produce a compact reduced model. Furthermore, these techniques are not applicable to the system of (4.1) due to the presence of the complex frequency dependence of the propagation constant $\beta(s)$.

In order to address the above concerns, a new PMR methodology is presented in section 4.3.2 based on the multidimensional moment matching technique which performs Krylov reduction directly on (4.1) and (4.2) without having to convert the original FEM equations into a linear first order representation. The next section describes the multidimensional model reduction methodology used to derive parameterized reduced order models.

4.3 – Multidimensional Model Reduction Methodology

In this section, we describe a multidimensional model reduction algorithm for the systems in (4.1) and (4.2) to address both the Krylov incompatibility of the discrete conventional FEM systems and to include design parameters in the reduced order model. The main objective of the multidimensional MOR method is to approximate the original system (having a large number of unknowns) with a reduced system (having a small number of unknowns) by capturing the behaviour of the original system with respect to frequency and other design parameters. This can be accomplished by calculating the multidimensional derivatives (moments) of the response of the system. Subsection 4.3.1 describes the multidimensional model reduction methodology and the PMR technique used to derive parameterized reduced order models based on converting the conventional FEM system into linear first order representations in order to perform Krylov subspace based reduction. This technique is referred to as the state space approach [53]. Subsection 4.3.2 describes a new PMR technique based on multidimensional Krylov subspace methods which perform reduction directly on (4.1) and (4.2) without having to convert the FEM equations into a linear first order representation. This is accomplished by using a parametric frequency approach which treats each frequency variables in (4.1) and (4.2) as independent multi frequency parameters.

4.3.1 –PMR Technique based on the State Space Approach

This section discusses a PMR methodology based on the state space approach to derive a parameterized reduced order model for the conventional FEM system in (4.2).

The state approach refers to the technique which converts the conventional FEM system in (4.2) into a linear first order representation as in (4.3) in order to take advantage of the Krylov subspace methods.

4.3.1.1 – Formulation of the Parametric System

The linear system in (4.3), can be expressed as a function of k and the other design parameters $\lambda_1, \dots, \lambda_n$ as

$$(\mathbf{G}(\lambda_1, \dots, \lambda_n) + k\mathbf{C}(\lambda_1, \dots, \lambda_n))\mathbf{X}(k, \lambda_1, \dots, \lambda_n) = \mathbf{B} \quad (4.5)$$

where n is the number of design parameters of interest in the system.

4.3.1.2 – Computation of Multidimensional Subspace

The computation of a multidimensional reduced model begins with the evaluation of the multidimensional subspace. This can be accomplished by calculating the block moments of the system with respect to k and the other design parameters $\lambda_1, \dots, \lambda_n$ including the cross-derivatives as

$$\text{colspan}(\mathbf{Q}) = \text{colspan}(\mathbf{Q}_k \ \mathbf{Q}_{\lambda_1} \ \dots \ \mathbf{Q}_{\lambda_n} \ \mathbf{Q}_x) \quad (4.6)$$

where \mathbf{Q}_k denotes the moments of the system \mathbf{X} with respect to k ; $\mathbf{Q}_{\lambda_1} \ \dots \ \mathbf{Q}_{\lambda_n}$ are the moments of \mathbf{X} with respect to the design parameters $(\lambda_1, \dots, \lambda_n)$ and \mathbf{Q}_x are the cross-derivatives. The system in (4.5) exhibits linear dependency with respect to k and therefore the moments \mathbf{Q}_k can be computed efficiently using techniques based on the Krylov subspace such as the Arnoldi process [2] which was described in section 2.4.2. Similarly, the Arnoldi process can also be used to calculate $\mathbf{Q}_{\lambda_1} \ \dots \ \mathbf{Q}_{\lambda_n}$ for the case

when the variation of the matrices \mathbf{G} and \mathbf{C} with respect to design parameters $(\lambda_1, \dots, \lambda_n)$ are linear.

4.3.1.3 – Model Reduction through Congruent Transformation

The computed multidimensional subspace \mathbf{Q} is a constant real matrix independent of k and the design parameters $(\lambda_1, \dots, \lambda_n)$. The multidimensional reduced model is obtained by a change of variables in (4.5) as

$$\mathbf{X}(k, \lambda_1, \dots, \lambda_n) = \mathbf{Q}\hat{\mathbf{X}}(k, \lambda_1, \dots, \lambda_n) \quad (4.7)$$

where $\hat{\mathbf{X}} \in \mathfrak{R}^q$ and $q = q_k + q_x + \sum_{i=1}^n q_{\lambda_i}$; q_k, q_{λ_i} and q_x are the number of columns in $\mathbf{Q}_k, \mathbf{Q}_{\lambda_i}$ and \mathbf{Q}_x , respectively. The reduced order system is obtained by a congruence transformation by substituting (4.7) into (4.5) and pre-multiplying by \mathbf{Q}^T , as

$$(\hat{\mathbf{G}}(\lambda_1, \dots, \lambda_n) + k\hat{\mathbf{C}}(\lambda_1, \dots, \lambda_n))\hat{\mathbf{X}}(k, \lambda_1, \dots, \lambda_n) = \hat{\mathbf{B}} \quad (4.8)$$

where

$$\hat{\mathbf{G}} = \mathbf{Q}^T \mathbf{G} \mathbf{Q} \quad \hat{\mathbf{C}} = \mathbf{Q}^T \mathbf{C} \mathbf{Q} \quad \hat{\mathbf{B}} = \mathbf{Q}^T \mathbf{B} \quad (4.9)$$

It is to be noted that the size of the reduced system q is very small compared to the size of the original system N i.e., $q \ll N$. Once the response of the reduced model is obtained from (4.8), the response at any node of the original system can be computed using (4.7). It can be shown that the reduced system preserves the dominant eigen values of the original system [30].

The above described PMR technique based on the state space approach derived a parameterized reduced order system given by (4.8) as a function of frequency and a set of other design parameters of interest. The key advantage of this technique is that the reduced order models derived using this method are valid over the parameter ranges of interest and hence does not require redoing the model order reduction process each time a parameter is modified in the problem. However, this method has the effect of making the original system twice large in order to derive an efficient parameterized reduced order model based on Krylov subspace techniques. Moreover, they cannot handle systems such as in (4.1) which have complex frequency dependence $\beta(s)$ introduced in the model due to frequency dependent boundary conditions.

In order to address the above issues, a new PMR technique based on multidimensional Krylov subspace methods is presented in the next section.

4.3.2 – PMR technique based on the Parametric Frequency

Approach

The PMR described in this section performs multidimensional Krylov subspace based reduction directly on the conventional FEM system in (4.1) and (4.2) obtained through the discretization of the vector wave equation. The method does not result in doubling the size of the original system in order to derive parameterized reduced order models. Furthermore, the method is also applicable to problems which include complex frequency dependence that can be introduced in the system due to frequency dependent material properties and frequency dependent boundary conditions.

4.3.2.1 – Formulation of the Multidimensional System

The proposed algorithm is based on multidimensional Krylov subspace methods to perform reduction directly on (4.1) and (4.2). In order to accomplish this, the frequency variables in (4.1) and (4.2) are treated as independent multi-frequency parameters. For the case of (4.1), the system is expressed as

$$(s_1 \mathbf{A}_0 + \mathbf{A}_1 + s \mathbf{A}_2 + s_2 \mathbf{A}_3) \mathbf{e}_s = s_2 \mathbf{b} \quad (4.10)$$

where

$$s_1 = \frac{1}{s}; \quad s_2 = \frac{j\beta(s)}{s} \quad (4.11)$$

Since the frequency variables s , s_1 and s_2 are linear with respect to (4.10), multidimensional Krylov subspace method can be used to reduce the system, where the moments of s , s_1 and s_2 are calculated using the Arnoldi algorithm [76]. It should be noted that for high frequency microwave applications, the frequency parameters s_1 and s_2 are quite small and hence very few moments are required for s_1 and s_2 to capture the original response.

Similarly, the system in (4.2) can also be expressed as a function of multi-frequency variables as

$$(k_1 \tilde{\mathbf{A}}_0 + \tilde{\mathbf{A}}_1 + k \tilde{\mathbf{A}}_2) \mathbf{e}_k = \mathbf{b} \quad (4.12)$$

where

$$k_1 = \frac{1}{k} \quad (4.13)$$

The system of (4.12) is reduced using multidimensional Krylov subspace method where the moments of k and k_1 are obtained using the Arnoldi algorithm. For high frequency microwave problems, the frequency parameter k_1 is also small and hence very few moments are required for k_1 to capture the original response.

Numerical examples presented in Section 4.4 have shown that to reduce the systems in (4.10) and (4.12), only one moment was required for each s_1 , s_2 and k_1 .

4.3.2.2 – Parametric System Formulation

The systems of (4.10) and (4.12) can be expressed as a function of the frequency variables and other design parameters as

$$(s_1 \mathbf{A}_0(\bar{\lambda}) + \mathbf{A}_1(\bar{\lambda}) + s \mathbf{A}_2(\bar{\lambda}) + s_2 \mathbf{A}_3(\bar{\lambda})) \mathbf{e}_s = s_2 \mathbf{b}(\bar{\lambda}) \quad (4.14)$$

$$(k_1 \tilde{\mathbf{A}}_0(\bar{\lambda}) + \tilde{\mathbf{A}}_1(\bar{\lambda}) + k \tilde{\mathbf{A}}_2(\bar{\lambda})) \mathbf{e}_k = \mathbf{b}(\bar{\lambda}) \quad (4.15)$$

where $\bar{\lambda} = \lambda_1, \lambda_2, \dots, \lambda_n$ are the design parameters of interest in the system.

4.3.2.3 – Computation of the Multidimensional Subspace

The multidimensional subspace can be constructed by calculating the block moments of the system with respect to the frequency variables, and the other design parameters ($\lambda_1, \dots, \lambda_n$) including the cross-derivatives using techniques elaborated in [30]. For the system of (4.14), an orthonormal matrix \mathbf{Q}_I is constructed using the moments of the system with respect to the frequency variables (s, s_1, s_2) and with respect to design parameters ($\lambda_1, \dots, \lambda_n$), as well as the cross moments, as

$$\text{colspan}(\mathbf{Q}_1) = \text{colspan}(\mathbf{Q}_s \mathbf{Q}_{s_1} \mathbf{Q}_{s_2} \mathbf{Q}_{\lambda_1} \dots \mathbf{Q}_{\lambda_n} \mathbf{Q}_x) \quad (4.16)$$

where $\mathbf{Q}_s, \mathbf{Q}_{s_1}$ and \mathbf{Q}_{s_2} denote the moments of the system e_s with respect to s, s_1 and s_2 , respectively; $\mathbf{Q}_{\lambda_1} \dots \mathbf{Q}_{\lambda_n}$ are the moments of e_s with respect to the design parameters $(\lambda_1, \dots, \lambda_n)$ and \mathbf{Q}_x are the cross-derivatives. The system in (4.14) exhibits linear dependency with respect to s, s_1 , and s_2 therefore the moments $\mathbf{Q}_s, \mathbf{Q}_{s_1}$ and \mathbf{Q}_{s_2} can be computed efficiently using techniques based on the Krylov subspace such as the Arnoldi process [76]. Similarly, the Arnoldi process can also be used to calculate $\mathbf{Q}_{\lambda_1} \dots \mathbf{Q}_{\lambda_n}$ for the case when the variation of the system matrices with respect to design parameters $(\lambda_1, \dots, \lambda_n)$ are linear.

For the system of (4.15) the orthonormal matrix \mathbf{Q}_2 is constructed as

$$\text{colspan}(\mathbf{Q}_2) = \text{colspan}(\mathbf{Q}_k \mathbf{Q}_{k_1} \mathbf{Q}_{\lambda_1} \dots \mathbf{Q}_{\lambda_n} \mathbf{Q}_x) \quad (4.17)$$

where \mathbf{Q}_k and \mathbf{Q}_{k_1} denote the moments of the system e_k with respect to k and k_1 , respectively; $\mathbf{Q}_{\lambda_1} \dots \mathbf{Q}_{\lambda_n}$ are the moments of e_k with respect to the design parameters $(\lambda_1, \dots, \lambda_n)$ and \mathbf{Q}_x are the cross-derivatives. The system (4.15) exhibits linear dependency with respect to k and k_1 and therefore the moments \mathbf{Q}_k and \mathbf{Q}_{k_1} can be computed efficiently using the Arnoldi process.

4.3.2.4 – MOR Through Congruent Transformation

The computed multidimensional subspace matrix \mathbf{Q}_1 and \mathbf{Q}_2 in (4.16) and (4.17), respectively are constant real matrices independent of the frequency variables and the

design parameters. For the system of (4.14) the multidimensional reduced model is obtained by a change of variables as

$$\mathbf{e}_s = \mathbf{Q}_1 \hat{\mathbf{e}}_s \quad (4.18)$$

where $\hat{\mathbf{e}}_s \in \mathbb{R}^q$; $q = q_s + \sum_{i=1}^2 q_{s_i} + \sum_{i=1}^n q_{\lambda_i} + q_x$; q_s , q_{s_i} , q_{λ_i} and q_x are the number of columns in \mathbf{Q}_s , \mathbf{Q}_{s_i} , \mathbf{Q}_{λ_i} and \mathbf{Q}_x respectively. The parametric reduced order system is obtained by a congruence transformation by substituting (4.18) into (4.14) and pre-multiplying by \mathbf{Q}_1^T , as

$$(s_1 \hat{\mathbf{A}}_0(\bar{\lambda}) + \hat{\mathbf{A}}_1(\bar{\lambda}) + s \hat{\mathbf{A}}_2(\bar{\lambda}) + s_2 \hat{\mathbf{A}}_3(\bar{\lambda})) \hat{\mathbf{e}}_s = s_2 \hat{\mathbf{b}}(\bar{\lambda}) \quad (4.19)$$

where

$$\begin{aligned} \hat{\mathbf{A}}_0 &= \mathbf{Q}_1^T \mathbf{A}_0 \mathbf{Q}_1; & \hat{\mathbf{A}}_1 &= \mathbf{Q}_1^T \mathbf{A}_1 \mathbf{Q}_1; & \hat{\mathbf{A}}_2 &= \mathbf{Q}_1^T \mathbf{A}_2 \mathbf{Q}_1; \\ \hat{\mathbf{A}}_3 &= \mathbf{Q}_1^T \mathbf{A}_3 \mathbf{Q}_1; & \hat{\mathbf{b}} &= \mathbf{Q}_1^T \mathbf{b}; \end{aligned} \quad (4.20)$$

Substituting (4.11) into (4.19) and multiplying by s on both sides, results in a parametric reduced order system corresponding to (4.1) as

$$(\hat{\mathbf{A}}_0(\bar{\lambda}) + \hat{\mathbf{A}}_1(\bar{\lambda})s + \hat{\mathbf{A}}_2(\bar{\lambda})s^2 + \hat{\mathbf{A}}_3(\bar{\lambda})j\beta(s)) \hat{\mathbf{e}}_s = \beta(s) \hat{\mathbf{b}}(\bar{\lambda}) \quad (4.21)$$

A similar approach to obtain the multidimensional reduced model for the system of (4.15) begins with a change of variables as

$$\mathbf{e}_k = \mathbf{Q}_2 \hat{\mathbf{e}}_k \quad (4.22)$$

where $\hat{\mathbf{e}}_k \in \mathbb{R}^q$; $q = q_k + q_{k_1} + \sum_{i=1}^n q_{\lambda_i} + q_x$; q_k , q_{k_1} , q_{λ_i} and q_x are the number of columns in \mathbf{Q}_k , \mathbf{Q}_{k_1} , \mathbf{Q}_{λ_i} and \mathbf{Q}_x respectively. The parametric reduced order system is obtained by a congruence transformation by substituting (4.22) into (4.15) and pre-multiplying by \mathbf{Q}_2^T , as

$$(k_1 \hat{\tilde{A}}_0(\bar{\lambda}) + \hat{\tilde{A}}_1(\bar{\lambda}) + k \hat{\tilde{A}}_2(\bar{\lambda})) \hat{e}_k = \hat{b}(\bar{\lambda}) \quad (4.23)$$

where

$$\begin{aligned} \hat{\tilde{A}}_0 &= \mathbf{Q}_2^T \tilde{\mathbf{A}}_0 \mathbf{Q}_2; & \hat{\tilde{A}}_1 &= \mathbf{Q}_2^T \tilde{\mathbf{A}}_1 \mathbf{Q}_2; \\ \hat{\tilde{A}}_2 &= \mathbf{Q}_2^T \tilde{\mathbf{A}}_2 \mathbf{Q}_2; & \hat{b} &= \mathbf{Q}_2^T b \end{aligned} \quad (4.24)$$

Substituting (4.13) into (4.23) and multiplying by k on both sides, results in a parametric reduced order system corresponding to (4.2) as

$$\left(\hat{\tilde{A}}_0(\bar{\lambda}) + \hat{\tilde{A}}_1(\bar{\lambda})k + \hat{\tilde{A}}_2(\bar{\lambda})k^2 \right) \hat{e}_k = k \hat{b}(\bar{\lambda}) \quad (4.25)$$

The size of the reduced system depends on the order q which is very small compared to the size of the original system N (i.e., $q \ll N$). Once the response of the reduced model is obtained from (4.21) and (4.25), the response at any node of the original system can be computed using (4.18) or (4.22) respectively.

An important advantage of this formulation is that the parameterized reduced order models of (4.21) and (4.25) preserve the original structure of the FEM formulation. Since (4.21) and (4.25) have linear and quadratic dependence with respect to frequency, they require fewer unknown variables when compared to the linear first order reduced models in (4.8) that were derived by the state space approach. Furthermore, the parametric frequency approach provides a flexible way to perform Krylov subspace reduction directly on the FEM system without having to introduce extra unknown variables. Numerical examples demonstrate that the parameterized reduced order models of (4.21) and (4.25) are more compact and require fewer unknown variables when compared to reduction techniques that convert the FEM equations to a linear first order representation.

4.3.3 –Selecting the Order of the Reduced Model

The accuracy of the reduced model depends on the order q . The value of q must be large enough to capture the frequency and parameter variances of interest and small enough for the reduced model to be computationally efficient. To select the appropriate order q , error bounds are required to estimate the accuracy of the reduced systems in (4.8), (4.21) and (4.25) with respect to the original systems of (4.1) and (4.2). Some interesting error bounds in [77]-[79] could be applied to automatically select the order of the reduced models for in (4.8),(4.21) and (4.25); however, the implementation of these methods require extra memory resources. In this work, the approach used to estimate the accuracy of (4.8), (4.21) and (4.25) is to compute the differences between two successive orders of approximations as described in [18]. If the error difference between the two models is below a given tolerance, the reduced model is assumed to be accurate and the reduction process is terminated. This approach is computationally efficient and does not require additional memory resources.

4.3.4 –Sparsification of the Reduced Model

Model order reduction through the congruent transformation process typically results in reduced order matrices that degrade the sparsity of the reduced order model. Consequently, the dense reduced model presents storage and simulation run-time problems. In order to overcome this issue, diagonalization methods were presented in [79] to construct sparse reduced order models. In the proposed work, the sparsification of

the reduced order models obtained using the parametric frequency approach and state space approach were performed by applying the method in [79].

In order to sparsify the reduced model obtained using the state space approach of reduction, the reduced matrices $\hat{G}(\lambda_1, \dots, \lambda_n)$ and $\hat{C}(\lambda_1, \dots, \lambda_n)$ in (4.8) are evaluated at specific values taken on by the design parameters that affect $\hat{C}(\lambda_1, \dots, \lambda_n)$ and $\hat{G}(\lambda_1, \dots, \lambda_n)$. After having evaluated the matrices $\hat{G}(\lambda_1, \dots, \lambda_n)$ and $\hat{C}(\lambda_1, \dots, \lambda_n)$ at specific design parameter values, equation (4.8) can be rewritten as

$$(I + k\hat{G}^{-1}\hat{C})\hat{X} = \hat{B} \quad (4.26)$$

where I is the identity matrix.

A standard eigenvalue decomposition technique can then be employed on the dense matrix $\hat{G}^{-1}\hat{C}$ resulting in

$$\hat{G}^{-1}\hat{C} = S\Lambda S^{-1} \quad (4.27)$$

where Λ is a diagonal matrix that contains the eigen values. Since $\hat{G}^{-1}\hat{C}$ is a real matrix any complex eigen value or eigen vector will have a conjugate and hence, real matrices can be obtained using the following similarity transform

$$S_r = SP^{-1} \text{ and } \Lambda_r = P\Lambda P^{-1} \quad (4.28)$$

where the entries in the transformation matrix P are defined in the following manner

- If $A_{i,i}$ is real, $P_{i,i} = 1$
- If $A_{i,i} = \bar{A}_{i+1,i+1}$, $P_{i:i+1, i:i+1} = \begin{bmatrix} 1 & 1 \\ j & -j \end{bmatrix}$

The eigen decomposition of the real matrix $\hat{G}^{-1}\hat{C}$ can then be expressed as

$$\hat{\mathbf{G}}^{-1}\hat{\mathbf{C}} = \mathbf{S}_r \Lambda_r \mathbf{S}_r^{-1} \quad (4.29)$$

Using this eigen value decomposition, equation (4.26) becomes

$$(\mathbf{I} + k\Lambda_r)\tilde{\mathbf{X}} = \tilde{\mathbf{B}} \quad (4.30)$$

where

$$\tilde{\mathbf{X}} = \mathbf{S}_r^{-1}\hat{\mathbf{X}} \quad \tilde{\mathbf{B}} = \mathbf{S}_r^{-1}\hat{\mathbf{G}}^{-1}\hat{\mathbf{B}} \quad (1.31)$$

The resulting equation (4.30) characterizes a real sparse reduced order model that can be very efficient for storage and simulation run time.

In order to sparsify the reduced model obtained using the parametric frequency approach, the reduced matrices $\hat{\mathbf{A}}_0(\bar{\lambda})$, $\hat{\mathbf{A}}_1(\bar{\lambda})$ and $\hat{\mathbf{A}}_2(\bar{\lambda})$ in (4.25) are evaluated at specific values taken on by the design parameters that affect $\hat{\mathbf{A}}_0(\bar{\lambda})$, $\hat{\mathbf{A}}_1(\bar{\lambda})$ and $\hat{\mathbf{A}}_2(\bar{\lambda})$. Once the matrices $\hat{\mathbf{A}}_0(\bar{\lambda})$, $\hat{\mathbf{A}}_1(\bar{\lambda})$ and $\hat{\mathbf{A}}_2(\bar{\lambda})$ are evaluated at specific design parameter values, the second order system can be converted to a linear state space form using (4.3)-(4.4) in order to perform sparsification using a similar approach as described for the sparsification of state space approach.

Numerical examples presented in the next section demonstrate the efficiency of sparsification of the reduced order models. In the proposed work, the sparsification was not performed for the reduced system in (4.21) due to the presence of the frequency dependent term $\beta(s)$ in the reduced model. Sparsification of the reduced order system that exhibit frequency dependent parameters is still a topic to be researched.

4.4 – Numerical Examples

In this section, three numerical examples are presented. Within the context of this section, parametric frequency approach refers to the parameterized reduction algorithm described in Section 4.3.2, which treats each frequency variable in (4.1) or (4.2) as multi-frequency parameters to perform multidimensional Krylov subspace reduction. State space approach refers to the parameterized reduction technique described in section 4.3.1 [53], which converts the conventional FEM system based on the vector wave equation into a linear first order representation. Modified Gram Schmidt approach refers to the parameterized reduction technique that explicitly matches the moments of (4.1) or (4.2) using modified Gram Schmidt to construct the orthonormal matrix. All computations are performed on a Pentium 4 (2.80 GHz) PC with 2048 MB memory. The developed algorithms were programmed in MATLAB [80] and the LU decompositions were performed using the direct method of [81].

4.4.1 – Example 4.1

Dielectric Post Inside a WR90 Waveguide.

This problem considers a dielectric post inside a WR90 waveguide which was proposed in [44],[53] (Figure 4.1). This example was considered to study the scattering effects due to the variations in the dielectric permittivity of the post inside the waveguide. Parameterized model order reduction techniques are used to model variations with respect to frequency and dielectric permittivity. The structure was discretized using 6699 tetrahedral elements; the total number of FEM degrees of freedom in the original system of (4.2) is equal to 10288. The range of interest of the relative permittivity ϵ_r of the

dielectric obstacle is from 6 to 10 and bandwidth of interest is from 8 GHz to 12 GHz. The expansion point for both the frequency variables and electric permittivity are chosen to be in the middle of the range of interest. In this example, the parametric frequency approach is compared with the state space approach. To make a fair comparison the size of the parameterized reduced order model for the state space approach will be twice the size of the parametric frequency approach, since state space approach yields first order models (i.e. linear dependency with respect to k) while the parametric frequency approach yields second order models (i.e. linear and quadratic dependency with respect to k). To reduce the system of (4.2) using the parametric frequency approach required 16 moments for k , 1 moment for k_1 and 2 moments for the parameter ε_r (total number of moments 19). For the state space approach, 34 moments for k and 4 moments for ε_r were used (total number of moments 38) to obtain a reduced order system twice the size of the parametric frequency model. Figure 4.2 to Figure 4.4 shows the magnitude of the reflection coefficient S_{11} as a function of frequency for different relative permittivity values at $\varepsilon_r = 6$, $\varepsilon_r = 8$, and $\varepsilon_r = 10$ for the original system and the parameterized reduced models given by the parametric frequency approach and the state space approach. For $\varepsilon_r = 8$, both parametric frequency approach and the state space approach match the response of the original system as shown in Figure 4.3. However as the relative permittivity ε_r deviates from the point of expansion of $\varepsilon_r = 8$ the accuracy of the frequency response for the state space approach deteriorates as shown in Figure 4.2 for $\varepsilon_r = 6$ and Figure 4.4 for $\varepsilon_r = 10$. To match the response of the original system over the entire range of interest using a single expansion point, the state space approach required a total of 87 moments as reported in [53] and shown in Figure 4.5. For this example the

size of the parametric frequency approach is 4 times smaller than the state space approach. Table 4.1 compares the total size and CPU times to generate the parametric reduced order systems for both the approaches. It should be noted that the state space approach makes use of the modified block Arnoldi approach proposed in [48], and hence the generation of Krylov subspace can be formulated at the same computational cost of the solution of (4.2) at a single frequency. The CPU times taken to generate the 3D plot of Figure 4.5 using 100 frequency points and 15 different values of the relative permittivity of the dielectric obstacle ranging from $\epsilon_r = 6$ to 10 for the original system and for the reduced systems obtained using the parametric frequency approach and the state space approach with and without sparsification is shown in Table 4.2. The total simulation time using the sparse reduced order models includes the time taken for eigen decompositions performed at each design parameter point in order to sparsify the reduced order model. It is clear from Table 4.2, that once the reduced models are sparsified, the total simulation time taken to solve the sparse reduced model is negligibly small when compared to the original simulation time.

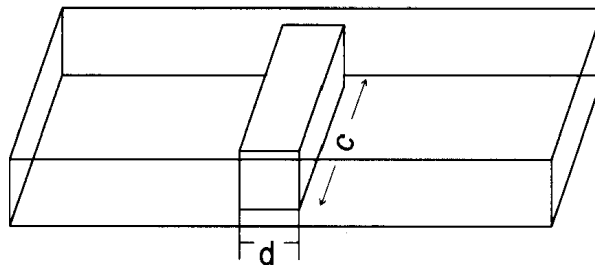


Figure 4.1: Dielectric Post inside WR90 waveguide ; $d= 6$ mm, $c = 12$ mm.

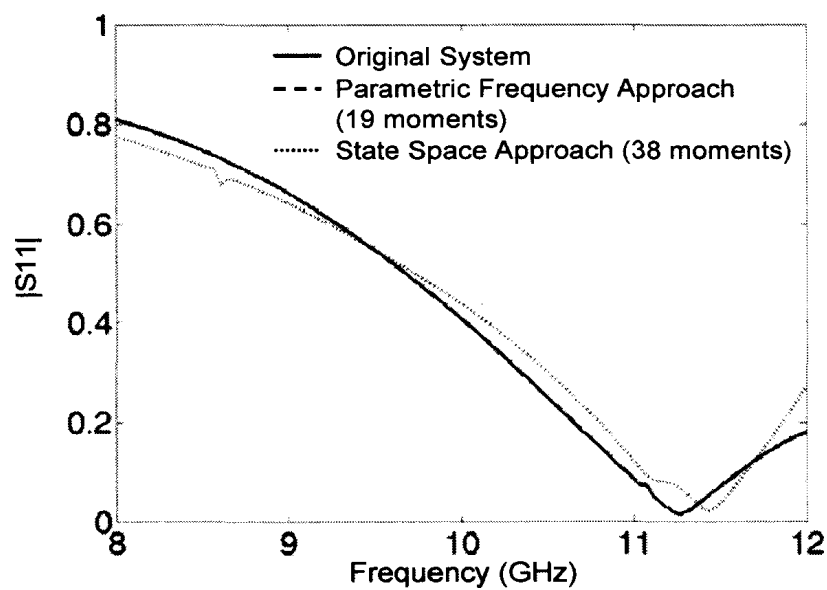


Figure 4.2: Frequency response comparison of the magnitude of reflection coefficient for Example 1 when $\epsilon_r = 6$.

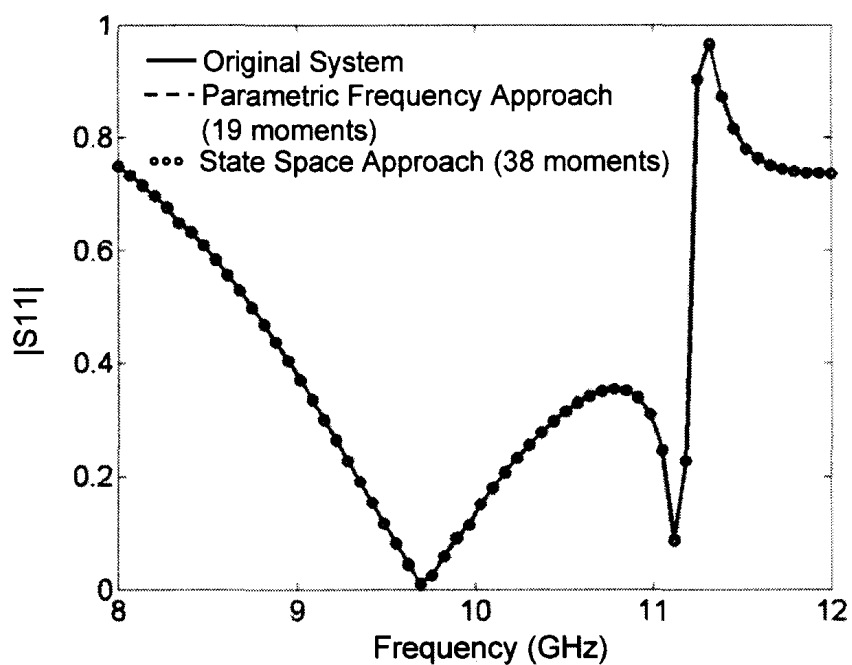


Figure 4.3: Frequency response comparison of the magnitude of reflection coefficient for Example 1 when $\epsilon_r = 8$.

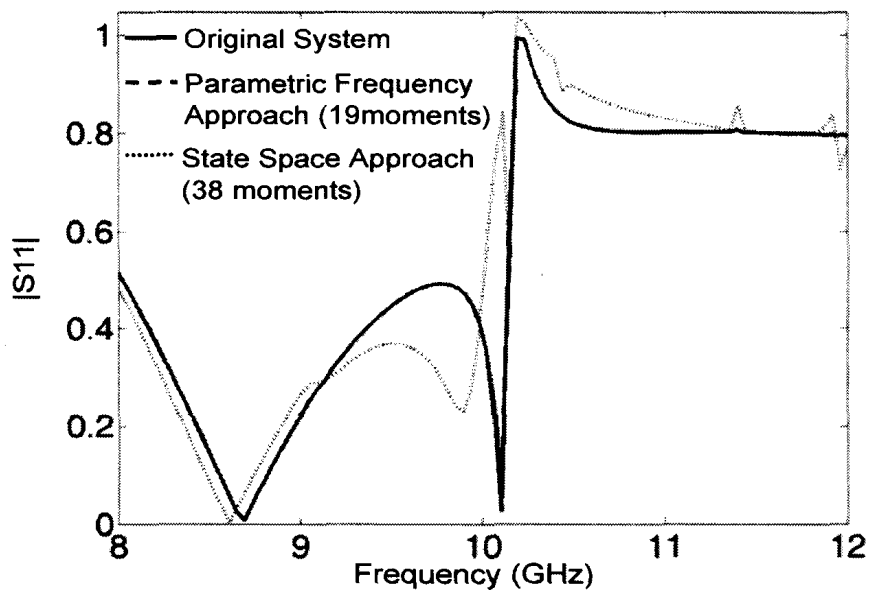


Figure 4.4: Frequency response comparison of the magnitude of reflection coefficient for Example 1 when $\epsilon_r = 10$.

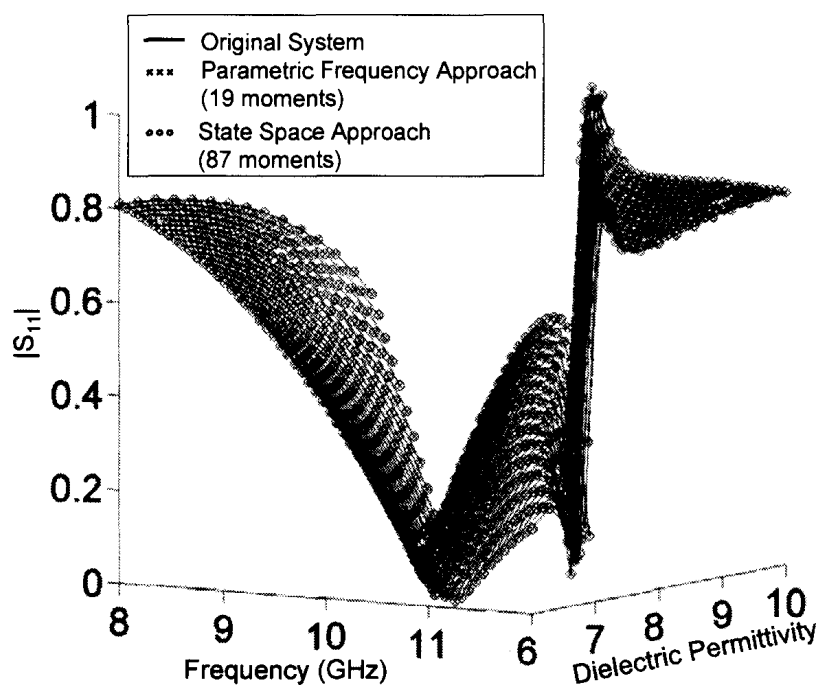


Figure 4.5: 3D comparison of the magnitude of reflection coefficient (S_{11}) for Example 1 with different dielectric permittivity values.

TABLE 4.1
COMPUTATIONAL INFORMATION – EXAMPLE 1

Solution Method	Size	CPU Time to generate reduced system	Savings in Size
Original System	10288	-	-
Parametric Frequency Approach	38	1.59 sec	99.63%
State Space Approach	174	1.74 sec	98.31%

TABLE 4.2
COMPUTATIONAL INFORMATION – EXAMPLE 1

Solution Method		Size	Eigen Decomposition (Sparsification)	Simulation Time	Total Solution Time	Speed Up Factor
Original System		10288	-	1641 sec	1641 sec	-
Parametric Frequency Approach	Without Sparsification	38	-	7.02 sec	7.02 sec	234
	With Sparsification	76	1.17 sec	0.7035 sec	1.874 sec	876
State Space Approach	Without Sparsification	174	-	68.85 sec	68.85 sec	24
	With Sparsification	174	3.98 sec	0.945 sec	4.925 sec	333

4.4.2 – Example 4.2

H-plane Waveguide T-junction loaded with a partial height cylindrical post

An H-plane WR75 (0.75in x 0.375in) rectangular waveguide T-junction loaded with a cylindrical post proposed in [70],[82] is shown in Figure 4.6. This example is important to test due to the fact that the cylindrical post loaded inside the waveguide could be a metallic conducting post and the original system for the corresponding problem exhibits complex frequency dependence due to the presence of $\beta(s)$ in (4.1). Hence the efficiency and validity of the parametric frequency approach could be tested for this special case. The radius and height of the post are chosen as 0.05in and 0.3in respectively. The waveguide structure was discretized using 14468 tetrahedral elements; the total number of FEM degrees of freedom in the original system of (4.1) is equal to 17875. The bandwidth of interest for this problem is 10GHz-15GHz. A parameterized reduced order model is generated which can be used to investigate the scattering effects of two different cases: a) when the cylindrical post is a metallic conducting post (i.e, $\sigma = 5.889e7$ and $\varepsilon_r = 1$); b) when the post is a lossy dielectric post (i.e, $\sigma = 0$ and the relative complex permittivity varies from $\varepsilon_r = 1-j0.1$ to $4-j0.25$). To derive a compact parametric reduced order model two expansion points were selected corresponding to the two cases: a) frequency = 12.5GHz, $\sigma = 5.889e7$ and $\varepsilon_r = 1$; b) frequency = 12.5GHz, $\sigma = 0$ and $\varepsilon_r = 2.5-j0.175$.

In this example, since the frequency dependent term $\beta(s)$ is present in (4.1) the PMR technique cannot be performed based on the state space approach. Hence the parameterized reduced order models are derived for the system of (4.1) using the parametric frequency approach and the traditional modified Gram Schmidt approach. To derive equivalent size reduced order models for both approaches, the following moments were selected. The parametric frequency approach used 8 moments for s , 1 moment for s_1 , 1 moment for s_2 , 1 moment for σ and 1 moment for ε_r , for the expansion of case a); and 8 moments for s , 1 moment for s_1 , 1 moment for s_2 , 1 moment for σ and 3 moments for ε_r , for the expansion of case b) (total number of moments 26). The modified Gram Schmidt approach used 10 moments for s , 1 moment for σ and 1 moment for ε_r , for the expansion of case a); and 10 moments for s , 1 moment for σ and 3 moments for ε_r , for the expansion of case b) (total number of moments 26). Figure 4.7 to Figure 4.9 shows the magnitude S_{11} as a function of frequency for different parameter values when $\sigma = 5.889e7$ and $\varepsilon_r = 1$; when $\sigma = 0$ and $\varepsilon_r = 1-j0.1$ and when $\sigma = 0$ and $\varepsilon_r = 4-j0.25$. As expected, the parametric frequency approach is able to achieve better accuracy than modified Gram Schmidt approach, since it takes advantage of the Arnoldi algorithm to calculate moments. For this example, modified Gram Schmidt failed to capture the frequency moments beyond tenth moment with respect to s and was not able to capture entire range of interest without using additional expansion points. On the other hand, parametric frequency approach required 10 moments for s , 1 moment for s_1 , 1 moment for s_2 , 1 moment for σ and 1 moment for ε_r , for the expansion of case a); and 14 moments for s , 1 moment for s_1 , 1 moment for s_2 , 1 moment for σ , 10 moments for ε_r , and 7 cross moments for the expansion of case b) (total number of moments 48) to

capture the entire range of interest as shown in Figure 4.10 and Figure 4.11 to Figure 4.13. The CPU times taken by the original system and the reduced system using parametric frequency approach in order to generate the 3D plots of Figure 4.11 to Figure 4.13 using 100 frequency points and 10 different values of the complex relative permittivity of the post ranging from $\epsilon_r = 1-j0.1$ to $4-j0.25$ are shown in Table 4.3. A speed up of 99 was achieved using the reduced system obtained through the parametric frequency approach when compared to the original simulation time. The sparsification of the reduced system was not performed for this example due to the presence of the frequency dependent term $\beta(s)$ in the reduced system. Table 4.3 also compares the total size of both the systems and CPU time taken to generate the parametric reduced order model using parametric frequency approach.

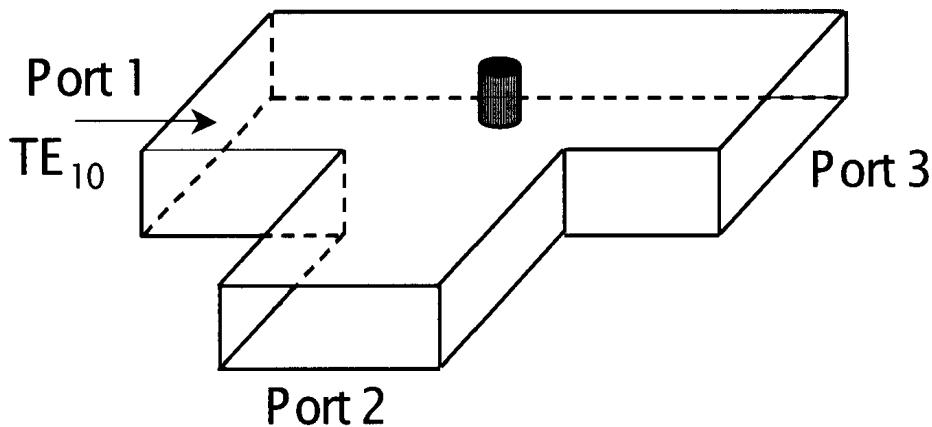


Figure 4.6: H-plane waveguide T-junction loaded with a partial height post. (Example 2)

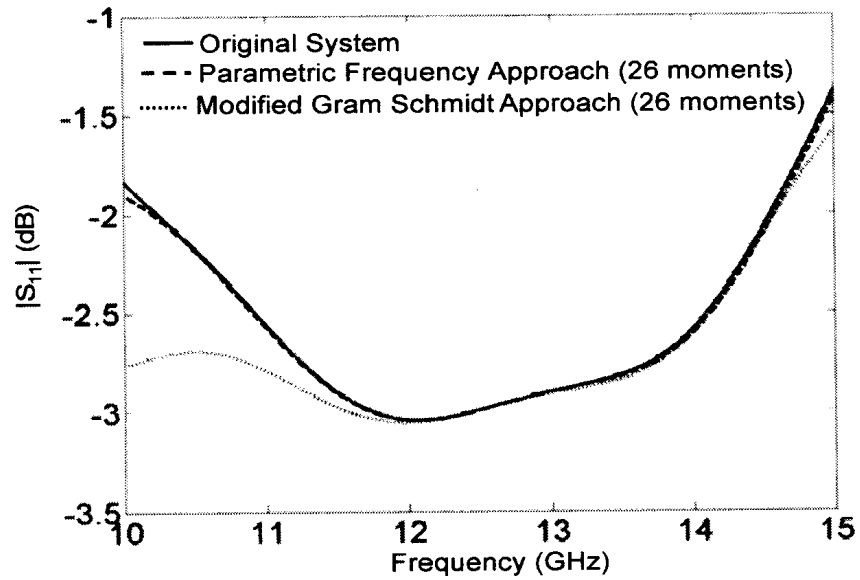


Figure 4.7: Frequency response comparison of the magnitude of reflection coefficient for Example 2 at parameter values $\sigma = 5.889e7$ and $\epsilon_r = 1$

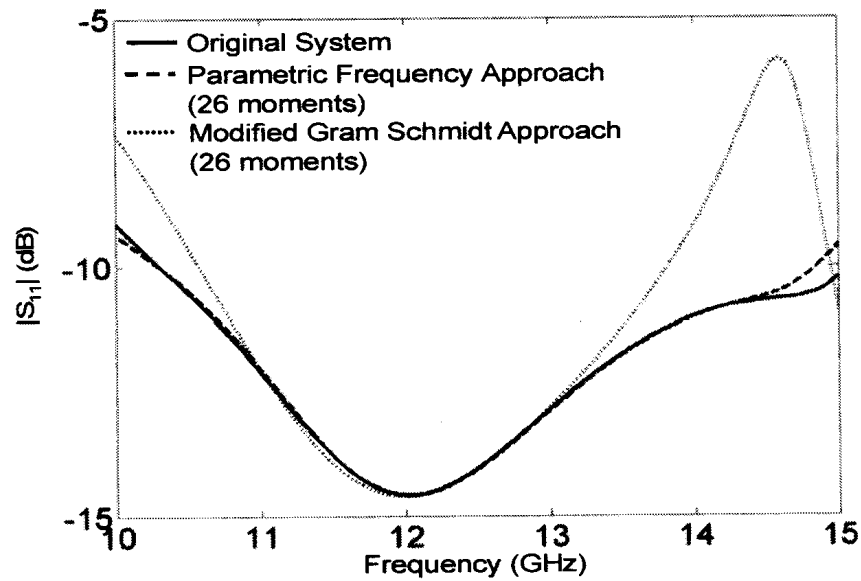


Figure 4.8: Frequency response comparison of the magnitude of reflection coefficient for Example 2 at parameter values $\sigma = 0$ and $\epsilon_r = 1 - j0.1$.

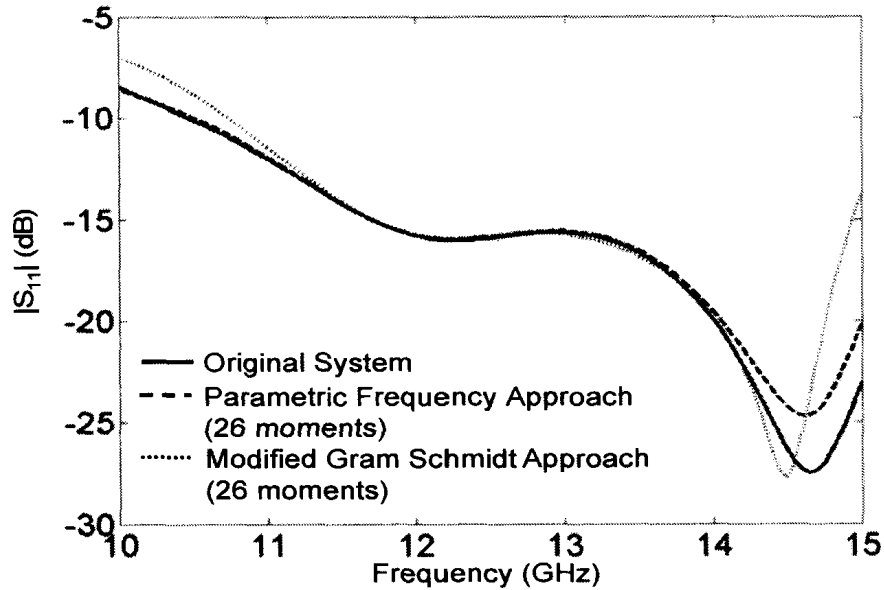


Figure 4.9: Frequency response comparison of the magnitude of reflection coefficient for Example 2 at parameter values $\sigma = 0$ and $\epsilon_r = 4 - j0.25$.

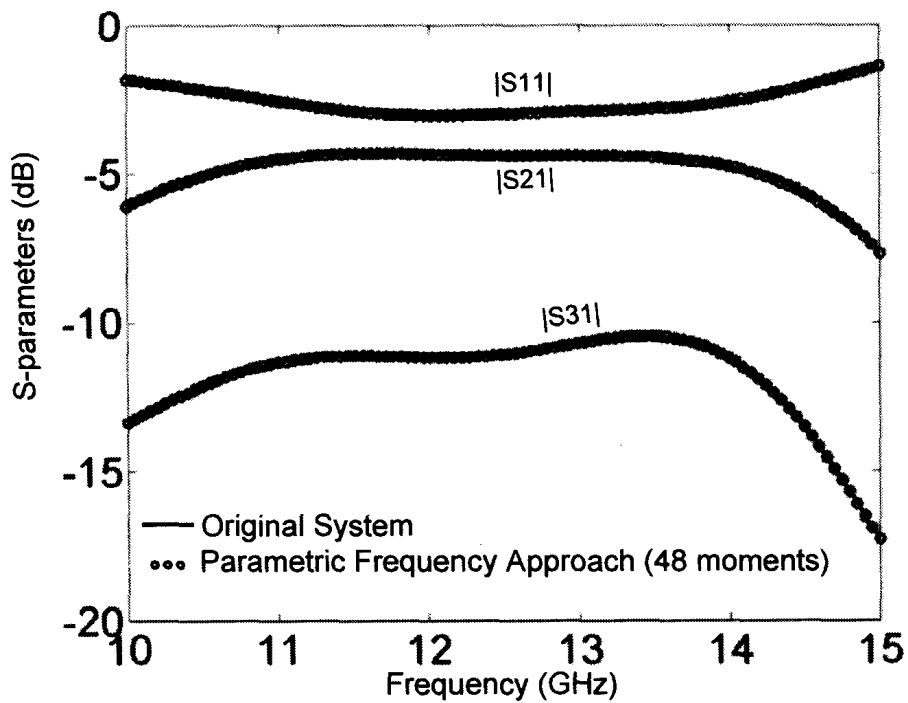


Figure 4.10: Comparison of Frequency response of S-parameters for Example 2 for the case when post is a metal ($\sigma = 5.889e7$ and $\epsilon_r = 1$).

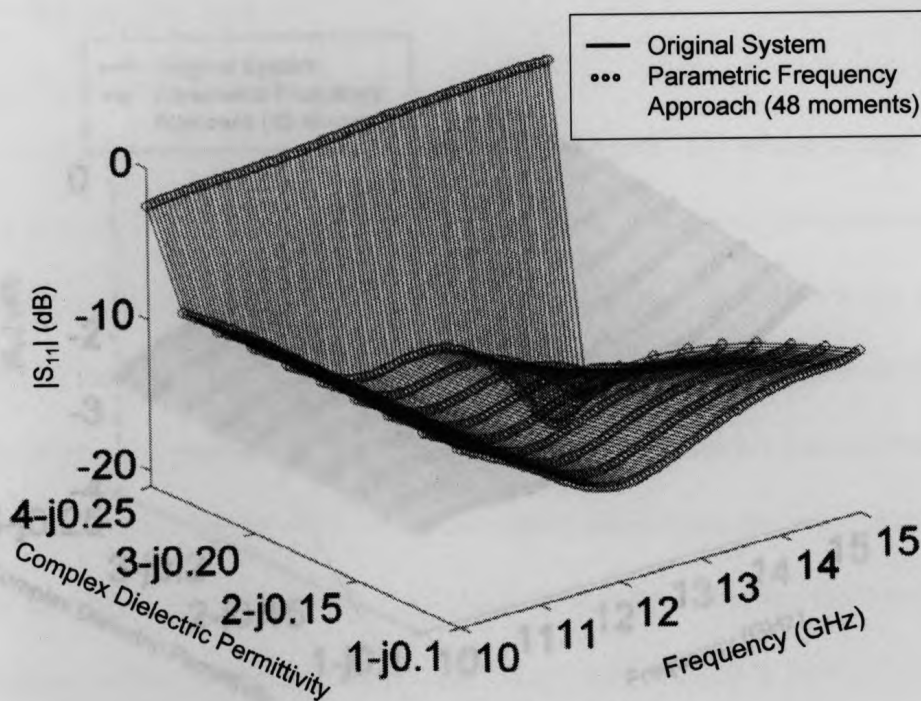


Figure 4.11: 3D comparison of the magnitude of S_{11} for Example2 when $\sigma = 0$ and at different dielectric permittivity values.

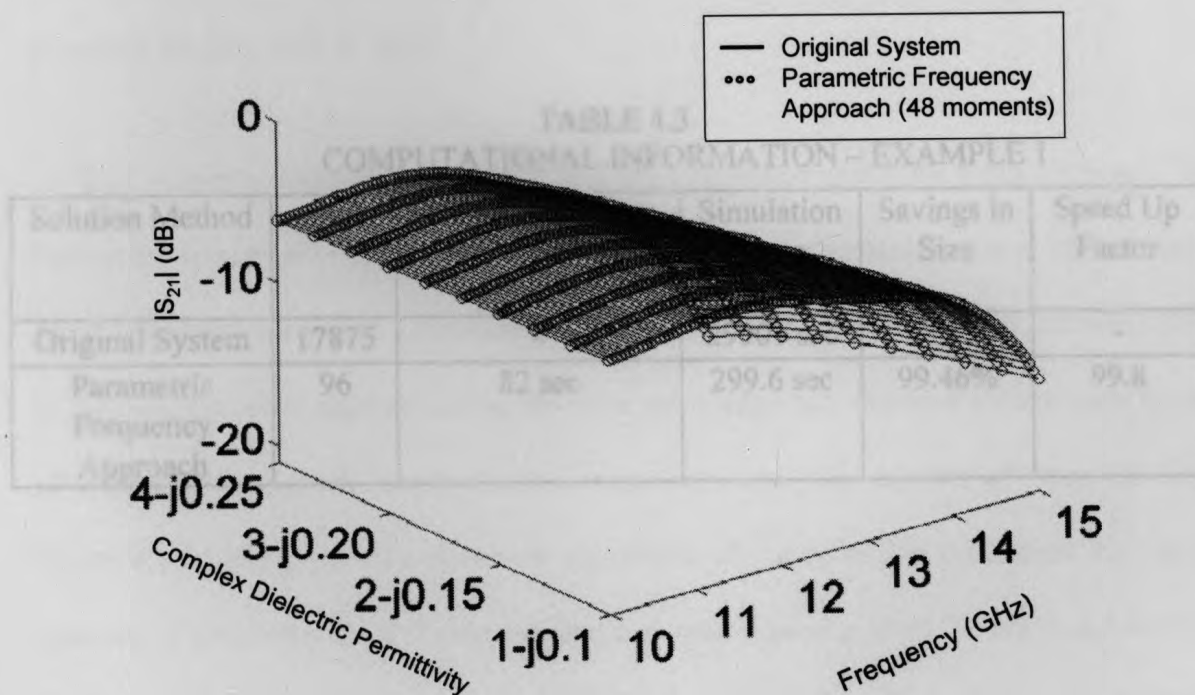


Figure 4.12: 3D comparison of the magnitude of S_{21} for Example2 when $\sigma = 0$ and at different dielectric permittivity values.

4.4.3 – Example 4.3

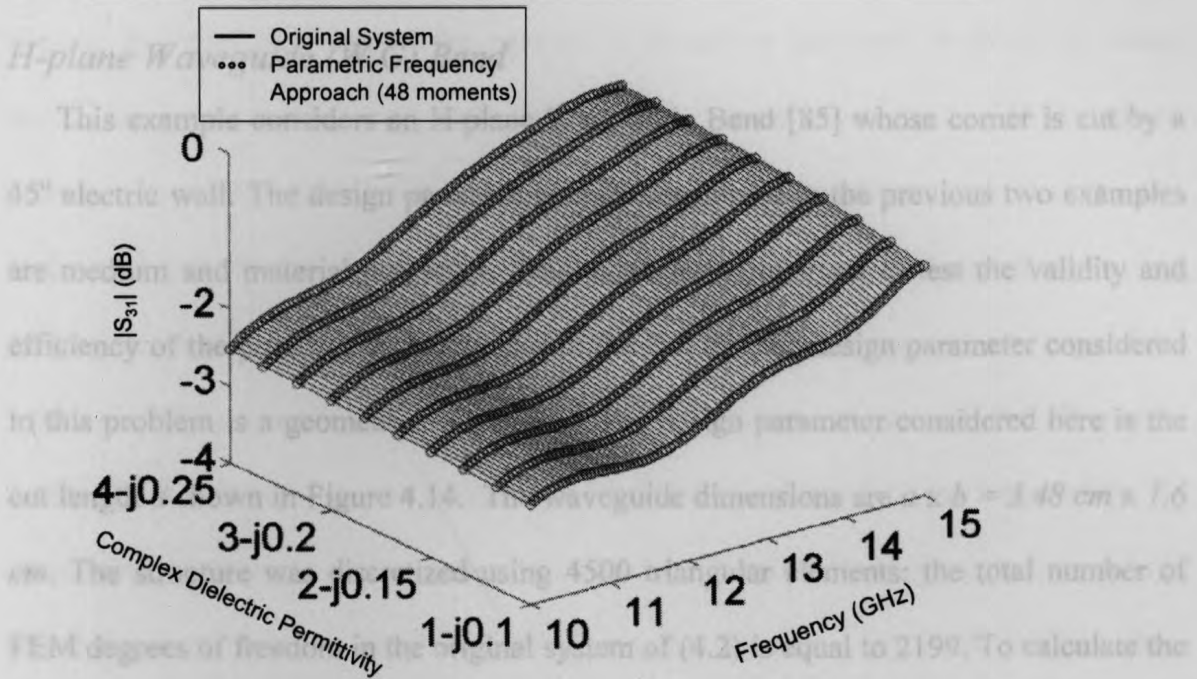


Figure 4.13: 3D comparison of the magnitude of S_{31} for Example 2 when $\sigma = 0$ and at different dielectric permittivity values.

TABLE 4.3
COMPUTATIONAL INFORMATION – EXAMPLE 1

Solution Method	Size	CPU Time to generate reduced system	Simulation Time	Savings in Size	Speed Up Factor
Original System	17875	-	29901 sec	-	-
Parametric Frequency Approach	96	82 sec	299.6 sec	99.46%	99.8

Figure 4.15 and Figure 4.16 shows the magnitude of the reflection coefficient ($|S_{11}|$) as a function of frequency for different cut length d values ranging from 2.6 cm to 2.9 cm for the original system and the parameterized reduced models given by the parametric frequency approach and the state space approach. For their respective orders both

4.4.3 – Example 4.3

H-plane Waveguide (W.G) Bend

This example considers an H-plane Waveguide Bend [85] whose corner is cut by a 45° electric wall. The design parameters so far considered in the previous two examples are medium and material properties. This example is important to test the validity and efficiency of the proposed technique due to the fact that the design parameter considered in this problem is a geometrical parameter. The design parameter considered here is the cut length d shown in Figure 4.14. The waveguide dimensions are $a \times b = 3.48 \text{ cm} \times 1.6 \text{ cm}$. The structure was discretized using 4500 triangular elements; the total number of FEM degrees of freedom in the original system of (4.2) is equal to 2199. To calculate the moments of the original system with respect to the cut length d , the polynomial fitting based parameterized moment matching method proposed in [31], [34], [37] was used. The range of interest of cut length d is from 2.6cm to 2.9cm and the bandwidth of interest is from 5.16 GHz to 7.74 GHz.

This example compares parametric frequency approach with state space approach. To reduce the system of (4.2) using the parametric frequency approach required 20 moments for k , 1 moment for k_1 and 4 moments for the cut length d (total number of moments 25). To achieve the same accuracy using the state space approach required 42 moments for k , 12 moments for the cut length d and 8 cross-moments (total number of moments 62). Figure 4.15 and Figure 4.16 shows the magnitude of the reflection coefficient (S_{11}) as a function of frequency for different cut length d values ranging from 2.6 cm to 2.9 cm for the original system and the parameterized reduced models given by the parametric frequency approach and the state space approach. For their respective orders both

parametric reduced order models match the original system over the entire range of interest; however, the size of the parametric frequency approach is about 2.5 times smaller than the state space approach. Table 4.4 compares the total size and CPU times to generate the parametric reduced order systems for both the approaches. Once again, use of the modified block Arnoldi algorithm [48] for the state space approach makes possible the generation of Krylov subspace to be formulated at the same computational cost of the solution of (4.2) at a single frequency. The CPU times taken to generate the 3D plot of Figure 4.16 using 100 frequency points and 25 different values of the cut length of the H-plane waveguide bend ranging from $d = 2.6$ cm to 2.9 cm for the original system and for the reduced systems obtained using the parametric frequency approach and the state space approach with and without sparsification is shown in Table 4.5. Once again, the total simulation time using the sparse reduced order models includes the time taken for Eigen decompositions performed at each design parameter point in order to sparsify the reduced order model. It is clear from Table 4.5, that once the reduced models are sparsified, the total simulation time taken to solve the sparse reduced model is negligibly small when compared to the original simulation time.

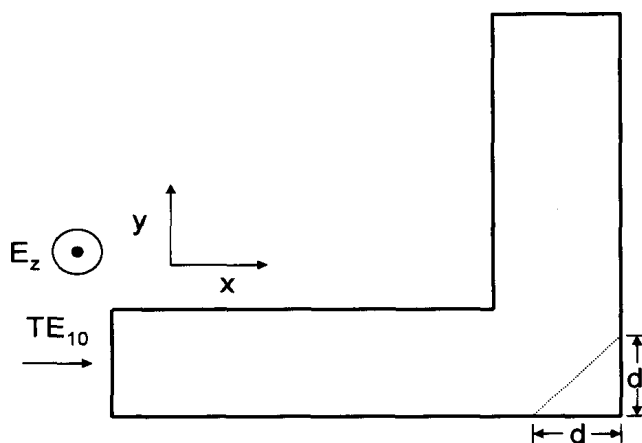


Figure 4.14: H-plane waveguide bend (Example 3)

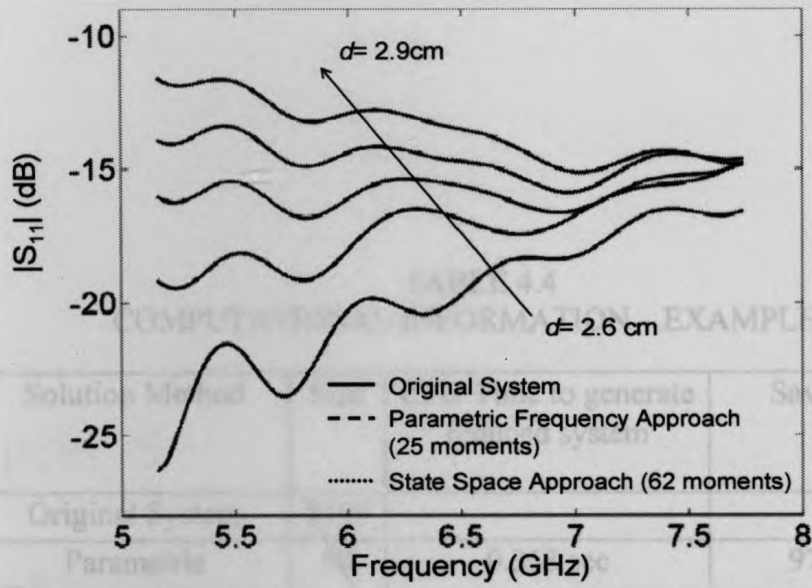


Figure 4.15: Frequency response of the magnitude of the reflection coefficient (S_{11}) for Example 3 at different cut lengths of the Hbend waveguide.

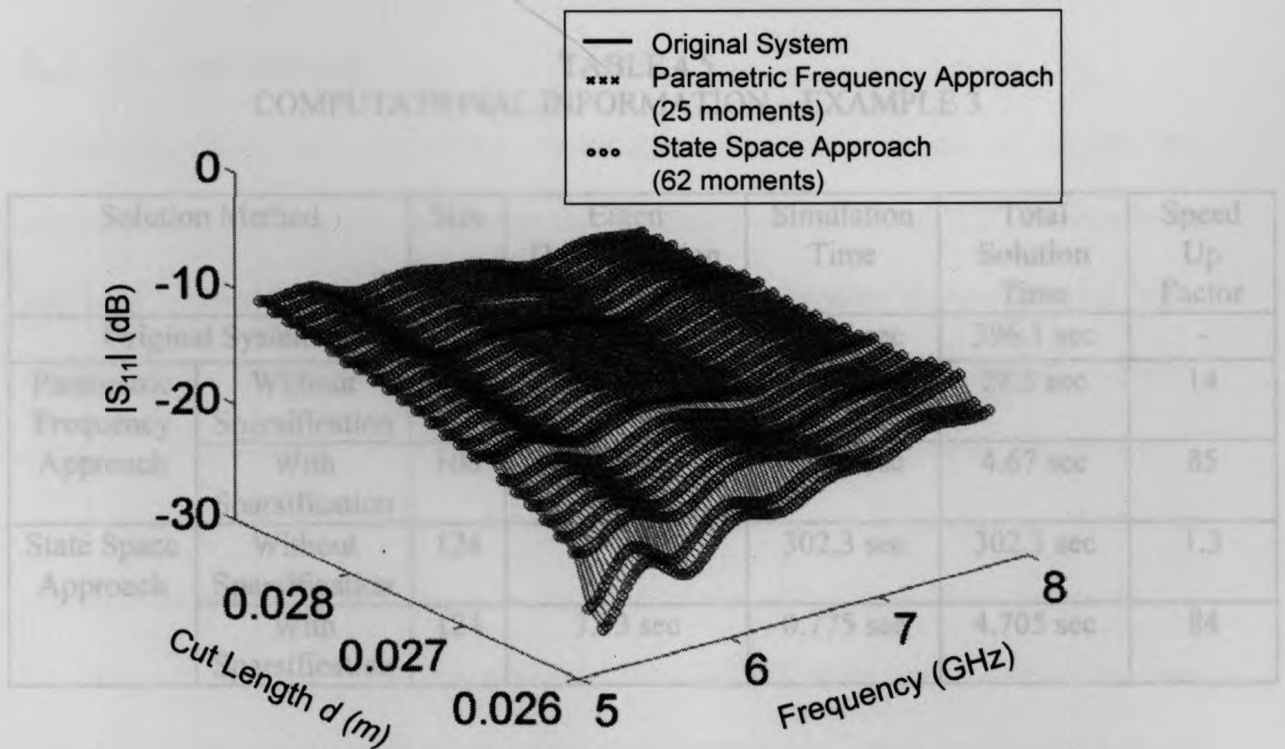


Figure 4.16: 3D comparison of the magnitude of reflection coefficient (S_{11}) for example3 at different cut length values.

TABLE 4.4
COMPUTATIONAL INFORMATION – EXAMPLE 3

Solution Method	Size	CPU Time to generate reduced system	Savings in Size
Original System	2199	-	-
Parametric Frequency Approach	50	0.363 sec	97.73%
State Space Approach	124	0.377 sec	94.36%

TABLE 4.5
COMPUTATIONAL INFORMATION – EXAMPLE 3

Solution Method		Size	Eigen Decomposition (Sparsification)	Simulation Time	Total Solution Time	Speed Up Factor
Original System		2199	-	396.1 sec	396.1 sec	-
Parametric Frequency Approach	Without Sparsification	50	-	28.5 sec	28.5 sec	14
	With Sparsification	100	3.90 sec	0.770 sec	4.67 sec	85
State Space Approach	Without Sparsification	124	-	302.3 sec	302.3 sec	1.3
	With Sparsification	124	3.93 sec	0.775 sec	4.705 sec	84

Chapter 5

Conclusion and Future Research

5.1 – Conclusion

In this thesis, two significant contributions have been made to combat the computational complexities involved in the simulation of high speed VLSI interconnects and high frequency microwave devices. Firstly, a new passive macromodel for lossy multiconductor transmission lines based on a high order FEM approximation has been presented [38]. The coefficients describing the macromodel are computed analytically in terms of predetermined constants and the transmission line p.u.l. parameters. Numerical examples demonstrated that due to the high efficiency of the sixth order approximation the proposed method offers an efficient means to discretize the transmission lines compared to the conventional lumped model, while preserving passivity. The formulation described was based on a sixth order FEM approximation; however, the method can be extended to higher orders while ensuring the passivity of the macromodel. The developed

macromodel is applicable to model interconnects with frequency dependent p.u.l. parameters and can be incorporated with passive model order reduction techniques. Secondly, a parametric model order reduction methodology was developed for high frequency microwave problems solved using the finite element method [53]. Multidimensional Krylov subspace techniques were used to derive reduced order models as a function of frequency as well as other design parameters of the systems. This eliminates the need to redo the reduction for each optimization point and thus results in significant CPU cost savings. Furthermore, the method presented performs multidimensional Krylov subspace based reduction directly on the conventional FEM system obtained through discretization of vector wave equation. The new approach does not result in doubling the size of the original system in order to perform Krylov-based MOR and also enables one to handle frequency dependent parameters in the system which arises due to frequency dependent material properties and frequency dependent boundary conditions.

5.2 – Suggestions for Future Research

This section provides some suggestions for future research based on the work presented in this thesis.

1. In many situations sensitivity analysis is frequently required for the optimization of circuits and systems. If the proposed FEM macromodel for transmission lines is able to support sensitivity analysis, it becomes an important tool for interconnect optimization. Since the coefficients of the interconnect model are obtained analytically in terms of the predetermined

constants and per unit length parameters, the proposed transmission line model should be able to support sensitivity analysis with respect to any interconnect parameter.

2. High speed interconnects in modern printed circuit boards and multi chip modules are complex in geometry and hence extending the macromodel to handle nonuniform transmission lines is important. The proposed macromodel can be applied to transmission lines with nonuniform line parameters by expanding the line parameters as FEM basis function with respect to the position x .
3. The PMR technique presented in this thesis can be extended to solve various other electromagnetic problems. In electromagnetics, eigenvalue problems are often encountered in cavity resonance and wave propagation in both closed and open structures, such as metallic waveguides, microstrip transmission lines, and optical waveguides [7]. Application of FEM to these problems, results in a large generalized eigenvalue problem to be solved for each frequency. Solving these for many frequency points and design parameter values is a very high computational burden. Extending the PMR technique to these problems, would help in addressing these issues. Furthermore, the parametric frequency approach based PMR can be investigated to solve electromagnetic problems with frequency dependent material properties.

References

- [1] B.M. Notaros, M. Djordjevic, and M.M Ilic, "High order electromagnetic modeling for wireless technology applications," *IEEE Topical Conference On Wireless Communication Technology*, pp. 229-232, 2003.
- [2] H.B. Bakoglu, *Circuit, interconnections and packaging for VLSI*. Reading, MA: Addison-Wesley, 1990.
- [3] M. Celik, L. Pileggi, and A. Odabasioglu, *IC interconnect analysis*. Norwell, MA: Kluwer, 2002.
- [4] C.R. Paul, *Analysis of multiconductor transmission lines*. New York: Wiley, 1994.
- [5] R. Achar, M. Nakhla, "Simulation of high-speed interconnects," *Proceedings of the IEEE*, vol. 49, pp. 693-728, May 2001.
- [6] P. P. Silvester and R. L. Ferrari, *Finite elements for electrical engineers*. Cambridge UK: Cambridge University Press, 1996.
- [7] J.M. Jin, *The finite element method in electromagnetics*. Wiley, New York, 2002.
- [8] M.N.O. Sadiku, *Numerical techniques in electromagnetics*. CRC Press LLC, 2001.
- [9] A.F. Peterson, S.L. Ray, and R. Mittra, *Computational methods for electromagnetics*. IEEE Press, 1998.
- [10] M.N.O Sadiku and A.F Peterson, "A comparison of numerical methods for computing electromagnetic fields," *Proceedings of IEEE Southeastcon*, 1990.
- [11] Olgierd A. Palusinski and Anyu Lee, "Analysis of transients in nonuniform and uniform multiconductor transmission Lines," *IEEE Trans. On Microwave Theory and Techniques*, vol. 37, no. 1, pp. 127-138, Jan.1989.
- [12] T. Dhane and D. Zutter, "Selection of lumped element models for coupled lossy transmission lines," *IEEE Trans. Computer-Aided Design*, vol. 11, pp. 57-67, July 1992.
- [13] J. Bracken, V.Raghavan, and R. Rohrer, "Interconnect simulation with asymptotic waveform evaluation," *IEEE Trans. Circuit Syst. I*, vol. 39, pp. 879-878, Nov.1992.
- [14] J.S. Roychowdury, A.R. Newton, and D.O. Pederson, "Algorithms for the transient simulation of lossy interconnects," *IEEE Trans. Computer-Aided Design*, vol. 13, pp. 96-104, Jan. 1994.

- [15] E. Chiprout and M.S. Nakhla, "Analysis of interconnect networks using complex frequency hopping (CFH)," *IEEE Trans. Computer-Aided Design*, vol. 14, pp. 186-200, Feb.1995.
- [16] M. Celik, and A.C. Cangellaris, "Efficient transient simulation of lossy packaging interconnects using moment matching techniques," *IEEE Trans. Comp., Packag. Manuf. Technol. B*, vol 19, pp. 64-73, Feb. 1996.
- [17] M. Celik and A. C. Cangellaris, "Simulation of dispersive multiconductor transmission lines by Padé via Lanczos process," *IEEE Trans. Microwave Theory Tech.*, vol. 44, pp. 2525-2535, Dec. 1996.
- [18] E. Grimme, *Krylov projection methods for model reduction*, Ph.D. thesis, University of Illinois, Urbana-Champaign, 1997.
- [19] M. Celik, A. C. Cangellaris and A. Yaghmour, "An all-purpose transmission-line model for interconnect simulation in SPICE," *IEEE Trans. Microwave Theory Tech.*, vol. 45, pp. 1857-1867, Oct. 1997.
- [20] I.M. Elfadel and D.D. Ling, "A block rational Arnoldi algorithm for multipoint passive model order reduction for multiport RLC networks," *IEEE/ACM Proc. ICCAD*, pp. 66-71, 1997.
- [21] A. Odabasioglu, M. Celik, L. T. Pileggi, "PRIMA: passive reduced-order interconnect macromodeling algorithm," *IEEE Trans. Computer- Aided Design*, vol. 17, pp. 645-654, Aug. 1998.
- [22] P.Gunupudi, M. Nakhla and R. Achar, "Efficient simulation of high-speed distributed interconnects using Krylov subspace techniques," *Proc. IEEE EPEP Topical Meeting*, pp. 295-298, Oct. 1998.
- [23] Q. Yu, J.M.L. Wang, E.S. Kuh, "Passive multipoint moment matching model order reduction algorithm on multiport distributed interconnect networks," *IEEE Trans. Circuits Syst. I*, vol. 46, Jan. 1999.
- [24] Andreas. C. Cangellaris, Soheila Pasha, John L. Prince, Mustafa Celik, "A new discrete transmission line model for passive model order reduction and macromodeling of high-speed interconnections," *IEEE Trans. On Adv. Packaging*, vol. 22, no. 3, pp. 356-364, Aug. 1999.
- [25] A. Dounavis, X. Li, M. Nakhla and R. Achar, "Passive closed-form transmission line model for general purpose circuit simulators," *IEEE Trans. Microwave Theory Tech.*, vol. 47,no. 12, pp. 2450-2459, Dec. 1999.
- [26] P. Gunupudi and M. Nakhla, "Multi-dimensional model reduction of VLSI interconnects," in *Proc. IEEE Custom Integrated Circuits Conf.*, May 2000, pp. 499-502.

- [27] A. Dounavis, R. Achar and M. Nakhla, "A general class of passive macromodels for lossy multiconductor transmission lines," *IEEE Trans. Microwave Theory Tech.*, vol. 49, no. 10, pp. 1686-1696, Oct. 2001.
- [28] I. Erdin, A. Dounavis, R. Achar and M.S. Nakhla, "A SPICE model for incident field coupling to lossy multiconductor transmission lines," *IEEE Trans. On Electromagnetic Compatibility*, vol. 43, no. 4, pp. 485-494, Nov. 2001.
- [29] I.M Elfadel, H. Hao-Ming, A.E. Ruehli, A. Dounavis, and M.S. Nakhla, "A comparative study of two transient analysis algorithms for lossy transmission lines with frequency-dependent data," *IEEE Trans. On Advanced Packaging.*, vol. 25, no. 2, pp. 143-153, May. 2002.
- [30] P. Gunupudi, R. Khazaka, and M. Nakhla, "Analysis of transmission line circuits using multidimensional model reduction techniques," *IEEE Trans. On Advanced Packaging.*, vol. 25, no. 2, pp. 174-180, May. 2002.
- [31] Daniel, L.; White, J.K., "Automatic generation of geometrically parameterized reduced order models for integrated spiral RF-inductors," *IEEE Behavioral Modeling and Simulation BMAS 2003*, Oct. 7-8 2003, San Jose, CA.
- [32] P.K. Gunupudi, R. Khazaka, M.S. Nakhla, T.Smy, and D. Celso, "Passive parameterized time-domain macromodels for high-speed transmission-line networks," *IEEE Trans. Microwave Theory Tech.*, vol. 51, no. 12, pp. 2347-2354, Dec. 2003.
- [33] Q. Xu, P. Mazumder, "Equivalent circuit interconnect modeling based on the fifth-order differential quadrature methods," *IEEE Trans. VLSI Systems.*, vol. 11, no. 6, pp. 1068-1079, Dec. 2003.
- [34] L. Daniel, O.C. Siong, L.S. Chay, K.H. Lee and J. White, "A multiparameter moment-matching model-reduction approach for generating geometrically parameterized interconnect performance models," *IEEE Trans. of CAD of integrated Circuits and Systems.*, vol. 23, no.5 , pp. 678-693, May 2004.
- [35] D. Saraswat, R. Achar, and M.S. Nakhla, "Passive reduction algorithm for RLC interconnect circuits with embedded state space systems (PRESS)," *IEEE Trans. Microwave Theory Tech.*, vol. 52, no. 9, pp. 2215-2226, Sept. 2004.
- [36] N.M. Nakhla, A. Dounavis, R. Achar, and M.S. Nakhla, "DEPACT: Delay extraction-based passive compact transmission-line macromodeling algorithm," *IEEE Trans. On Advanced Packaging.*, vol. 28, no. 1, pp. 13-23, Feb. 2005.
- [37] J.H. Lee, D. Vasilyev, A. Vithayathil, L. Daniel, and J. White, "Accelerated optical topography inspection using parameterized model order reduction," *IEEE Int. Microwave Symp.*, Long Beach, CA, 2005, pp. 1771-1774.

- [38] M.K. Sampath and A. Dounavis, "Efficient passive macromodels for lossy multiconductor transmission lines using high order finite element method," *Proc. IEEE EPEP 14th Topical Meeting*, pp. 191-194, Oct. 2005.
- [39] M. Ma, T.-M. Leung, and R. Khazaka, "Multi level parametric model order reduction for interconnect networks," *Proc. IEEE EPEP 14th Topical Meeting*, pp. 57-60, Oct. 2005.
- [40] G.S. Shin, N.M. Nakhla, R. Achar, M.S. Nakhla, A. Dounavis, and I. Erdin, "Fast transient analysis of incident field coupling to multiconductor transmission lines," *IEEE Trans. On Advanced Packaging*, vol.48, no. 1, pp. 57-73, Feb. 2006.
- [41] M.A Kolbehdari, M. Srinivasan, M.S. Nakhla, Q.-J. Zhang and R. Achar, "Simultaneous time and frequency domain solutions of EM problems using finite element and CFH techniques," *IEEE Trans. Microwave Theory Tech.*, vol. 44, no. 9, pp. 1526-1534, Sept. 1996.
- [42] J. Gong and J.L. Volakis, "AWE implementation for electromagnetic FEM analysis," *Electronics Letters*, vol. 32, no. 24, pp. 2216-2217, Nov. 1996.
- [43] X.-M. Zhang and J.-F. Lee, "Application of the AWE method with the 3-D TVFEM to model spectral responses of passive microwave components," *IEEE Trans. Microwave Theory Tech.*, vol. 46, no. 11, pp. 1735-1741, Nov. 1998.
- [44] L. Zhao and A.C.Cangellaris, "Reduced-order modeling of electromagnetic field interactions in unbounded domains truncated by perfectly matched layers," *Microwave Opt. Technol. Lett.*, vol. 17, no. 1, pp. 62-66, Jan. 1998.
- [45] M.R. Zunoubi, K.C. Donepudi, J.M. jin, and W.C. Chew, "Efficient time-domain and frequency-domain finite-element solution of Maxwell's equations using spectral Lanczos decomposition method," *IEEE Trans. Microwave Theory Tech.*, vol. 46, pp. 1141-1149, Aug. 1998.
- [46] A. Cangellaris, M.Celik, S.Pasha, and L.Zhao, "Electromagnetic model order reduction for system-level modeling," *IEEE Trans. Microwave Theory Tech.*, vol. 47, pp. 840-849, June 1999.
- [47] D.-K. Sun, Z. Cendes, and J.-F. Lee, "ALPS-A new fast frequency-sweep procedure for microwave devices," *IEEE Trans. Microwave Theory Tech.*, vol. 49, pp. 398-402, Feb. 2001.
- [48] Y.Zhu and A.C.Cangellaris, "A new finite element model for reduced order electromagnetic modeling," *IEEE Microwave and Wireless Components Letters*, vol. 11, no. 5, May 2001.

- [49] Y. Zhu and A.C. Cangellaris, "Finite element-based model order reduction of electromagnetic devices," *Int.J.Numer.Model.*, vol 15, no.1, pp. 73-92, Jan. 2002.
- [50] H. Wu and A.C. Cangellaris, "Model-order reduction of finite-element approximations of passive electromagnetic devices including lumped electrical-circuit models," *IEEE Trans. Microwave Theory Tech.*, vol. 52, no.9, pp.2305-2313, Sept. 2004.
- [51] E.B. Rudnyi, and J.G. Korvink, "Review: Automatic model reduction for transient simulation of MEMS-based devices," *Sensors Update*, Feb 2003.
- [52] J.V. Clark, and et. Al., "3D MEMS simulation modeling using modified nodal analysis," *Proc. of the Microscale Systems: Mechanics and Measurements Symposium*, Portland, OR, Jun. 2001.
- [53] M.K. Sampath, A. Dounavis, and R. Khazaka, "Parameterized model order reduction techniques for finite element based full wave analysis," *IEEE MTT-S International Microwave Symposium Digest*, San Francisco, CA, June 2006.
- [54] International Technology Roadmap for Semi-conductors, 2003 Edition.
- [55] R. Wang and O. Wing, "A circuit model of a system of VLSI interconnects for time response computation," *IEEE Trans. Microwave Theory Tech.*, vol. 39, pp.688-693, April 1991.
- [56] J. Cullum, A. Ruehli, and T. Zhang, "A method of reduced-order modeling and simulation of large interconnect circuits and its application to PEEC models with retardation," *IEEE Trans. Circuit and Systems II*, vol. 47, pp. 261-273, April 2000.
- [57] F.H. Branin, Jr., "Transient analysis of lossless transmission lines," *Proc. IEEE*, vol. 55, pp. 2012-2013, 1967.
- [58] F.Y. Chang, "The generalized method of characteristics for waveform relaxation analysis of coupled transmission lines," *IEEE Trans. Microwave Theory Tech.*, vol. 37, pp.2028-2038, Dec. 1989.
- [59] R. W. Newcomb, *Linear Multiport Synthesis*, New York: McGraw 1966.
- [60] HSPICE, Synopsis, Inc. Release U-2003.09-RA, Mountain View, CA.
- [61] K. Israel, and R. Miniowitz, "Hermitian finite-element method for inhomogeneous waveguides," *IEEE Trans. Microwave Theory Tech.*, vol. 38, no. 9, Sept. 1990.
- [62] A.C. Cangellaris, and R. Lee, "Finite element analysis of electromagnetic scattering from inhomogeneous cylinders at oblique incidence," *IEEE Trans. Antennas and Propagation*, vol. 39, no. 5, pp. 645-650, May 1991.

- [63] K. Ise, K. Inoue, and M. Koshiba, "Three-dimensional finite element method with edge elements for electromagnetic waveguide discontinuities," *IEEE Trans. Microwave Theory Tech.*, vol. 39, no. 8, Aug. 1991.
- [64] M. Zhang, "Finite-element analysis of waveguide scattering problems," *IEEE Trans. On Magnetics*, vol. 27, no. 5, Sept. 1991.
- [65] M.R. Lyons, A.C. Polycarpou, and C.A. Balanis, "On the accuracy of the perfectly matched layers using a finite element formulation," *IEEE MTT-S Digest*, 1996, pp. 205-208.
- [66] J.R. Brauer, and G.C.Lizalek, "Microwave filter analysis using a new 3-D finite element modal frequency method," *IEEE Trans. Microwave Theory Tech.*, vol. 45, no. 5, pp. 810-818, May 1997.
- [67] R. Dyczij-Edlinger, G. Peng, and J.-F. Lee, "Efficient finite element solvers for the Maxwell equations in the frequency domain," *Comput. Methods Appl. Mech. Eng.*, vol. 169, no. 3-4, pp.297-309, Feb. 1999.
- [68] Y. Zhu, and A.C. Cangellaris, "Macro-elements for efficient FEM simulation of small geometric features in waveguide components," *IEEE Trans. Microwave Theory Tech.*, vol. 48, pp. 2254-2260, Dec. 2000.
- [69] J. Rubio, J. Arroyo and J. Zapata, "SFELP- An efficient methodology for microwave circuit analysis," *IEEE Trans. Microwave Theory Tech.*, vol. 49, no. 3, pp. 509-516, Mar. 2001.
- [70] J.Liu, J.M.Jin, E.K.N.Yung, and R.S.Chen, "A fast three-dimensional higher order finite element analysis of microwave waveguide devices," *Microwave Opt. Tech. Lett.*, vol. 32, no. 5, pp. 344-352, March 2002.
- [71] V. Hill, O. Farle, and R.D. Edlinger, "Finite element basis functions for nested meshes of nonuniform refinement level," *IEEE Trans. On Magnetics*, vol. 40, no. 2, march 2004.
- [72] H. Wu, and A.C. Cangellaris, "Finite element analysis of passive electromagnetic devices including lumped electrical circuit models," *IEEE Proc. Electronic Components and Technology*, June 2004, pp. 231-236.
- [73] M.M. Ilic, A.Z.Ilic, and B.M. Notaros "Higher order large-domain FEM modeling of 3-D multiport waveguide structures with arbitrary discontinuities" *IEEE Trans. Microwave Theory Tech.*, vol. 52, no. 6, June 2004.
- [74] J.C. Nedelec, "Mixed finite elements in R^3 ," *Numer.Meth.*, vol. 35, pp. 315-341, 1980.

- [75] M.K. Sampath, A. Dounavis, and R. Khazaka, "Parameterized model order reduction techniques for FEM based full wave analysis," submitted to *IEEE Transactions on Microwave Theory and Techniques*.
- [76] J.W. Demmel, *Applied Numerical Linear Algebra*. Philadelphia, PA: SIAM, 1997.
- [77] C. Prud'homme, D. Rovas, K. Veroy, Y. Maday, A. T. Patera, and G. Turinici, "Reliable real-time solution of parameterized partial differential equations: Reduced-basis output bounds methods," *J. Fluids Eng.*, 2002.
- [78] Bai Z, Slone Rd, Smith WT, Ye Q, "Error bound for reduced system model by Pade approximation via the Lanczos process," *IEEE Trans. Of CAD of Integrated Circuits and Systems.*, vol. 18, no.2, pp. 133-141, Feb 1999.
- [79] Odabasioglu A, Celik M, Pileggi LT, "Practical considerations for RLC circuit reduction," *IEEE/ACM Proceedings of the ICCAD*, San Jose, CA, Nov. 1999.
- [80] MATLAB 7.0.0.19920 (R14) *User's Guide* 2004, The Mathworks Inc., Natick, MA.
- [81] T.A Davis, "UMFPACK v4.3," [Online document], Jan. 16 2004, [cited 2005 Sept 14], Available HTTP: <http://www.cise.ufl.edu/research/sparse/umfpack>.
- [82] K.L.Wu and H.Y. Wang, "A rigorous modal analysis of H-plane waveguide T-junction loaded with a partial-height post for wideband applications," *IEEE Trans. Microwave Theory Tech.*, vol. 49, no. 5, May 2001.
- [83] Z. Bai, and Y. Su, "SOAR: A second-order Arnoldi method for the solution of the quadratic eigenvalues problem," *Computer Science Technical report*, CSE-2003-21, University of California, Davis, 2003.
- [84] Y.Su, J. Wang, X. Zeng, Z. Bai, C. Chiang, and D. Zhou, "SAPOR: Second-order Arnoldi method for passive order reduction of RCS circuits," *IEEE Proc. ICCAD*, pp. 74-79, 2004.
- [85] D. Li, and N.K. Nikolova, "S-parameter sensitivity analysis of waveguide structures with femlab," *Comsol Multiphysics Conference*, Boston, Oct 23-25, 2005.
- [86] D. Saraswat, R.Achar, and M.Nakhla, "Global passivity enforcement algorithm for macromodels of interconnect subnetworks characterized by tabulated data," *IEEE Trans. VLSI Systems*, vol. 13, no. 17, July 2005.
- [87] T. Kailath, *Linear Systems*. Toronto: Prentice-Hall Inc., 1980.
- [88] B. Friedland, *Control System Design: An Introduction to State-Space Methods*. New York: McGraw-Hill Inc., 1986.

- [89] S. Grivet Talocia, H-M Huang, A.E. Ruehli, F. Canvero, and I. Elfadel, "Transient analysis of lossy transmission lines: An efficient approach based on the method of characteristics," *IEEE Trans on Adv. Packag.*, pp. 1-12, 2004.
- [90] A. Dounavis, R. Achar and M. Nakhla, "Efficient passive circuit models for distributed networks with frequency dependent parameters," *IEEE Trans. On Adv. Packag.*, vol. 23, pp. 382-392, Aug 2000.
- [91] L. Weinberg, *Network Analysis and Synthesis*. New York: McGraw-Hill Book Company Inc., 1962.
- [92] E.A. Guillemin, *Synthesis of Passive Networks*. New York, NY: John Wiley and Son Inc., 1957.
- [93] W.H. Press, S.A. Teukolsky, W.T. Vetterling, B.P. Flannery, *Numerical Recipes in C*, 2nd ed., Cambridge, U.K.: Cambridge University Press, 1992.
- [94] A. Deutsch, "Electrical characteristics of interconnections for high performance systems," *Proceedings of IEEE*, vol. 86, pp. 315-355, Feb. 1998.
- [95] S. Grivet-Talocia, "Passivity enforcement via perturbation of hamiltonian matrices," *IEEE Trans. On Circuits and Systems*, vol. 51, 2004.